Available online at www.sciencedirect.com

ScienceDirect

Geochimica et Cosmochimica Acta 133 (2014) 479–522

Geochimica et Cosmochimica Acta

www.elsevier.com/locate/gca

Presolar graphite from the Murchison meteorite: An isotopic study

Sachiko Amari [a,*], Ernst Zinner [a], Roberto Gallino [b]

[a] McDonnell Center for the Space Sciences and the Physics Department, Washington University, St. Louis, MO 63130, USA
[b] Dipartimento di Fisica, Università di Torino, I-10125 Torino, Italy

Received 28 November 2012; accepted in revised form 9 January 2014; available online 19 January 2014

Abstract

We studied presolar graphite grains from four density fractions, KE3 (1.65–1.72 g/cm^3), KFA1 (2.05–2.10 g/cm^3), KFB1 (2.10–2.15 g/cm^3), and KFC1 (2.15–2.20 g/cm^3), extracted from the Murchison (CM2) meteorite, with the ion microprobe. One of the most interesting features of presolar graphite is that isotopic features depend on density. There are grains with ^{15}N and ^{18}O excesses, Si isotopic anomalies, high ^{26}Al/^{27}Al ratios (~0.1), and Ca and Ti isotopic anomalies, including the initial presence of short-lived ^{41}Ca and ^{44}Ti. These isotopic features are qualitatively explained by nucleosynthesis in core collapse supernovae. We estimate that 76%, 50%, 7% and 1% of the KE3, KFA1, KFB1 and KFC1 grains, respectively, are supernova grains. We performed 3- and 4-zone supernova mixing calculations to reproduce the C, O (^{18}O/^{16}O) and Al isotopic ratios of the KE3 grains, using 15 $M_\odot$ model calculations by Rauscher et al. (2002). Isotopic ratios of grains with high ^{12}C/^{13}C ratios (>200) can be reproduced, whereas those of grains with ratios $\leqslant$200 are hard to explain if we assume that graphite grains form in C-rich conditions.

We compared the distributions of the ^{12}C/^{13}C ratios of KFB1 and KFC1 grains and their *s*-process ^{86}Kr/^{82}Kr ratios inferred from bulk noble gas analysis to model calculations of asymptotic giant branch (AGB) stars with a range of mass and metallicity. We conclude that KFB1 grains with ^{12}C/^{13}C $\geqslant$ 100 formed in the outflow of low-mass (1.5, 2 and 3 $M_\odot$) low-metallicity ($Z = 3 \times 10^{-3}$ for 1.5, 2 and 3 $M_\odot$, $Z = 6 \times 10^{-3}$ for 3 $M_\odot$ only) AGB stars and that KFC1 grains with ^{12}C/^{13}C $\geqslant$ 60 formed in those stars as well as in 5 $M_\odot$ stars of solar and/or half-solar metallicities. Grains with ^{12}C/^{13}C < 20 in all the fractions seem to have multiple origins. Some of them formed in the ejecta of core-collapse supernovae. J stars and born-again AGB stars are also possible stellar sources.

We calculated the abundances of graphite grains from supernovae and AGB stars in the Murchison meteorite to be 0.24 ppm and 0.44 ppm, respectively, whereas those of SiC grains from supernovae and AGB stars are 0.063 ppm and 5.6 ppm, respectively. In contrast to graphite, AGB stars are a dominant source of SiC grains.

Since different mineral types have different residence times in the interstellar medium, their abundances in meteorites may not reflect original yields in stellar sources. Even if graphite grains are more easily destroyed than SiC grains, graphite grains from supernovae are more abundant than SiC grains from supernovae (0.24 ppm vs. 0.063 ppm), indicating that supernovae are a prolific producer of graphite grains. Graphite grains from AGB stars are less abundant than SiC grains from AGB stars (0.44 ppm vs. 5.6 ppm). This difference may reflect the difference in their parent stars: graphite grains formed in low-metallicity stars, while SiC grains formed in close-to-solar metallicity stars.

* Corresponding author. Tel.: +1 314 935 6248; fax: +1 314 935 4083.
E-mail address: sa@wuphys.wustl.edu (S. Amari).

http://dx.doi.org/10.1016/j.gca.2014.01.006
0016-7037/

1. INTRODUCTION

Elemental and isotopic abundances of the Galaxy change with time. When stars reach the later stages of their lives, their nucleosynthetic products are expelled into space as gas and dust. Stars with masses less than 8 $M_\odot$ become asymptotic giant branch (AGB) stars and lose significant material as stellar wind during the thermally-pulsing AGB phase. Stars with masses $\geqslant 8\ M_\odot$ become core-collapse supernovae and the nucleosynthetic products in these stars are distributed into space through explosion. Gas and dust expelled from these stars are eventually incorporated into molecular clouds. Our solar system, located at 8.5 kpc from the center of the Galaxy, formed from such a molecular cloud ~4.6 billion years ago. The parent molecular cloud of the solar system was believed to have been completely homogenized during solar system formation (Cameron, 1962). This idea of an isotopically uniform solar system was reinforced by analyses of meteorites in the 50's and 60's, which showed uniform isotopic ratios (e.g., Podosek, 1978).

However, when Black and Pepin (1969) analyzed Ne in primitive meteorites by step-wise heating, they found a new ^{22}Ne-rich component (see Fig. 4 in Black and Pepin, 1969), which later was named Ne-E (Black, 1972). The lowest ^{20}Ne/^{22}Ne ratio (3.4, air: 9.8) observed in their experiment was such that it was difficult to explain the ^{22}Ne enrichment by processes that occurred in the solar system, thus a nucleosynthetic origin was proposed (Clayton, 1975). Subsequent studies indicated the presence of two kinds of Ne-E: Ne-E(H), released at *h*igh temperature (1200–1400 °C) and concentrated in *h*igh-density mineral separates (3–3.5 g/cm^3), and Ne-E(L), released at *l*ow temperature (500–700 °C) and concentrated in *l*ow-density separates (<2.3 g/cm^3) (Jungck, 1982).

Isotopically distinct components were identified also in heavy noble gases. Xe-HL is characterized by excesses in both light and *p*-process-only isotopes, 124 and 126, and heavy and *r*-process-only isotopes, 134 and 136 relative to solar (Lewis et al., 1975). Xe-S and Kr-S, with excesses in even-numbered isotopes, are components that show the signature of the slow neutron-capture process (the *s*-process) (Srinivasan and Anders, 1978). These Kr and Xe components were well hidden in bulk meteorites and their presence was detected only in chemically processed residues, after more than 99 percent of bulk meteorites had been dissolved. This indicates that minerals containing these noble gases have extremely low abundances in meteorites.

Edward Anders, Roy S. Lewis and their colleagues at The University of Chicago undertook the task to identify and isolate the minerals with the anomalous noble gas components (≡carriers). Without knowing the mineral types of these carriers, they used the anomalous noble gas components as a navigator. They separated small portions of meteorites from bulk meteorites by chemical and physical methods and analyzed noble gases in these fractions. Fractions enriched in anomalous noble gas components would be further processed to achieve a greater enrichment. This effort, on and off but spanning more than a decade, finally bore fruit when diamond, the carrier of Xe-HL, was isolated and identified from the Allende meteorite (Lewis et al., 1987). Soon the identification and isolation of silicon carbide (SiC), the carrier of Xe-S, Kr-S and Ne-E(H), followed (Bernatowicz et al., 1987; Tang and Anders, 1988), as did the isolation of graphite (Amari et al., 1990). Interestingly, all carriers of these anomalous noble gas components are carbonaceous and fairly resistant to chemicals. Otherwise, this method, "burning a haystack to find the needle" as Edward Anders once phrased it, would not have worked. A historical account of the discoveries of those noble gas components and their carriers has been given by Anders (1988).

Presolar grains identified to date include diamond (Lewis et al., 1987), SiC (Bernatowicz et al., 1987; Tang and Anders, 1988), graphite (Amari et al., 1990), oxides (Hutcheon et al., 1994; Huss et al., 1994; Nittler et al., 1994; Choi et al., 1999; Floss et al., 2008), silicon nitride (Si_3N_4) (Nittler et al., 1995), refractory carbides in SiC (Bernatowicz et al., 1992; Hynes et al., 2010) and graphite (Bernatowicz et al., 1991, 1996; Croat et al., 2003, 2010), and silicates (Messenger et al., 2003; Nguyen and Zinner, 2004; Nagashima et al., 2004; Mostefaoui and Hoppe, 2004; Haenecour et al., 2013). In addition, a variety of metal, carbide, oxide, sulfide and silicide subgrains were identified inside of SiC and graphite grains (Bernatowicz et al., 1996; Croat et al., 2003, 2008, 2013; Hynes et al., 2010, 2011). Except for the three carbonaceous presolar grain types, they were identified by secondary ion mass spectrometry (SIMS) and transmission electron microscopy (TEM). Abundances of presolar grains in meteorites range from ~1000 ppm (diamond) to a few ppb (Si_3N_4). The isolation and identification of presolar grains have opened a new field of astronomy: we are able to study stardust in great detail with unprecedented precisions in the laboratory. Analyses of presolar grains have provided a wealth of information about nucleosynthesis in stars, mixing in stellar ejecta, and Galactic chemical evolution. Reviews of presolar grains and related topics can be found in various papers and book chapters (Bernatowicz and Zinner, 1997; Hoppe and Zinner, 2000; Clayton and Nittler, 2004; Zinner, 2004; Lodders and Amari, 2005; Davis, 2011; Zinner, 2013).

In this paper, we report the results of a comprehensive study of presolar graphite from the Murchison meteorite by SIMS. We will describe experimental procedures in Section 2, and results in Section 3. We will discuss the results and their implications in Section 4 and summarize our work in Section 5. Part of the data have already been reported by Amari et al. (1993, 1995c, 1996), Hoppe et al. (1995), Nittler et al. (1996), Travaglio et al. (1999), Croat et al. (2003), Heck et al. (2009a) and Meier et al. (2012).

2. EXPERIMENTAL PROCEDURES

2.1. Separation of presolar graphite from the Murchison meteorite

The separation procedure of carbonaceous presolar grains is described in detail by Amari et al. (1994); we briefly summarize it here with emphasis on presolar graphite. The separation of presolar graphite is more complicated

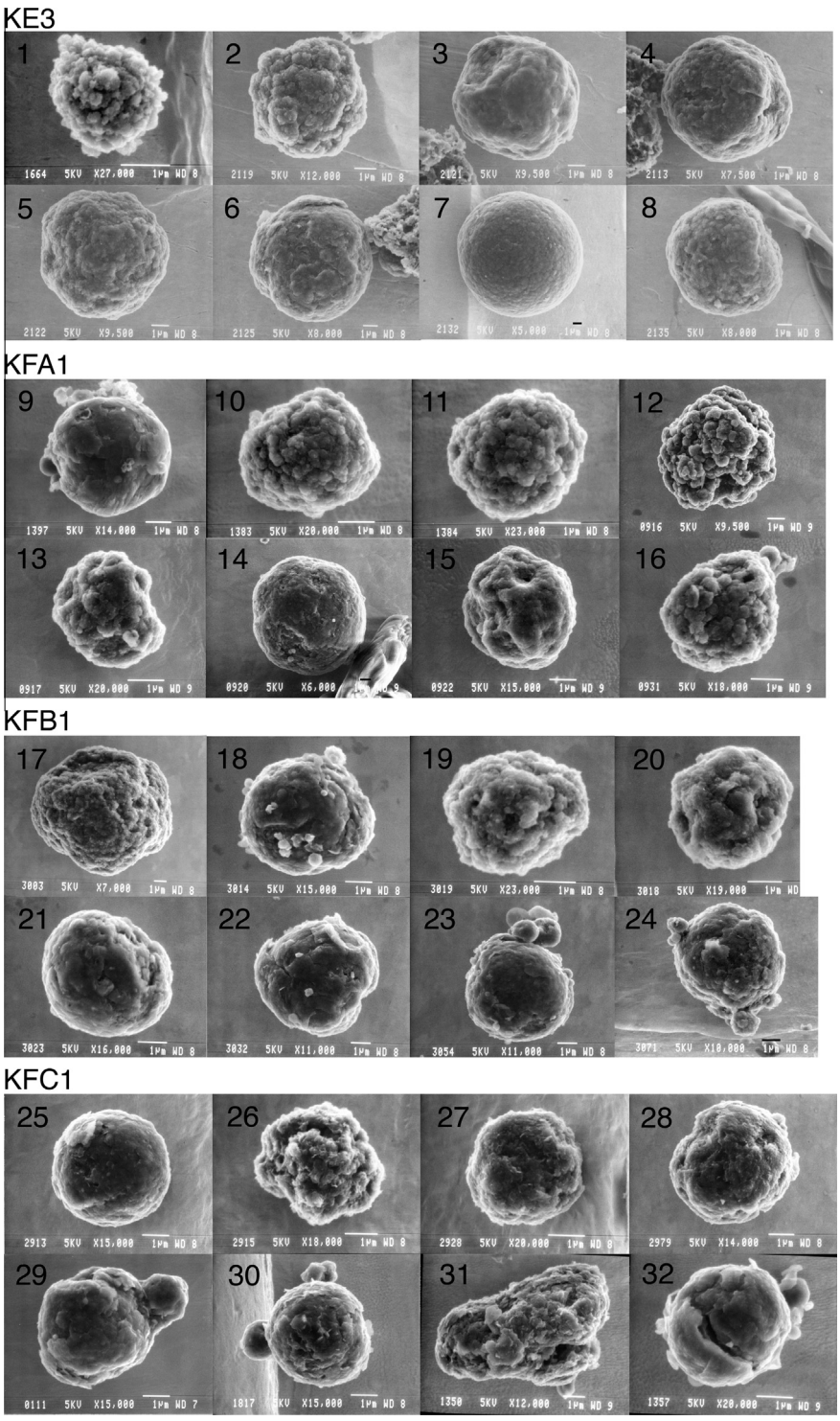

Fig. 1. Secondary electron images of presolar grains from the Murchison graphite fractions. The scale bars are 1 μm. C stands for cauliflower, O for onion. $^{12}C/^{13}C$ ratios are also given. For the grains' morphologies see the text. The lowercase letters following the fraction names indicate different mounts. (1) KE3a-411, C, 93.8 ± 1.8. (2) KE3c-111, C, 120 ± 1. (3) KE3c-131, O, 17.1 ± 0.1. (4) KE3c-351, C, 61.8 ± 0.2. (5) KE3c-401, C, 37.8 ± 0.2. (6) KE3c-411, O, 14.22 ± 0.04. (7) KE3c-551b, O, 7223 ± 111. (8) KE3c-621, C, 1493 ± 44. (9) KFA1c-121, O, 645 ± 21. (10) KFA1c-m132, C, 55.3 ± 0.7. (11) KFA1c-m133, C, 92.2 ± 1.1. (12) KFA1f-101, C, 89.2 ± 0.9. (13) KFA1f-131, C, 147 ± 2. (14) KFA1f-161, O, 24.9 ± 0.1. (15) KFA1f-182, C, 17.2 ± 0.2. (16) KFA1f-581, C, 31.2 ± 0.1. (17) KFB1a-151, C, 43.5 ± 0.2. (18) KFB1a-212, O, 587 ± 40. (19) KFB1a-261, C, 90.0 ± 1.1. (20) KFB1a-262, C, 6.72 ± 0.07. (21) KFB1a-311, O, 1163 ± 10. (22) KFB1a-332, O, 117 ± 1. (23) KFB1a-421, O, 156 ± 2. (24) KFB1a-575, O, 25.0 ± 0.2. (25) KFC1a-115, O, 187 ± 2. (26) KFC1a-117, C, 12.3 ± 0.1. (27) KFC1a-173, C, 123 ± 2. (28) KFC1a-364, C, 1293 ± 61. (29) KFC1b2–0m11, O, 671 ± 13. (30) KFC1b2–303, O, 4.51 ± 0.02. (31) KFC1b2–661, C, 386 ± 4. (32) KFC1b2–751, O, 559 ± 12.

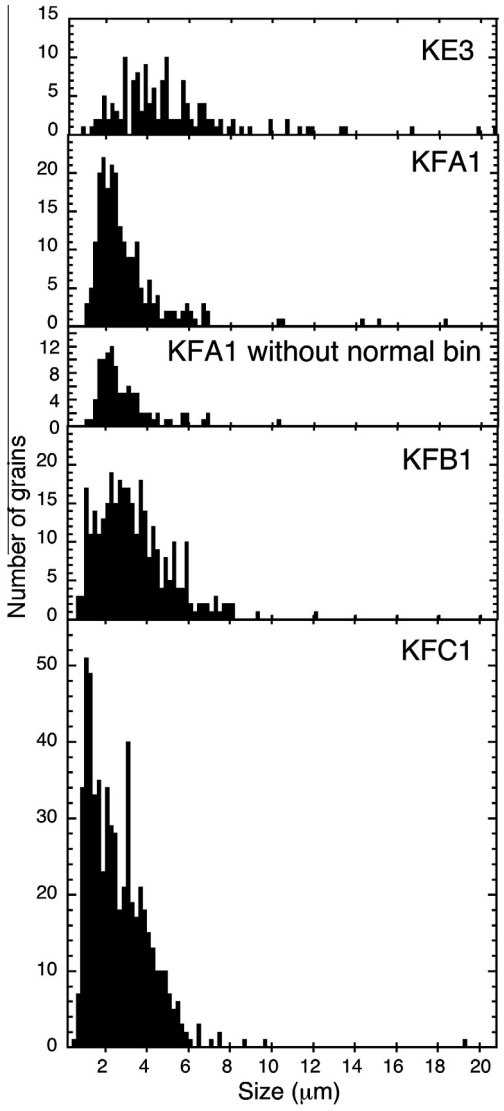

Fig. 2. Size distributions of the grains in the different graphite fractions. The total numbers of grains examined for their sizes and their average sizes are given in Table 3. There are a number of KFA1 grains with close-to-normal $^{12}C/^{13}C$ ratios, many of which may be of solar system origin. Thus, the sizes of KFA1 grains excluding those with $79.4 < {}^{12}C/{}^{13}C < 100$, indicated as "KFA1 without normal bin" in the figure, are also shown. There are no significant size differences between these grains and the entire KFA1 population. Part of the data have previously been published by Hoppe et al. (1995), Croat et al. (2003), Heck et al. (2009a) and Meier et al. (2012).

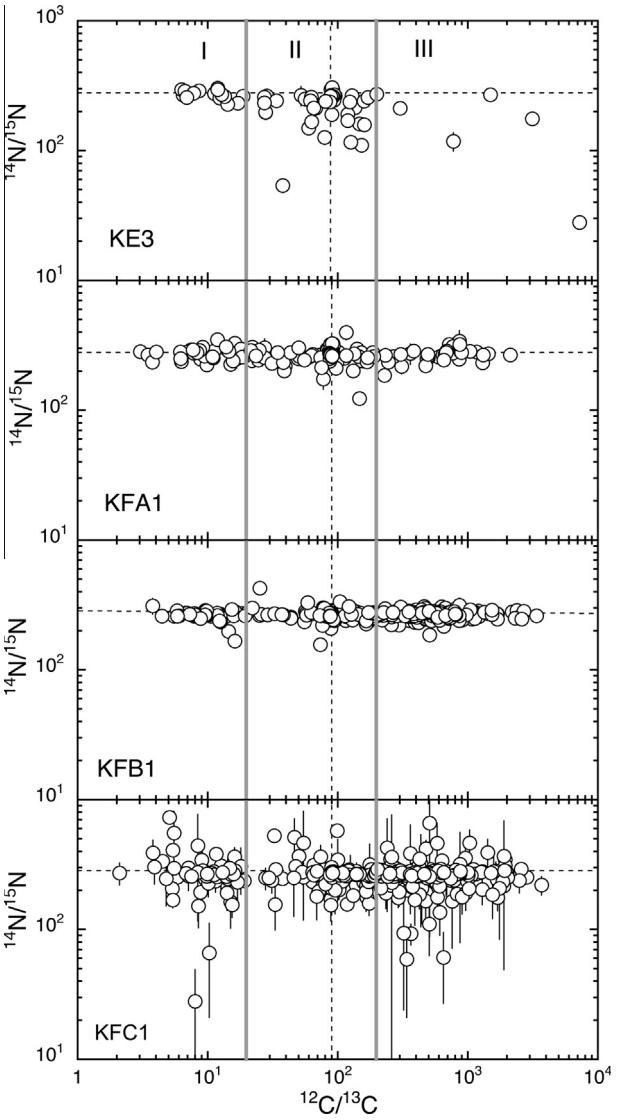

Fig. 3. Nitrogen and C isotopic ratios of the grains from the graphite fractions. The two gray solid lines crossing the four plots in this figure and the subsequent figures indicate the boundaries of Populations I, II and III (20 and 200). In this and all following figures showing isotopic ratios errors are 1σ. The dotted lines in this figure and subsequent figures indicate the solar ratios. An exception is the N isotopic ratio, which is that of air. Part of the data have previously been published by Hoppe et al. (1995), Amari et al. (1993, 1995c, 1996) and Travaglio et al. (1999).

than those of diamond and SiC because graphite is less resistant to chemicals than the other carbonaceous presolar minerals. Moreover, presolar graphite is found only in primitive meteorites which also contain abundant organic matter that has similar characteristics as graphite. Usually strong oxidants are used to destroy organic matter, but this cannot be done for the separation of graphite because it would be also destroyed by such a treatment. Therefore, mild oxidation in combination with density and size separations is applied to extract graphite grains.

The separation of the Murchison K-series started by combining a few already-present Murchison separates that had been enriched in matrix through freeze–thaw disaggregation. Due to this start, the effective initial mass was estimated to be 83 ± 8 g of bulk Murchison meteorite. This Murchison sample was alternately treated with 1 M HCl – 10 M HF and 6 M HCl to remove silicates, followed by another alternating treatment with 6 M HCl – 0.6 M H_3BO_3 and 6 M HCl – 2 M HF to dissolve insoluble fluorides and remaining silicates. The residue was immersed in 4 M KOH at 70 °C for 24 h to dissolve reactive kerogen (organic matter) and sulfur. Hydrogen peroxide (H_2O_2) was

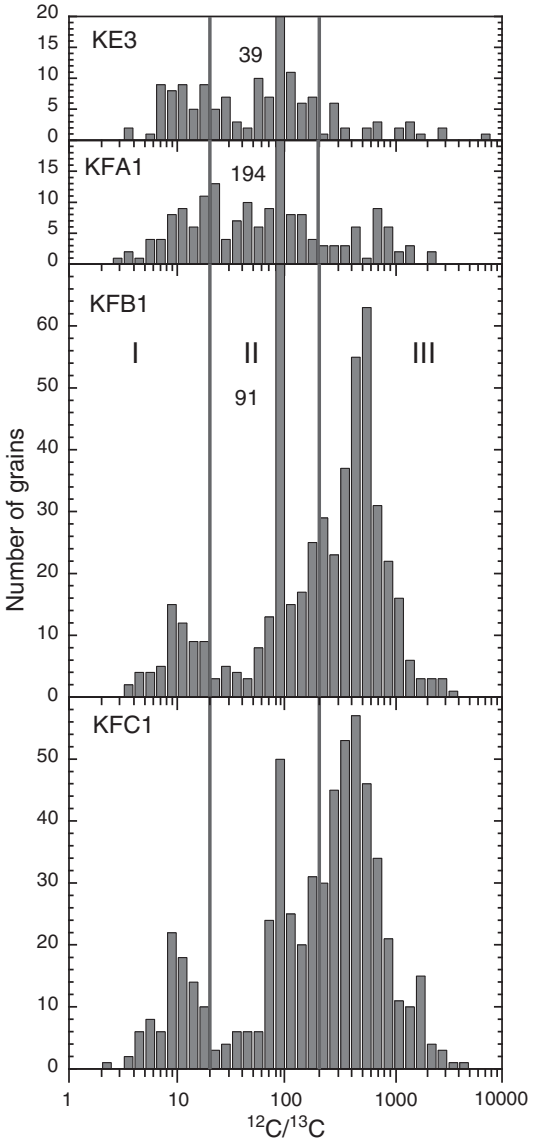

Fig. 4. $^{12}C/^{13}C$ histograms of grains from the graphite fractions. The numbers in the plots for KE3, KFA1 and KFB1 indicate the numbers of grains in the "normal" bin that includes the solar ratio ($^{12}C/^{13}C = 89$). The lower-density fractions KE3 and KFA1 have more grains with $^{12}C/^{13}C$ ratios lower than solar, while the higher-density fractions KFB1 and KFC1 have more grains with $^{12}C/^{13}C$ ratios higher than solar. Part of the data have previously been published by Hoppe et al. (1995), Amari et al. (1993, 1995c, 1996), Travaglio et al. (1999), Croat et al. (2003), Heck et al. (2009a) and Meier et al. (2012).

added at 0–20 °C to destroy polysulfides and thiosulfate, and to oxidize some of the kerogen to organic acids. Colloidal separation was performed with 0.1 M NH_3 in four cycles to extract presolar diamond. The remaining residue was oxidized with 0.5 N $Na_2Cr_2O_7$ – 2 N H_2SO_4 at 85 °C for 20 h to remove reactive kerogen that had survived the H_2O_2 treatment. Another colloidal separation was performed to further remove presolar diamond.

The residue was subjected to density separation using sodium polytungstate [$Na_6(H_2W_{12}O_{40})$] with a surfactant (Brij-35, polyoxyethylene (23) lauryl ether) to disperse the residue in suspension, yielding seven fractions. The lowest-density fraction (1.5–1.6 g/cm^3) consisted mostly of organic matter. The next four fractions were size-separated with a size cutoff of 1 μm, yielding the graphite-rich fractions KE1, KFA1, KFB1, and KFC1 (Table 1). KE3 was later separated from KE1 to increase the number of presolar grains and the size cutoff was 2 μm (Amari et al., 1995c). Noble gases were not analyzed for KE3. The highest-density fraction (>2.3 g/cm^3) was treated with $HClO_4$ at 200 °C to destroy any remaining organic matter and then with concentrated H_2SO_4 at 180–190 °C for 2–6 h six times to dissolve oxides. This residue was separated by size, yielding nine SiC fractions, KJA, KJB, KJC, KJD, KJE, KJF, KJG, KJH and KJI.

2.2. Observation with the scanning electron microscope

Grains were suspended in a mixture of 20% water – 80% isopropanol and drops were deposited onto Au foil pressed onto SEM Al mounts or onto stainless disks. The deposited grains were examined in the scanning electron microscope (JEOL JSM-840A) at Washington University in St. Louis. Their chemical compositions were analyzed with EDX (Energy dispersive X-ray Spectroscopy) to confirm that they were carbonaceous, and secondary electron images were taken to record the sizes and morphologies of the grains. While many grains were spheres, a few grains were elongated (Fig. 1 and 31). We calculated their average sizes (D) using the formula $D = (A \times B^2)^{1/3}$, where A is the long axis and B the short axis. Low magnification pictures (× ~300) of the mounts were also taken to locate grains for subsequent ion probe analysis.

2.3. Ion probe analyses

Grains were analyzed with the modified CAMECA IMS-3f and the NanoSIMS at Washington University in St. Louis. The numbers of the grains analyzed for various elements are summarized in Table 2.

2.3.1. IMS-3f

A Cs^+ beam (14.5 keV) was used to analyze H, C, N, O and Si isotopes while an O^- beam (17 keV) was used to analyze Al–Mg, Ca, Ti, Fe and Ni isotopes. The method for isotopic analysis has been described in detail by Zinner et al. (1989). Nitrogen isotopic ratios were analyzed as $^{12}C^{14}N^-$ and $^{12}C^{15}N^-$ ions at a mass-resolving power ($M/\Delta M$) of ~ 6,000 to separate $^{12}C^{15}N^-$ and $^{13}C^{14}N^-$. $^{17}O/^{16}O$ ratios were analyzed in a fraction of the grains at $M/\Delta M$ of ~5000. Isotopic analyses for the other elements and $^{18}O/^{16}O$ were performed at a mass-resolving power of ~3500. Standards were used for peak centering and instrumental mass-fractionation corrections. For C and N standards, we used 1-hydroxybenzotriazole hydrate ($C_6H_5N_3O{\cdot}H_2O$) ($\delta^{13}C = -37.96 \pm 1.6‰$, $\delta^{15}N = -12.16‰$) and carbon paint (DAG) [$\delta^{13}C = (-29.3 \sim -24.6) \pm 1.7‰$, $\delta^{15}N = -12.2 \pm 3.1‰$]. DAG was also used as standard for H isotopic analysis. For O and Al–Mg, Burma spinel was used as a standard, for Si, synthetic SiC was used, and for O, Al–Mg, Ca, Ti, Fe, and Ni, augite was used.

Table 1
Graphite-rich fractions from Murchison.

Fraction	Density (g/cm^3)	Abundance of the fraction[a] (ppm)	Abundance of presolar graphite[b] (ppm)
KE1	1.65–2.05	1.2	–
KE3	1.65–1.72	~0.26[c]	~0.22
KFA1	2.05–2.10	0.22	0.11
KFB1	2.10–2.15	0.15	0.13
KFC1	2.15–2.20	0.44	0.42

[a] These numbers are relative to bulk Murchison.
[b] These numbers were derived from the numbers in Table 4.
[c] See text how this number was derived.

Table 2
The numbers of the grains analyzed for various isotopic ratios.

Fraction	Density (gcm^3)	Total	D/H	$^{12}C/^{13}C$	$^{14}N/^{15}N$	$^{17}O/^{16}O$	$^{18}O/^{16}O$	$\delta^{25,26}Mg/^{24}Mg$	$^{26}Al/^{27}Al$	$\delta^{29,30}Si/^{28}Si$
KE3	1.65–1.72	163	4	163	65	94	155	58	58 (44)[a]	154
KFA1	2.05–2.10	347	0	347	291	98	126	96	96 (40)[a]	119
KFB1	2.10–2.15	536	0	535[**]	400	173	329	46	46 (6)[a]	216
KFC1	2.15–2.20	594	0	593[**]	381	n.m.	120	59	59 (0)[a]	342

Fraction	$\delta^{41}K/^{39}K$	$^{41}Ca/^{40}Ca$	$\delta^{42,43,44}Ca/^{40}Ca$	$^{44}Ti/^{48}Ti$	$\delta^{46,47,49,50}Ti/^{48}Ti$	$\delta^{57}Fe/^{56}Fe$	$\delta^{60,61}Ni/^{62}Ni$
KE3	20	20 (7)[a]	31	31 (4)[a]	22	14	14
KFA1	15	15 (9)[a]	34	34 (4)[a]	28	15	15
KFB1	n.m.	n.m.	n.m.	n.m.	n.m.	n.m.	n.m.
KFC1	n.m.	n.m.	14	–	40	n.m.	n.m.

$\delta^{i}Mg/^{24}Mg \equiv [(^{i}Mg/^{24}Mg)_{grain}/(^{i}Mg/^{24}Mg)_{solar} - 1] \times 1000$.
Mount KFA1e was contaminated and huge Ca counts were detected. Therefore, for Ca and Ti isotopic ratios, only anomalous grains (11 for Ca and 4 for Ti) were counted.
[**] One KFB1 grain and one KFC1 grain were analyzed only for their $^{18}O/^{16}O$ ratios.
[a] The numbers in parentheses are the numbers of the grains with resolvable ^{26}Al, or ^{41}Ca or ^{44}Ti in form of excesses of their daughter isotopes.

2.3.2. NanoSIMS

The NanoSIMS at Washington University is equipped with five electron multipliers, four of which are movable. Five adjacent masses up to mass number 30 can be simultaneously analyzed. Isotopic ratios of C, N, O, Al–Mg and Si were analyzed in multi-detection mode, using these electron multipliers. Potassium, Ca, Ti, Fe and Ni isotopes were analyzed using combined analysis mode, where magnetic peak jumping and multi-detection were involved. Carbon, N, O and Si were analyzed with a Cs^+ beam (16 keV) and Al–Mg, K, Ca, Ti, Fe, and Ni were analyzed with an O^- beam (16 keV). The beams were rastered over a 2–3 μm square to cover the grain with the beam. Various standards were used for different mounts: For C, synthetic SiC, carbon paint (DAG), and Murchison matrix were used. For O, DAG, Al_2O_3, and Murchison matrix; for N, a mix of synthetic SiC and synthetic Si_3N_4; for Si, synthetic SiC and Murchison matrix; for Al–Mg, Murchison matrix; for K, Ca and Ti, Murchison matrix and terrestrial pervoskite; for Ti–Cr, terrestrial pervoskite and chromite; for Fe–Ni, NBS610 standard glass.

3. RESULTS

3.1. Grain size

Grain sizes and grain size distributions are shown in Table 3 and Fig. 2. The uncertainties for the average grain sizes in the table are standard deviations. KFA1, KFB1 and KFC1 are nominally the fractions larger than 1 μm and KE3 is the fraction larger than 2 μm. Although there were grains smaller than these cutoffs in these fractions, we tended to select larger grains ($\geqslant$1 μm) to analyze isotopic ratios of as many elements as possible in a given grain. Therefore, grain selection was biased toward large grains and grains smaller than 1 μm are underrepresented. Even with this bias, it is clearly seen that the grain size distributions are different among the four density fractions.

On average, grains become smaller with increasing density: KE3 > KFB1 > KFA1 > KFC1. The average size of KE3 grains is 5.3 ± 3.2 μm, while those of the other fractions are around 3 μm Table 3). Since we estimated that 48% of the KFA1 grains are of solar system origin (see Section 3.2), we show the grain size distributions in two ways: one with all the KFA1 grains and the other without KFA1 grains with $^{12}C/^{13}C$ ratios between 79.4 and 100 (labeled as "KFA1 without normal bin"). The distributions are not markedly different, indicating that solar system and presolar KFA1 grains are not distinguishable by their size.

3.2. Carbon and N isotopic ratios

The isotopic ratios of the grains mentioned in the text and figures are given in Tables 4a and 4b. The uncertainties in the tables are 1σ. $\delta D/H$ values $\{\delta D/H\ (‰) = [(D/H)_{grain}/(D/H)_{standard} - 1] \times 1000\}$ and Fe and Ni isotopic ratios of

Table 3
Grain sizes of the Murchison fractions.

Fraction	Average (μm)	Min (μm)	Max (μm)	Median (μm)	Number of grains	Grains ⩾ 5 μm	Grains ⩾ 10 μm	Fraction of grains ⩾ 5 μm (%)	Fraction of grains ⩾ 10 μm (%)
KE3	5.3 ± 3.2	1.1	20.9	4.68	140	62	12	44	9
KFA1	3.3 ± 2.1	1.3	18.5	2.67	220	25	5	11	2
KFA1 w/o NB*	3.1 ± 1.4[a]	1.4	10.6	2.63	103	10	1	10	1
KFB1	3.6 ± 1.7	0.86	12.3	3.30	327	63	1	19	0.3
KFC1	2.8 ± 1.6	0.76	19.5	2.53	569	43	1	8	0.2

* KFA1 without the normal bin (see the text).
[a] 3.43 ± 2.54 μm for the grains in the normal bin.

a few KE3 grains are not included: δD/H values were obtained only for 4 KE3 grains and will be discussed in Section 3.5 and the Fe and Ni isotopic ratios are normal within huge errors. Complete data tables are available online as Supplementary content.

The $^{12}C/^{13}C$ ratios of the graphite grains span more than 3 orders of magnitude in all the fractions (Figs. 3 and 4). The lowest $^{12}C/^{13}C$ ratio (2.09 ± 0.06) is found in KFC1b-202 and the highest $^{12}C/^{13}C$ (7223 ± 111) is observed in KE3c-551b.

In contrast to the wide range of C isotopic ratios of the grains, the N isotopic ratios of most of the graphite grains are surprisingly close to that of air ($^{14}N/^{15}N_{air} = 272$) (Fig. 3) and within the range of ratios found in bulk meteorites (e.g., Table 1 by Grady and Wright, 2003 and the references therein). Grains with N isotopic anomalies are most abundant in KE3. Of 65 KE3 grains analyzed for their N isotopic ratios, 12 grains have $^{14}N/^{15}N$ ratios lower than 200 outside of 2σ errors. We found only one grain with $^{14}N/^{15}N < 200$ outside of 2σ errors among 291 KFA1 grains. Out of 400 KFB1 grains, 3 grains have $^{14}N/^{15}N < 200$ and one grain > 400. The number of grains with N isotopic anomalies in KFC1 is higher than in KFA1 and KFB1. Six grains have ratios lower than 200 and three grains higher than 400 among 381 KFC1 grains. Since isotopically anomalous C and close-to-normal N cannot be produced simultaneously by any nucleosynthetic processes, Hoppe et al. (1995) explained the close-to-normal N isotopic ratios of many graphite grains by partial isotopic exchange or dilution of the original N with close-to-normal N, either in the solar system, on earth and/or in the laboratory. If this is the case, anomalous N isotopic ratios in these grains should be taken either as lower or upper limits.

Fig. 4 shows C isotopic ratio histograms of all the fractions. The two lower-density fractions KE3 and KFA1 have similar C isotopic distributions, broad and containing more grains with isotopically heavy C than with light C. On the other hand, KFB1 and KFC1 have many more isotopically light ($^{12}C/^{13}C >$ solar) grains than heavy ($^{12}C/^{13}C <$ solar) grains and they show bimodal distributions as has previously been shown by Hoppe et al. (1995). The smaller distribution peaks around 10, while the larger distribution peaks around 400–630. These distributions of presolar graphite are quite different from those of SiC (see Fig. 3 in Hoppe et al., 1994). The majority of SiC grains have ratios between 20 and 100, most of which are mainstream grains that are believed to have formed in low-mass (1.5–3 $M_\odot$) AGB stars with close-to-solar metallicity (Lewis et al., 1990, 1994; Gallino et al., 1990, 1994; Prombo et al., 1993; Hoppe et al., 1994; Savina et al., 2003; Podosek et al., 2004). As among the graphite grains, there are also SiC grains with low $^{12}C/^{13}C$ ratios (<10).

All the fractions have elevated numbers of grains in the bin with $^{12}C/^{13}C$ ratios between 79.4 and 100, compared with those in the adjacent bins. Since the solar ratio (89) falls into this bin, we name it "normal bin". The sudden increase of the number of the grains in the normal bin most likely results from the presence of solar system grains in addition to indigenous presolar grain populations in the density fractions. There is no reason that presolar grains should have an excessive component with normal C isotopic compositions and we can safely assume a smooth C isotopic distribution for presolar grains. Thus, the excess must come from the presence of solar system grains.

We calculated the numbers of presolar grains in the normal bin for the different fractions as follows. Assuming that presolar graphite grains have smooth C isotopic ratio distributions, we estimated the number of presolar grains in the normal bin by averaging the number of grains in the adjacent bins for each fraction. Then we checked the isotopic signatures of the grains in the normal bins. If the numbers of grains isotopically anomalous in other elements were larger than the estimated numbers from the adjacent bins, we took the former. This was the case for KE3 and KFA1. Nine was the number of presolar KE3 grains estimated from the averaging method [(7 + 11)/2], while 13 grains in the normal bin are isotopically anomalous in other elements (10 with ^{18}O excesses and 3 with Si isotopic anomalies) (Table 5). Therefore, we used 13 as the number of presolar grains in the KE3 normal bin. Similarly, 9 KFA1 grains were estimated to be presolar, while actual analyses indicated that 27 grains were presolar. For KFB1, there are 11 isotopically anomalous grains, while the number of anomalous grains estimated from the adjacent bins is 14. For KFC1, the interpolated number was used.

Hoppe et al. (1995) classified graphite grains into four groups. (1) Grains with $2 < ^{12}C/^{13}C < 20$, (2) Grains with $20 < ^{12}C/^{13}C < 80$, (3) Grains with normal or close-to-normal C and (4) Grains with isotopically light C. Since we estimated the number of solar system grains with the

Table 4a
Isotopic ratios of graphite grains.

Grain	$^{12}C/^{13}C$	$^{14}N/^{15}N$	$^{17}O/^{16}O$ (10^{-4})	$^{18}O/^{16}O$ (10^{-3})	$\delta^{25}Mg/^{24}Mg$ (‰)	$^{26}Al/^{27}Al$ (10^{-3})	$\delta^{29}Si/^{28}Si$ (‰)	$\delta^{30}Si/^{28}Si$ (‰)	$\delta^{41}K/^{39}K$ (‰)
KE3a-022	27.8 ± 0.2	197 ± 5	–	4.65 ± 0.06	654 ± 125	87.9 ± 4.5	−90 ± 42	−124 ± 38	–
KE3a-071	6.46 ± 0.08	269 ± 19	3.61 ± 0.51	3.30 ± 0.27	−88 ± 151	19.6 ± 1.3	−76 ± 47	−64 ± 68	–
KE3a-141	777 ± 27	118 ± 19	3.48 ± 0.72	208 ± 4	491 ± 587	130 ± 7	−141 ± 66	−65 ± 40	–
KE3a-152	27.9 ± 0.3	198 ± 21	–	6.03 ± 0.12	280 ± 290	146 ± 8	−121 ± 92	32 ± 111	–
KE3a-157	79.0 ± 0.7	127 ± 10	3.45 ± 0.68	38.2 ± 1.3	1585 ± 301	99.9 ± 5.1	−127 ± 60	−179 ± 50	–
KE3a-301	302 ± 6	212 ± 6	15.3 ± 3.2	17.2 ± 1.8	205 ± 94	22.4 ± 1.5	63 ± 69	−25 ± 64	–
KE3a-321	136 ± 1	214 ± 10	10.9 ± 2.3	63.7 ± 3.3	816 ± 354	104 ± 5	−214 ± 37	−314 ± 33	–
KE3a-322	147 ± 2	161 ± 9	3.80 ± 0.45	17.3 ± 0.5	22 ± 18	125 ± 6	−120 ± 27	−179 ± 17	–
KE3a-411	93.8 ± 1.8	270 ± 17	–	2.21 ± 0.24	–	–	486 ± 511	109 ± 150	–
KE3a-573	27.3 ± 0.3	259 ± 17	0.90 ± 1.0	1.48 ± 0.67	–	–	−235 ± 97	−327 ± 128	–
KE3a-613	55.9 ± 0.36	250 ± 9	3.26 ± 0.51	21.1 ± 0.7	638 ± 259	116 ± 6	58 ± 68	−29 ± 44	–
KE3a-662	3138 ± 167	176 ± 14	–	192 ± 4	−20 ± 37	89.4 ± 4.5	−16 ± 51	−212 ± 41	–
KE3a-751	153 ± 3	110 ± 8	2.46 ± 0.90	119 ± 4	38 ± 218	47.0 ± 2.5	231 ± 47	−94 ± 48	–
KE3c-111	120 ± 1	171 ± 7	4.13 ± 0.71	4.76 ± 0.37	117 ± 48	8.9 ± 1.1	−99 ± 114	−303 ± 105	529 ± 130
KE3c-131	17.1 ± 0.1	232 ± 17	4.6 ± 1.0	1.89 ± 0.16	14 ± 36	0.28 ± 0.20	−71 ± 291	18 ± 324	−60 ± 35
KE3c-242	6.91 ± 0.02	257 ± 10	–	2.04 ± 0.12	53 ± 31	1.80 ± 0.33	197 ± 149	77 ± 149	−25 ± 16
KE3c-351	61.8 ± 0.2	242 ± 6	3.86 ± 0.37	11.6 ± 0.2	119 ± 43	37.0 ± 1.9	2 ± 86	135 ± 97	27 ± 25
KE3c-401	37.8 ± 0.2	53.5 ± 1.2	4.38 ± 0.68	44.3 ± 1.2	212 ± 53	63.9 ± 3.2	−324 ± 38	−497 ± 35	99 ± 55
KE3c-411	14.22 ± 0.04	228 ± 9	3.97 ± 0.62	1.84 ± 0.10	227 ± 192	1.59 ± 0.32	−30 ± 130	−103 ± 132	0 ± 16
KE3c-431	13.51 ± 0.05	262 ± 17	3.59 ± 0.91	9.68 ± 0.68	153 ± 127	48.0 ± 2.5	−162 ± 129	−247 ± 128	−54 ± 40
KE3c-551b	7223 ± 111	28.4 ± 1.6	2.18 ± 0.41	370 ± 14	−101 ± 447	72.3 ± 3.1	98 ± 64	−412 ± 48	10610 ± 326
KE3c-621	1493 ± 44	270 ± 15	2.64 ± 0.50	10.4 ± 0.5	105 ± 160	65.1 ± 3.3	45 ± 144	−146 ± 137	1863 ± 142
KE3c-721	65.3 ± 0.5	213 ± 7	3.95 ± 0.51	6.67 ± 0.38	65 ± 28	4.08 ± 0.24	−214 ± 143	−73 ± 166	218 ± 50
KE3d-1	9.05 ± 0.02	–	–	2.00 ± 0.05	–	–	−21 ± 72	53 ± 73	90 ± 119
KE3d-4	61.3 ± 0.2	–	–	9.24 ± 0.17	783 ± 383	36.4 ± 4.6	192 ± 56	−114 ± 45	–
KE3d-9	82.8 ± 0.3	–	–	8.77 ± 0.15	−76 ± 61	5.6 ± 1.1	1272 ± 75	937 ± 66	−48 ± 28
KE3e-10	125 ± 1	–	–	5.74 ± 0.22	–	94.5 ± 6.2	−85 ± 31	−123 ± 30	–
KE3j-020	12.79 ± 0.03	271 ± 2	–	7.76 ± 0.19	–	–	−360 ± 27	−422 ± 30	809 ± 33
KE3j-572	170.5 ± 0.5	257 ± 2	–	2.95 ± 0.07	–	–	−291 ± 40	−404 ± 43	55 ± 11
KE3j-941	80.3 ± 0.2	241 ± 2	–	4.10 ± 0.10	–	–	706 ± 42	448 ± 45	19 ± 12
KFA1a1-471	91.1 ± 0.6	–	–	–	–	2.5 ± 2.3	571 ± 119	−55 ± 134	–
KFA1c-121	645 ± 21	266 ± 6	–	–	–	–	–	–	–
KFA1c-m132	55.3 ± 0.7	254 ± 12	–	–	–	–	–	–	–
KFA1c-m133	92.2 ± 1.1	271 ± 5	–	–	–	–	–	–	–
KFA1e-274b	82.8 ± 0.6	295 ± 8	–	–	99 ± 11	93.8 ± 0.2	–	–	–
KFA1e-301	8.66 ± 0.06	288 ± 6	3.10 ± 0.15	1.45 ± 0.05	200 ± 12	–	−9 ± 18	45 ± 22	176 ± 18
KFA1e-412	96.8 ± 0.8	210 ± 10	3.69 ± 0.17	1.73 ± 0.06	16 ± 10	–	−35 ± 24	48 ± 29	–
KFA1e-413	189 ± 2	260 ± 11	3.52 ± 0.19	2.56 ± 0.09	9 ± 12	–	43 ± 15	71 ± 18	–
KFA1e-463	229 ± 2	186 ± 10	3.42 ± 0.12	2.16 ± 0.07	76 ± 12	7.37 ± 0.28	600 ± 19	435 ± 21	–
KFA1e-562	21.5 ± 0.2	289 ± 10	3.51 ± 0.16	2.06 ± 0.07	49 ± 22	0.150 ± 0.011	−23 ± 23	−57 ± 26	–
KFA1e-623	133 ± 1	272 ± 10	3.20 ± 0.16	4.08 ± 0.14	94 ± 16	12.2 ± 0.3	–	–	118 ± 12
KFA1e-631	15.7 ± 0.1	239 ± 10	3.62 ± 0.12	2.26 ± 0.08	3 ± 12	52.6 ± 0.4	−97 ± 13	−120 ± 15	
KFA1e-731	73.7 ± 0.6	255 ± 10	3.21 ± 0.16	2.19 ± 0.08	122 ± 12	19.1 ± 0.1	37 ± 18	−78 ± 19	602 ± 16

KFA1e-742	868 ± 12	322 ± 12	3.08 ± 0.24	1.56 ± 0.07	14 ± 18	–	−50 ± 17	−35 ± 20	–
KFA1e-743	34.6 ± 0.3	279 ± 12	2.33 ± 0.21	2.09 ± 0.09	312 ± 13	83.6 ± 0.4	−21 ± 16	−98 ± 18	44 ± 11
KFA1e-745	116 ± 1	264 ± 10	3.15 ± 0.16	1.66 ± 0.06	94 ± 18	40.4 ± 0.8	−13 ± 18	−69 ± 20	452 ± 14
KFA1e-753	305 ± 3	269 ± 11	3.66 ± 0.09	1.87 ± 0.06	1 ± 12	1.37 ± 0.37	−23 ± 35	110 ± 42	–
KFA1e-754	10.9 ± 0.1	258 ± 10	3.48 ± 0.09	1.75 ± 0.06	13 ± 11	9.97 ± 0.51	–	–	–
KFA1f-101	89.2 ± 0.9	268 ± 7	4.68 ± 0.51	1.93 ± 0.16	−76 ± 196	0.47 ± 0.72	−41 ± 58	−11 ± 55	–
KFA1f-131	147 ± 2	123 ± 5	4.26 ± 0.46	5.88 ± 0.28	2999 ± 1955	45.4 ± 3.3	318 ± 29	−97 ± 22	–
KFA1f-133	82.2 ± 0.6	244 ± 5	4.08 ± 0.36	9.17 ± 0.25	849 ± 373	52.8 ± 1.6	−226 ± 97	−176 ± 95	–
KFA1f-161	24.9 ± 0.1	291 ± 20	4.53 ± 0.53	2.13 ± 0.17	163 ± 99	<0.001	−235 ± 40	−329 ± 35	–
KFA1f-182	17.2 ± 0.2	265 ± 11	3.97 ± 0.34	2.46 ± 0.13	356 ± 230	0.522 ± 0.037	−146 ± 75	−267 ± 64	–
KFA1f-302	116.6 ± 0.5	398 ± 49	5.10 ± 0.73	11.6 ± 0.5	37 ± 113	0.39 ± 0.41	−272 ± 20	−349 ± 18	–
KFA1f-481	91.3 ± 0.8	272 ± 10	3.83 ± 0.46	2.06 ± 0.17	−60 ± 190	–	−35 ± 95	−89 ± 86	–
KFA1f-581	31.2 ± 0.1	229 ± 4	4.34 ± 0.39	3.06 ± 0.16	−31 ± 38	<0.001	−66 ± 43	−4 ± 42	–
KFA1f-712	78.7 ± 0.4	263 ± 9	3.45 ± 0.49	1.87 ± 0.18	103 ± 202	–	−26 ± 81	−115 ± 72	–
KFA1g-745	10.58 ± 0.05	–	4.04 ± 0.17	3.00 ± 0.06	813 ± 61	104 ± 3	−55 ± 10	−41 ± 14	–
KFA1i-031	87.0 ± 0.7	250 ± 3	–	2.46 ± 0.07	–	–	11 ± 21	−23 ± 24	15 ± 16
KFA1i-061	88.5 ± 0.7	271 ± 4	–	1.97 ± 0.06	–	–	1 ± 30	15 ± 35	12 ± 16
KFA1i-101	493 ± 4	270 ± 4	–	1.94 ± 0.07	–	–	−20 ± 26	13 ± 31	10 ± 23
KFA1i-151	50.0 ± 0.4	303 ± 5	–	1.99 ± 0.07	–	–	2 ± 21	34 ± 24	−15 ± 16
KFA1i-152	88.6 ± 0.7	271 ± 4	–	2.02 ± 0.06	–	–	−13 ± 23	31 ± 27	11 ± 16
KFA1i-201	90.3 ± 0.7	258 ± 7	–	1.98 ± 0.11	–	–	−6 ± 40	29 ± 48	10 ± 16
KFA1i-221	88.5 ± 0.7	268 ± 3	–	1.93 ± 0.06	–	–	37 ± 20	47 ± 24	−1 ± 16
KFA1i-271	75.2 ± 0.6	214 ± 2	–	10.9 ± 0.3	–	–	16 ± 26	−17 ± 30	7 ± 15
KFA1i-381	89.8 ± 0.7	266 ± 5	–	1.92 ± 0.08	–	–	32 ± 37	−2 ± 43	−3 ± 19
KFA1i-451	7.70 ± 0.09	292 ± 5	–	2.86 ± 0.09	–	–	−12 ± 32	−27 ± 38	23 ± 21
KFA1i-452	14.5 ± 0.1	285 ± 5	–	2.01 ± 0.07	–	–	7 ± 25	31 ± 30	26 ± 19
KFA1i-741	13.9 ± 0.1	307 ± 6	–	2.50 ± 0.10	–	–	19 ± 32	−21 ± 37	143 ± 33
KFA1i-m141	90.5 ± 0.7	262 ± 4	–	1.91 ± 0.06	–	–	15 ± 21	15 ± 24	−16 ± 17
KFB1a-122	14.5 ± 0.1	198 ± 5	–	–	670 ± 231	23.0 ± 2.3	36 ± 111	−65 ± 102	–
KFB1a-151	43.5 ± 0.2	256 ± 9	–	–	−159 ± 82	29.0 ± 2.3	116 ± 101	154 ± 101	–
KFB1a-212	587 ± 40	276 ± 16	–	–	222 ± 177	–	−193 ± 419	−601 ± 279	–
KFB1a-261	90.0 ± 1.1	238 ± 8	–	–	−41 ± 277	86 ± 18	−402 ± 66	−542 ± 114	–
KFB1a-262	6.72 ± 0.07	275 ± 6	–	–	−109 ± 108	–	50 ± 169	−252 ± 136	–
KFB1a-311	1163 ± 10	275 ± 10	–	–	–	–	–	–	–
KFB1a-332	117 ± 1	258 ± 8	–	–	–	–	–	–	–
KFB1a-415	13.6 ± 0.1	258 ± 11	–	–	100 ± 121	4.3 ± 1.1	−103 ± 74	−245 ± 66	–
KFB1a-421	156 ± 2	269 ± 12	–	–	27 ± 57	–	291 ± 532	633 ± 596	–
KFB1a-462	18.3 ± 0.3	273 ± 7	–	–	−306 ± 66	10.0 ± 1.3	−59 ± 71	−49 ± 70	–
KFB1a-542	221 ± 2	247 ± 6	–	–	−56 ± 88	9.7 ± 1.5	9 ± 88	29 ± 87	–
KFB1a-575	25.0 ± 0.2	263 ± 7	–	–	–	–	–	–	–
KFB1f-024	1531 ± 59	289 ± 5	2.44 ± 0.55	1.85 ± 0.15			21 ± 12	143 ± 17	
KFB1f-171	157 ± 6	254 ± 4	6.8 ± 1.1	2.10 ± 0.18	–	–	5 ± 14	−23 ± 17	–
KFB1f-202	758 ± 28	270 ± 4	2.56 ± 0.59	1.87 ± 0.16			2 ± 12	68 ± 16	
KFB1f-378	333 ± 12	265 ± 3	7.7 ± 1.4	2.14 ± 0.22	–	–	−9 ± 12	−30 ± 15	–

(*continued on next page*)

Table 4a (*continued*)

Grain	$^{12}C/^{13}C$	$^{14}N/^{15}N$	$^{17}O/^{16}O$ (10^{-4})	$^{18}O/^{16}O$ (10^{-3})	$\delta^{25}Mg/^{24}Mg$ (‰)	$^{26}Al/^{27}Al$ (10^{-3})	$\delta^{29}Si/^{28}Si$ (‰)	$\delta^{30}Si/^{28}Si$ (‰)	$\delta^{41}K/^{39}K$ (‰)
KFB1f-623	305 ± 11	306 ± 5	2.64 ± 0.64	1.71 ± 0.16			54 ± 14	117 ± 18	
KFB1f-632	166 ± 6	239 ± 3	3.40 ± 0.43	15.3 ± 0.4			−346 ± 7	−501 ± 7	
KFB1f-763	58.8 ± 2.1	331 ± 4	2.22 ± 0.69	2.19 ± 0.21	–	–	−82 ± 11	−114 ± 13	–
KFC1a-042	12.7 ± 0.1	310 ± 109	–	1.84 ± 0.12	1387 ± 522	–	–	–	–
KFC1a-115	187 ± 2	245 ± 28	–	2.08 ± 0.08	9 ± 113	–	−3 ± 93	−44 ± 87	–
KFC1a-117	12.3 ± 0.1	266 ± 22	–	1.96 ± 0.09	–	–	−25 ± 246	−26 ± 237	–
KFC1a-173	123 ± 2	289 ± 31	–	1.97 ± 0.06	121 ± 206	–	−57 ± 119	−52 ± 116	–
KFC1a-357b	77.3 ± 0.6	262 ± 17	–	1.98 ± 0.06	144 ± 294	–	285 ± 52	589 ± 59	–
KFC1a-364	1293 ± 61	280 ± 26	–	2.17 ± 0.10	237 ± 290	–	72 ± 211	208 ± 221	–
KFC1a-551	8.46 ± 0.04	273 ± 8	–	1.98 ± 0.12	−157 ± 443	–	84 ± 54	761 ± 72	–
KFC1b-102	365 ± 43	93 ± 17	–	3.63 ± 0.62	–	–	–	–	–
KFC1b-202	2.09 ± 0.06	273 ± 53	–	1.80 ± 0.21	–	–	–	–	–
KFC1b2-0m11	671 ± 13	264 ± 21	–	1.87 ± 0.08	–	–	–	–	–
KFC1b2-2113	12.02 ± 0.05	280 ± 16	–	2.07 ± 0.06	156 ± 116	–	−69 ± 43	−67 ± 43	–
KFC1b2-231	650 ± 11	272 ± 9	–	1.97 ± 0.04	36 ± 48	–	−9 ± 22	−20 ± 22	–
KFC1b2-262	737 ± 19	267 ± 11	–	1.93 ± 0.09	91 ± 133	–	−9 ± 55	−13 ± 54	–
KFC1b2-303	4.51 ± 0.02	336 ± 30	–	1.81 ± 0.18	–	–	−39 ± 110	−41 ± 108	–
KFC1b2-441	8.90 ± 0.03	266 ± 12	–	1.92 ± 0.08	–	–	48 ± 38	68 ± 38	–
KFC1b2-521	2007 ± 91	274 ± 27	–	1.68 ± 0.21	–	–	167 ± 58	257 ± 60	–
KFC1b2-551	254 ± 3	251 ± 13	–	1.97 ± 0.10	–	–	–	–	–
KFC1b2-661	386 ± 4	263 ± 7	–	1.93 ± 0.04	–	–	−28 ± 27	9 ± 27	–
KFC1b2-751	559 ± 12	264 ± 16	–	1.89 ± 0.09	–	–	48 ± 45	37 ± 44	–
KFC1d-012	411 ± 4	258 ± 3	–	–	–	–	−29 ± 7	−41 ± 10	–
KFC1d-051	486 ± 6	275 ± 4	–	–	–	–	−31 ± 7	22 ± 10	–
KFC1d-121	269 ± 3	256 ± 4	–	–	–	–	−25 ± 6	−30 ± 10	–
KFC1d-202	309 ± 3	265 ± 5	–	–	–	–	−33 ± 10	24 ± 14	–
KFC1d-212	58.6 ± 0.5	–	–	–	–	–	88 ± 13	229 ± 16	–
KFC1d-301	437 ± 4	260 ± 4	–	–	–	–	3 ± 9	66 ± 13	–

The isotopic ratios of the grains mentioned in the text and those in Figs. 12 and 14 are shown. The isotopic ratios of all grains are available as the supporting document online. The errors are 1σ.

Table 4b
Isotopic ratios of graphite grains.

Grain	$^{41}Ca/^{40}Ca$ (10^{-3})	$\delta^{42}Ca/^{40}Ca$ (‰)	$\delta^{43}Ca/^{40}Ca$ (‰)	$\delta^{44}Ca/^{40}Ca$ (‰)	$^{44}Ti/^{48}Ti$ (10^{-3})	$\delta^{46}Ti/^{48}Ti$ (‰)	$\delta^{47}Ti/^{48}Ti$ (‰)	$\delta^{49}Ti/^{48}Ti$ (‰)	$\delta^{50}Ti/^{48}Ti$ (‰)
KE3a-022	–	−71 ± 91	−31 ± 157	−48 ± 64	–	427 ± 214	198 ± 198	546 ± 232	–
KE3a-071	–	−28 ± 30	38 ± 52	40 ± 22	–	63 ± 11	22 ± 10	84 ± 11	–
KE3a-141	–	78 ± 67	2 ± 108	88 ± 46	–	270 ± 320	423 ± 331	1720 ± 486	–
KE3a-157	–	343 ± 122	168 ± 192	62 ± 75	–	79 ± 256	426 ± 311	356 ± 303	–
KE3a-321	–	30 ± 19	72 ± 41	76 ± 14	1.06 ± 0.22	22 ± 11	−5 ± 11	296 ± 13	–
KE3a-322	–	34 ± 33	69 ± 57	53 ± 23	2.4 ± 1.1	78 ± 27	−4 ± 26	576 ± 36	–
KE3a-662	–	175 ± 36	429 ± 66	70 ± 24	–	24 ± 29	−26 ± 29	862 ± 45	–
KE3c-111	16.5 ± 3.8	−372 ± 213	−361 ± 331	68 ± 205	–	−598 ± 358	−105 ± 595	229 ± 817	640 ± 2398
KE3c-131	–	50 ± 126	193 ± 207	−69 ± 87	–	368 ± 435	123 ± 398	7 ± 422	−128 ± 1114
KE3c-242	–	−28 ± 73	7 ± 114	194 ± 60	98 ± 38	16 ± 230	−271 ± 196	−4 ± 268	4962 ± 2488
KE3c-351	–	−75 ± 73	−76 ± 112	29 ± 57	–	13 ± 49	−38 ± 49	331 ± 68	54 ± 66
KE3c-401	–	74 ± 64	330 ± 109	93 ± 47	–	−10 ± 79	−81 ± 79	495 ± 120	18 ± 94
KE3c-411	–	91 ± 104	−45 ± 149	23 ± 74	–	289 ± 171	169 ± 167	854 ± 251	1521 ± 442
KE3c-431	–	−17 ± 156	−94 ± 231	−98 ± 110	–	99 ± 41	1 ± 40	314 ± 53	67 ± 45
KE3c-551b	10.4 ± 0.2	155 ± 29	492 ± 51	68 ± 21	–	12 ± 10	−62 ± 9	901 ± 16	200 ± 12
KE3c-621	7.56 ± 0.29	191 ± 52	508 ± 90	150 ± 38	–	−54 ± 261	319 ± 371	36 ± 296	1067 ± 749
KE3c-721	1.94 ± 0.43	58 ± 66	−28 ± 97	9 ± 47	–	39 ± 43	−98 ± 41	382 ± 61	117 ± 51
KE3d-1	–	−24 ± 154	−65 ± 232	266 ± 130	408 ± 301	–	–	–	–
KE3d-4	–	247 ± 385	877 ± 728	153 ± 272	–	18 ± 89	−162 ± 82	969 ± 157	636 ± 130
KE3d-9	–	580 ± 147	1799 ± 382	894 ± 109	3.18 ± 0.69	30 ± 31	521 ± 41	1717 ± 77	1825 ± 83
KE3e-10	–	39 ± 44	33 ± 83	−7 ± 27	–	44 ± 35	−53 ± 33	440 ± 53	10 ± 53
KE3j-020	24.6 ± 2.7	85 ± 21	87 ± 45	23 ± 15	–	–	–	–	–
KE3j-572	7.3 ± 1.7	26 ± 13	72 ± 27	16 ± 12	–	–	–	–	–
KE3j-941	–	164 ± 13	452 ± 30	73 ± 12	–	–	–	–	–
KFA1e-274b	–	–	–	–	–	64 ± 17	40 ± 16	613 ± 21	–
KFA1e-301	2.39 ± 0.23	149 ± 36	142 ± 80	102 ± 24	211 ± 60	–	–	–	–
KFA1e-412	–	58 ± 24	236 ± 58	28 ± 18	–	–	–	–	–
KFA1e-413	–	–	–	–	–	31 ± 28	184 ± 26	1002 ± 28	–
KFA1e-463	–	44 ± 14	228 ± 35	50 ± 14	–	–	–	–	–
KFA1e-562	–	33 ± 26	11 ± 55	41 ± 19	10.1 ± 4.7	12 ± 32	39 ± 32	171 ± 38	–
KFA1e-623	1.95 ± 0.19	96 ± 22	393 ± 56	69 ± 17	–	–	–	–	–
KFA1e-631	–	−115 ± 8	66 ± 21	10 ± 13	–	–	–	–	–
KFA1e-731	6.06 ± 0.12	289 ± 19	691 ± 49	106 ± 16	–	30 ± 15	35 ± 12	226 ± 19	–
KFA1e-742	–	–	–	–	–	1238 ± 64	−15 ± 89	1489 ± 71	–
KFA1e-743	1.01 ± 0.24	102 ± 22	123 ± 49	66 ± 17	11.1 ± 2.3	–	–	–	–
KFA1e-745	2.75 ± 0.07	45 ± 12	103 ± 28	39 ± 14	–	–	–	–	–
KFA1e-753	–	−51 ± 12	16 ± 28	12 ± 13	–	–	–	–	–
KFA1e-754	–	−81 ± 17	−101 ± 37	5 ± 15	–	–	–	–	–
KFA1f-101	–	895 ± 423	−524 ± 354	−68 ± 203	–	28 ± 200	−198 ± 198	−274 ± 173	
KFA1f-161	–	98 ± 227	430 ± 439	67 ± 155	–	−88 ± 123	72 ± 158	145 ± 153	–
KFA1f-182	–	−41 ± 143	203 ± 270	−4 ± 101		−100 ± 245	−108 ± 287	204 ± 287	–
KFA1f-302	–	365 ± 440	2069 ± 1119	137063 ± 7824	8.09 ± 0.53	118 ± 10	26 ± 10	443 ± 12	205 ± 12
KFA1f-481	–	203 ± 280	76 ± 446	83 ± 184	–	70 ± 319	155 ± 384	−589 ± 193	–

(*continued on next page*)

Table 4b (*continued*)

Grain	$^{41}Ca/^{40}Ca$ (10^{-3})	$\delta^{42}Ca/^{40}Ca$ (‰)	$\delta^{43}Ca/^{40}Ca$ (‰)	$\delta^{44}Ca/^{40}Ca$ (‰)	$^{44}Ti/^{48}Ti$ (10^{-3})	$\delta^{46}Ti/^{48}Ti$ (‰)	$\delta^{47}Ti/^{48}Ti$ (‰)	$\delta^{49}Ti/^{48}Ti$ (‰)	$\delta^{50}Ti/^{48}Ti$ (‰)
KFA1f-712	–	−207 ± 361	3616 ± 1492	−87 ± 268	–	51 ± 354	225 ± 448	−491 ± 244	–
KFA1i-031	–	−39 ± 26	54 ± 57	18 ± 16	–	−157 ± 218	−336 ± 205	1627 ± 501	–
KFA1i-061	–	−17 ± 25	43 ± 54	13 ± 15	–	−33 ± 68	−114 ± 69	−159 ± 79	–
KFA1i-101	–	95 ± 84	−22 ± 165	34 ± 48	–	119 ± 58	38 ± 59	−97 ± 64	–
KFA1i-151	–	11 ± 25	58 ± 53	9 ± 15	–	292 ± 142	65 ± 136	116 ± 163	–
KFA1i-152	–	−7 ± 18	44 ± 39	1 ± 11	–	50 ± 9	33 ± 10	54 ± 11	–
KFA1i-201	–	16 ± 20	−9 ± 42	48 ± 12	2.43 ± 0.61	−58 ± 9	−24 ± 10	10 ± 11	–
KFA1i-221	–	−2 ± 11	5 ± 22	−8 ± 7	–	−18 ± 9	−11 ± 10	27 ± 11	–
KFA1i-271	–	36 ± 19	124 ± 41	21 ± 11	–	137 ± 88	−81 ± 83	563 ± 130	–
KFA1i-381	–	0 ± 24	−52 ± 50	27 ± 15	–	139 ± 18	131 ± 19	170 ± 22	–
KFA1i-451	–	86 ± 66	54 ± 137	−2 ± 37	–	844 ± 215	822 ± 223	2038 ± 352	–
KFA1i-452	–	36 ± 57	32 ± 121	51 ± 34	–	894 ± 142	342 ± 123	1210 ± 189	–
KFA1i-741	25.2 ± 0.1	110 ± 54	−17 ± 107	64 ± 32	–	66 ± 41	10 ± 43	1021 ± 73	–
KFA1i-m141	–	−3 ± 13	8 ± 26	24 ± 8	66 ± 22	393 ± 45	246 ± 41	261 ± 44	–
KFC1a-357b	–	746 ± 94	703 ± 156	66 ± 50	–	384 ± 193	−225 ± 141	2751 ± 388	–
KFC1b2-0m11	–	−103 ± 113	−310 ± 187	29 ± 118	–	136 ± 125	−47 ± 137	188 ± 134	–
KFC1b2-2113	–	941 ± 145	953 ± 270	235 ± 111	–	319 ± 362	501 ± 506	3629 ± 1019	–
KFC1b2-231	–	−207 ± 95	−97 ± 171	58 ± 76	–	60 ± 239	−101 ± 282	391 ± 301	–
KFC1b2-262	–	59 ± 83	−18 ± 135	−96 ± 53	–	1115 ± 437	65 ± 341	1556 ± 522	–
KFC1b2-441	–	345 ± 238	1569 ± 557	395 ± 169	–	234 ± 516	289 ± 685	2452 ± 1187	–
KFC1b2-521	–	−59 ± 189	−690 ± 183	55 ± 139	–	41 ± 62	2 ± 80	224 ± 72	–
KFC1b2-551	–	−205 ± 186	718 ± 464	8 ± 145	–	564 ± 231	84 ± 230	596 ± 242	–
KFC1d-012	–	–	–	–	–	947 ± 266	203 ± 203	1364 ± 347	–
KFC1d-051	–	–	–	–	–	−508 ± 209	733 ± 464	654 ± 534	–
KFC1d-121	–	–	–	–	–	187 ± 174	267 ± 189	729 ± 256	–
KFC1d-202	–	–	–	–	–	−40 ± 8	−16 ± 10	23 ± 11	–
KFC1d-212	–	–	–	–	–	413 ± 295	498 ± 324	1380 ± 483	–
KFC1d-301	–	–	–	–	–	1307 ± 920	−44 ± 631	4692 ± 1916	–

The isotopic ratios of the grains mentioned in the text and those in Figs. 12 and 14 are shown. The isotopic ratios of all grains are available as the supporting document online. Some of the grains were analyzed for Fe and Ni isotopes. Since they are normal within 2σ errors, they are not listed.
The errors are 1σ.

Table 5
Grains in Populations I, II and III.

Fraction	Total	Estimated Solar Grains	Estimated Presolar Grains in the Normal Bin	Anomalous Grains	Anom./ Total	Population I	Population II	Population III	PI/Anom. Grains	PII/ Anom. Grains	PIII/ Anom. Grains
KE3	163	26	13	137	0.84	43	71	23	0.31	0.52	0.17
KFA1	347	167	27	180	0.52	46	96	38	0.26	0.53	0.21
KFB1	537	77	14	460	0.85	60	108	292	0.13	0.23	0.64
KFC1	593	25	25	568	0.95	87	151	330	0.15	0.27	0.58

method described above, we can set aside solar system grains and will be able focus on presolar graphite grains in the subsequent discussions. We classified graphite grains based on their $^{12}C/^{13}C$ ratios but used the term "Population" instead of "Group" to avoid confusions with the classification by Hoppe et al. (1995). We categorized grains with $^{12}C/^{13}C < 20$ as **Population I**, those with $20 \leqslant {}^{12}C/^{13}C \leqslant 200$ as **Population II**, and those with $^{12}C/^{13}C > 200$ as **Population III**. Table 5 summarizes the numbers and abundances of presolar grains in the Populations as well as those of solar system grains. In KFA1, only 52% of the grains are unambiguously presolar, while the fractions of presolar grains are 84–95 percent in the other fractions. The similarities of the C isotopic distributions between KE3 and KFA1, and between KFB1 and KFC1 are evident also in Table 5. In KE3 and KFA1, ~30% and ~50% of the grains belong to Populations I and II, respectively, and only ~20% of the grains belong to Population III. In contrast, in KFB1 and KFC1 ~15% and ~25% of the grains belong to Populations I and II, respectively and ~60% of the grains belong to Population III.

3.3. Abundances of presolar graphite in the Murchison meteorite

From the fractions of presolar grains in the density fractions estimated in Section 3.2, we calculated the abundances of presolar grains in the Murchison meteorite.

The abundances of KE1, KFA1, KFB1 and KFC1 (Table 1) (Amari et al., 1994) were derived from sample aliquots taken for noble gas analysis (Amari et al., 1995a). The KE3 abundance was not determined in this way because KE3 was separated from KE1 to further increase the fraction of presolar grains, and its noble gases were not analyzed. We estimated the abundance of KE3 in the following way. On a KE1 mount (KE1a), nine grains out of 56 grains are isotopically anomalous in C. The normal bin has 47 grains with one grain each in the two adjacent bins. Therefore, we estimate that one grain in the normal bin is anomalous, making the total 10 anomalous grains on the mount. Thus the fraction of anomalous grains is 0.18 (10/56) in KE1. In KE3, it is 0.84 (137/163 in Table 5), implying that a 4.7-fold enrichment in anomalous grains was achieved with the second purification. From this number, we estimated that the KE3 abundance is ~0.26 ppm. We assumed that solar system and presolar grains have similar size distributions. If solar system grains are significantly larger than presolar grains, the abundance of KE3 becomes lower than ~0.26 ppm. In fact, we encountered many large blocky grains in KE1 although it is hard to quantify the abundance of these grains. We note that the KE3 abundance bears a large uncertainty.

The abundances of presolar grains in all density fractions (Table 1) were calculated from the total abundances of the density fractions (Table 1) and the proportions of the anomalous grains among all grains (Table 5).

3.4. Morphologies

Two basic morphological types have been observed in graphite grains (Hoppe et al., 1995). Grains of the Onion type show a relatively smooth surface and layered structure (images 3, 6, 7, 9, 14, 18, 21, 22, 23, 24, 25, 29, 30, and 32 in Fig. 1). Grains of the Cauliflower type look like aggregates of small grains (1, 2, 4, 5, 8, 10, 11, 12, 13, 15, 16, 17, 19, 20, 26, 27, 28, and 31 in Fig. 1).

TEM observations revealed crystallographic differences of these two types (Bernatowicz et al., 1991, 1996; Croat et al., 2003, 2008). The Onion type consists of concentric layers of well-graphitized carbon with long-range order. Grains of this type often contain a core of nanocrystalline carbon consisting of up to 3–4 nm diameter graphene sheets (Bernatowicz et al., 1996). The Cauliflower type consists of short, curved and discontinuous platelets of turbostratic graphite. Raman studies have confirmed that, on average, onion grains are better crystallized than cauliflower grains (Wopenka et al., 2013).

Many grains show the distinct feature of either type: KE3a-411 (1 in Fig. 1), KFA1c-m133 (11) and KFA1f-101 (12) are typical Cauliflower grains, whereas KFA1c-121 (9), KFB1a-421 (23), and KFC1a-115 (25), with smooth layered surfaces, are classified as Onions. However, there are grains with intermediate features: they have a layered structure but the surface is not smooth and has aggregate features. In this case, we classified those grains as Cauliflower. An example is KFC1a-364 (28). The classification can be subjective for some of these grains.

KE3c-551b (7), having the highest $^{12}C/^{13}C$ ratio of 7223 ± 111 among the Murchison graphite grains analyzed so far, is an Onion grain. During the ion probe analysis, $^{12}C/^{13}C$, $^{14}N/^{15}N$ and $^{16}O/^{18}O$ ratios of this grain became more anomalous as the analysis progressed, indicating that contamination and/or outer layers that could have been

Table 6
Morphologies of the grains.

		Population I	Population II w/o Normal Bin	Normal Bin	Population III	Total*	Total (%)*
KE3	Cauliflower	7	14	12	1	34 (22)	59 (48)
	Onion	7	13	0	4	24 (24)	41 (52)
KFA1	Cauliflower	8	27	58	5	98 (40)	74 (61)
	Onion	6	8	9	12	35 (26)	26 (39)
KFB1	Cauliflower	11	4	15	4	34 (19)	23 (16)
	Onion	6	27	11	67	111 (100)	77 (84)
KFC1	Cauliflower	2	5	1	16	24 (23)	28 (27)
	Onion	10	13	1	38	62 (61)	72 (73)

* Numbers in parentheses indicate those without normal bins.

equilibrated with solar system material was sputtered away during the analysis (see Fig. 1 in Travaglio et al., 1999). If it is the latter, even tightly-packed-looking Onion grains had been affected by alteration, as evidenced by the largely normal N isotopic ratios of most KFC1 grains.

Grains with similar morphologies can have completely different $^{12}C/^{13}C$ ratios. KFA1c-m132 (10) and KFA1c-m133 (11) are of the Cauliflower type and look similar, but the $^{12}C/^{13}C$ of the former is 55.27 ± 0.67 and that of the latter is close to solar (92.2 ± 1.1). The Cauliflower grains KFB1a-261 (19) and KFB1a-262 (20) have $^{12}C/^{13}C$ of 90.0 ± 1.1 and 6.72 ± 0.07, respectively. Most of the grains are round, but there exist non-round grains such as KFC1b2-661 (31).

Table 6 summarizes the abundances of the grains of the two morphologies in the three Populations. Since the normal bin in Population II contains solar system grains, we list the numbers in the normal bin separately to see whether there are morphological differences between solar system and presolar grains. As shown in Table 6, the ratios of Cauliflowers to Onions in the normal bin are much larger than these ratios in the Population II without the normal bin, indicating that solar system grains are more likely to be Cauliflowers than Onions. As for presolar grains, Cauliflower grains are more abundant in the lower-density fractions KE3 and KFA1 (59% and 74% in KE3 and KFA1, respectively), while Onion grains are dominant in the higher-density fractions KFB1 and KFC1 (77% and 72% in KFB1 and KFC1, respectively). Similar results have been obtained for grains from the KFA1, KFB1, and KFC1 fractions by Wopenka et al. (2013).

3.5. Hydrogen isotopic ratios

Four grains from KE3 were analyzed for their H isotopic ratios. Hydrogen in KE3a-662 is depleted in the heavier isotope ($\delta D/H = -338 \pm 41‰$). The H isotopic ratios of the other 3 grains, KE3a-141, KE3a-321 and KE3a-751, are normal. All four analyzed grains show isotopic features characteristic of KE3 grains such as ^{15}N and ^{18}O excesses, and Si isotopic anomalies. They all have $^{12}C/^{13}C$ ratios higher than the solar ratio (KE3a-141: 777 ± 27, KE3a-321: 136 ± 1, KE3a-751: 153 ± 3). KE3a-662 has one of the highest $^{12}C/^{13}C$ ratios (3138 ± 167) among KE3 grains. The Si in KE3a-662 is depleted in ^{30}Si [$\delta^{29}Si$ (‰) $= -16 \pm 51$, $\delta^{30}Si$ (‰) $= -212 \pm 41$].

In stars, deuterium is completely converted to ^3He via $D(p,\gamma)^3He$ when they are on the Pre-Main Sequence and are fully convective (Clayton, 1968). Since stardust grains formed at the end of stars' lifetimes, D is not expected to be found in them. The normal D/H ratios in the 3 grains and the presence of D in KE3a-662, although D is much depleted in the grain, indicate that the H in the grains is dominated by contamination or the result of at least partial isotopic exchange.

3.6. Oxygen isotopic ratios

Oxygen-18 excesses are observed in many grains in KE3, KFA1, and, to a much lesser extent, KFB1 (Figs. 5 and 6, and Table 7). Not only is the number of the ^{18}O-rich grains highest in KE3 (see below), but also the highest ^{18}O excesses are found in KE3. Five KE3 grains have $^{18}O/^{16}O > 0.1$ (two in Population II and three in Population III, solar: 2×10^{-3}), while no grains in the other fractions show such large anomalies. The highest $^{18}O/^{16}O$ ratios in KFA1 and KFB1 are observed in Population II grains (four KFA1 and one KFB1 grains with ratios > 0.01).

At first glance, $^{12}C/^{13}C$ ratios and $^{18}O/^{16}O$ ratios seem to be positively correlated in KE3 (Fig. 5): the highest $^{18}O/^{16}O$ ratio (0.37 ± 0.01) is seen in the grain with the highest $^{12}C/^{13}C$ ratio (7223 ± 111), grain KE3c-551b in Population III. However, if we exclude the three KE3 grains from Population III with $^{18}O/^{16}O$ ratios > 0.1, that apparent trend does not exist any more and the highest $^{18}O/^{16}O$ ratios are seen in Population II grains. That is also observed in KFA1 and KFB1. KFC1 lacks ^{18}O-rich Population II grains and has only one ^{18}O-rich grain in Population III.

Only a subset of KE3, KFA1 and KFB1 grains and no KFC1 grains were measured for their $^{17}O/^{16}O$ ratios (Fig. 6). Many grains with ^{18}O anomalies have solar $^{17}O/^{16}O$ ratios. Even if they have ^{17}O anomalies, anomalies are much smaller in $^{17}O/^{16}O$ than in $^{18}O/^{16}O$: The highest $^{17}O/^{16}O$ ratio is only 3.8 times the solar ratio (KE3a-301), whereas the highest $^{18}O/^{16}O$ ratio is 185 times the solar ratio (KE3c-551b). There are also grains with $^{17}O/^{16}O$ ratios lower than the solar ratio by about a factor of two [$(2.18 \pm 0.41) \times 10^{-4}$ in KE3c-551b] (The $^{17}O/^{16}O$ ratio of KE3a-573 is $[8.98 \pm 9.99] \times 10^{-5}$ and it is even lower. However, it has a huge error).

The fractions of ^{18}O-rich grains are given in Table 7. We are interested in the fractions of ^{18}O-rich grains among

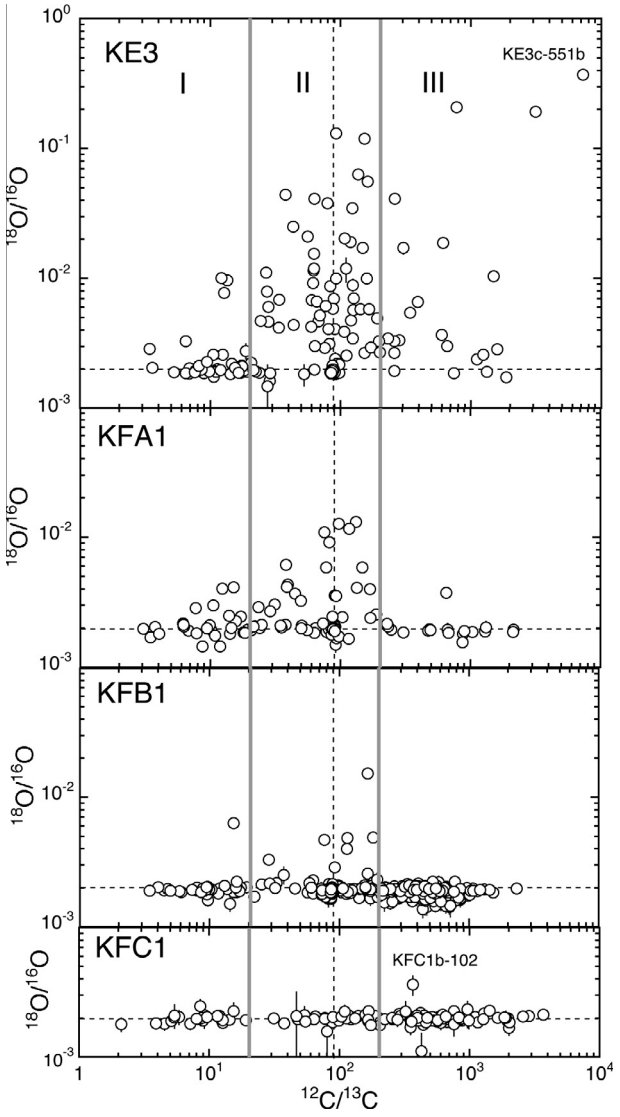

Fig. 5. $^{18}O/^{16}O$ vs. $^{12}C/^{13}C$ plots of grains from the graphite fractions. Oxygen-18 rich grains are most abundant in KE3 followed by KFA1. There are only a few such grains in KFB1and hardly any in KFC1. Part of the data have previously been published by Hoppe et al. (1995), Amari et al. (1993, 1995c, 1996), Travaglio et al. (1999), Croat et al. (2003) and Heck et al. (2009a).

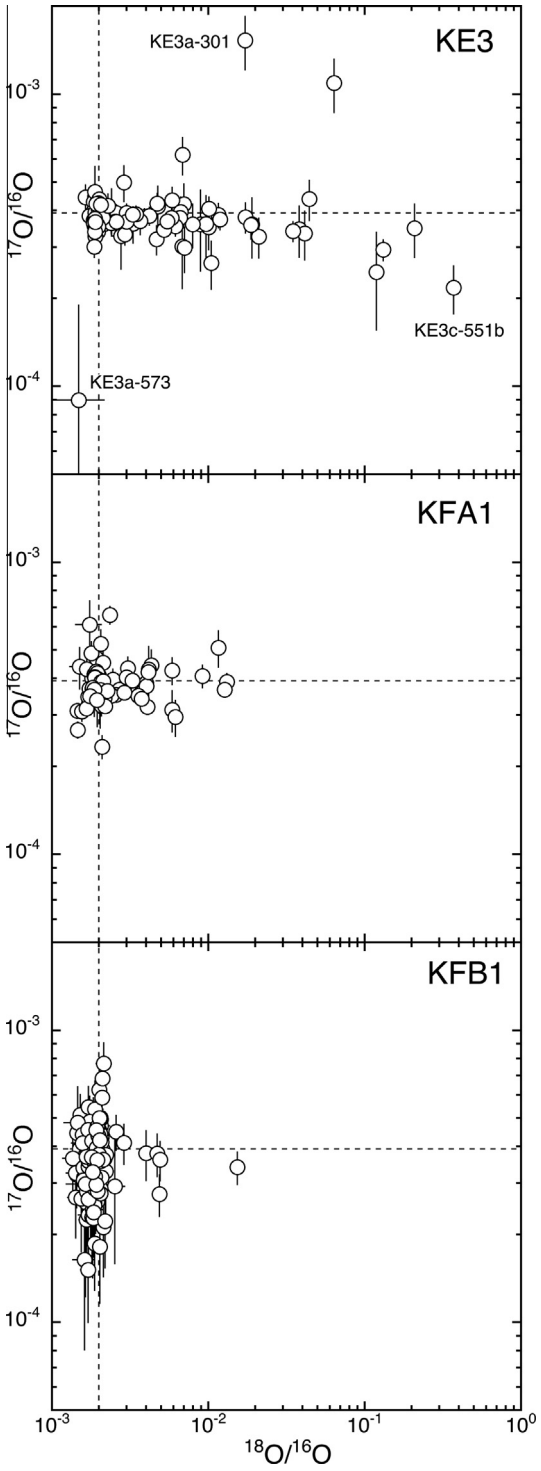

Fig. 6. $^{17}O/^{16}O$ vs. $^{18}O/^{16}O$ for KE3, KFA1 and KFB1. KFC1 grains were not analyzed for their $^{17}O/^{16}O$ ratios. Part of the data have previously been published by Hoppe et al. (1995), Amari et al. (1993, 1995c, 1996), Travaglio et al. (1999) and Croat et al. (2003).

presolar grains and not among all the grains analyzed. For this reason, special care had to be taken for grains that fall into the normal bin (Fig. 4). A few of them might have been solar system grains and thus have the solar $^{18}O/^{16}O$ ratio. For Population II we estimated the numbers of presolar grains analyzed for O isotopic ratios in the normal bin from the fractions of presolar grains in the normal bin (Table 5) and list the numbers in Table 7. The first numbers in the parentheses are the numbers of the O-anomalous grains (in the numerators) and the estimated numbers of presolar grains among the measured grains (in the denominators) in the normal bins.

The fraction of the ^{18}O-rich grains decreases with increasing density as seen in Fig. 5 and Table 7. The fraction of ^{18}O-rich grains is 70% for KE3 followed by 42% for KFA1. In KFB1 and KFC1, the numbers are 4.5% and <1%, respectively.

More than 80% of the KE3 grains from Populations II and III are ^{18}O-rich and a third of the KE3 grains in

Table 7
Grains with ^{18}O excesses.

Fraction	Population I		Population II		Population III		Total	
	Number of grains*	Fraction of ^{18}O-rich grains	Number of grains[a]	Fraction of ^{18}O-rich grains	Number of grains	Fraction of ^{18}O-rich grains	Number of grains	Fraction of ^{18}O-rich grains
KE3	15/41	0.37	(10 + 49)/(12 + 57)	0.86	18/22	0.82	92/132	0.70
KFA1	8/28	0.29	(6 + 21)/(6 + 36)	0.64	2/18	0.11	37/88	0.42
KFB1	2/35	0.057	(2 + 9)/(7 + 55)	0.16	0/189	0	13/286	0.045
KFC1	0/23	0	(0 + 0)/(2 + 24)	0	1/69	0.015	1/118	0.008

* (The number of ^{18}O-rich grains)/(the number of grains analyzed).
[a] [The number of ^{18}O-rich grains in the normal bin ($^{12}C/^{13}C = 79.4 - 100$) + that in the other bins in Population II ($20 < ^{12}C/^{13}C < 79.4$ and $100 < ^{12}C/^{13}C < 200$)]/[estimated number of presolar grains among analyzed grains in the normal bin + that in the other bins in Population II].

Population I also show ^{18}O excesses. The fractions of ^{18}O-rich grains in all Populations in KFA1 are lower than those of the corresponding Populations in KE3. In KE3, the fraction of ^{18}O-rich grains in Population II is about the same as that in Population III. In KFA1, the fraction of the ^{18}O-rich grains in Population III (11%) is significantly lower than in Population II (64%). Population II is the only Population in KFB1 that contains a notable number of ^{18}O-rich grains. In KFC1, we found only one ^{18}O-rich grain; it belongs to Population III.

3.7. $^{25}Mg/^{24}Mg$ ratios

Fig. 7 shows $\delta^{25}Mg/^{24}Mg$ values and $^{12}C/^{13}C$ ratios of the graphite grains. The anomalous grains (differing in their $^{25}Mg/^{24}Mg$ ratios by more than 2σ errors from solar) are shown as solid circles. In KE3, all eleven anomalous grains show ^{25}Mg excesses; these grains also have ^{18}O excesses. Except KE3a-301 in Population III, the other 10 anomalous grains are in Population II. Their inferred $^{26}Al/^{27}Al$ ratios range from 4.08×10^{-3} to 0.116, and 7 out of all 11 grains have Si isotopic anomalies. KE3a-157 shows the highest excess in ^{25}Mg ($\delta^{25}Mg/^{24}Mg = 1585 \pm 301‰$) as well as isotopic anomalies in other elements (Tables 4a and 4b).

Also in KFA1 have the anomalous grains only ^{25}Mg excesses. The ^{25}Mg-rich grains are most abundant in Population II (24), as in the case of KE3, followed by Population I (7) and Population III (3). In KE3 the highest excess is found in Population II, while in KFA1 it is found in a Population I grain ($813 \pm 61‰$ in KFA1g-745). In contrast to KE3 and KFA1, most of the anomalous grains in KFB1 and KFC1 show deficits in ^{25}Mg. Only one out of 4 KFB1 grains and one out of 5 KFC1 grains show excesses. The KFB1 and KFC1 grains with excesses are found in Population I.

3.8. Calculation of isotopic ratios of extinct radionuclides

The radionuclides we looked for include ^{26}Al ($T_{1/2} = 7.3 \times 10^5$ a), ^{41}Ca ($T_{1/2} = 1 \times 10^5$ a), ^{44}Ti ($T_{1/2} = 60$ a), and ^{60}Fe ($T_{1/2} = 2.6 \times 10^6$ a, Rugel et al., 2009), which decay to ^{26}Mg, ^{41}K, (via ^{44}Sc) ^{44}Ca and (via ^{60}Co) ^{60}Ni, respectively. We did not find any ^{60}Ni excesses in the few grains we analyzed. Because of their short half-lives, these radionuclides completely decayed in presolar grains and we inferred their abundances from the excesses in their daughter isotopes. To do so, we needed to determine the radiogenic portion of their daughter isotopes. In terrestrial and extra-terrestrial material of solar system origin, any excesses relative to the solar abundances can be attributed to the decay of radionuclides because solar system material can be safely assumed to have solar isotopic composition. Presolar grains have non-solar isotopic compositions in many elements, thus one may wonder how we can estimate the radiogenic portion of excesses in the daughter isotopes when the non-radiogenic portion is likely to be anomalous.

Considering the Al–Mg systematics, Mg is volatile and is expected to condense at much lower temperatures than host graphite grains, thus indigenous Mg contents in graphite grains are low. Therefore, it is likely that the Mg measured in some grains is dominated by contamination. In fact, the $^{25}Mg/^{24}Mg$ ratios in many grains we analyzed are normal within huge errors. In contrast, Al is much more refractory than Mg, and condenses preferentially over Mg into graphite grains. As a consequence, intrinsic Al/Mg ratios are high.

There are grains with ^{25}Mg excesses as seen in Fig. 7. However, in these cases, ^{26}Mg excesses are much larger than the ^{25}Mg excesses (Fig. 8). The $^{26}Mg/^{24}Mg$ in KE3a-321 is 433 times solar, while the $^{25}Mg/^{24}Mg$ is 1.8 times solar (Fig. 8a). If the ^{25}Mg excess is due to neutron capture, we expect that the ^{26}Mg excess is of the same order of magnitude as the ^{25}Mg excess. For example, in the 15 $M_\odot$ supernova (SN) model ("s15a28c" case) by Rauscher et al. (2002), the $^{25}Mg/^{24}Mg$ and $^{26}Mg/^{24}Mg$ ratios in the O/C zone, where neutron capture takes place, are expected to be 22.5 and 20.9 times solar, respectively. Therefore, not taking into account ^{26}Mg excesses due to neutron capture does not have a large effect on inferring $^{26}Al/^{27}Al$ ratios when ^{26}Mg excesses are disproportionally high. For one of the KFA1 mounts (KFA1e), we made a correction assuming that ^{26}Mg excesses due to neutron capture are of the same order as ^{25}Mg excesses. For all the other cases, we used the solar $^{26}Mg/^{24}Mg$ ratio to calculate ^{26}Mg excesses.

In the Ca-K systematics, the daughter element K has only 2 stable isotopes, ^{39}K and ^{41}K. Thus, there are no other

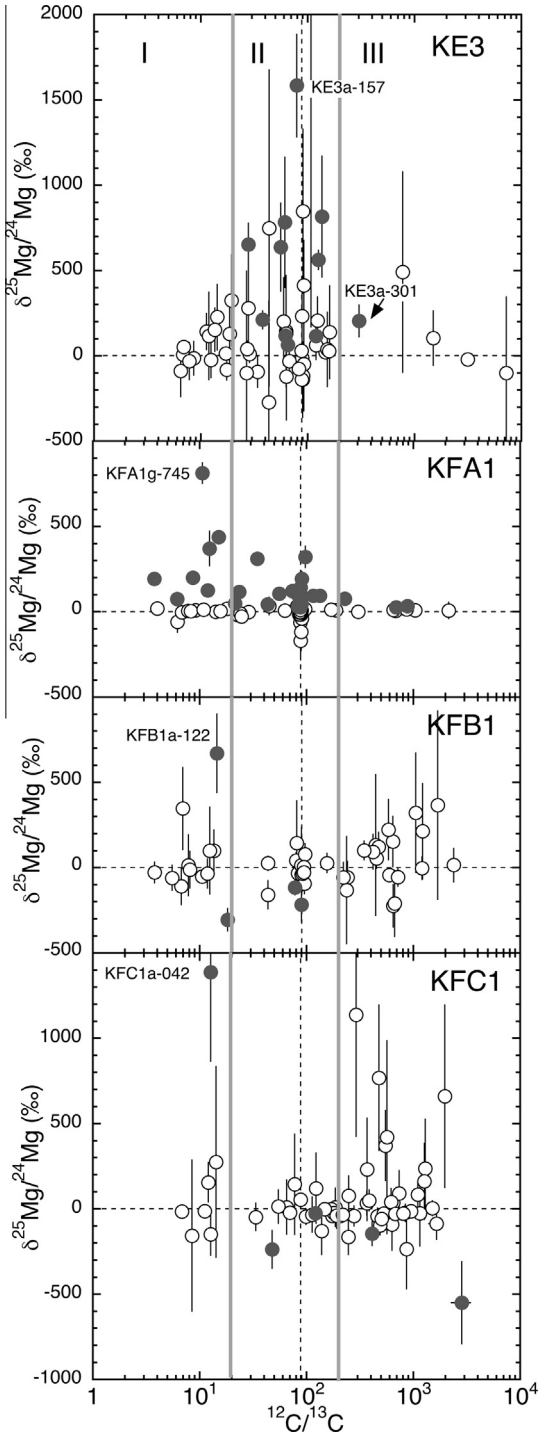

Fig. 7. $\delta^{25}Mg/^{24}Mg$ values of graphite grains are plotted against their $^{12}C/^{13}C$ ratios. The open circles indicate grains with a solar $^{25}Mg/^{24}Mg$ ratio within 2σ errors. The dark solid circles indicate anomalous grains.

isotopic ratios to estimate the radiogenic portion of ^{41}K as we do with the Al–Mg systematics. $\delta^{41}K/^{39}K$ values in the He/C, O/C and O/Ne zones of a 15 $M_\odot$ star are expected to be 3100‰, 1400‰ and 700‰, respectively (Rauscher et al., 2002). It is not likely that K, a volatile element, would have as readily condensed into graphite into the graphite grains as the more refractory Ca, similar to the case of volatile Mg and refractory Al. Of the 7 KE3 grains with evidence for ^{41}Ca, there are two grains with $\delta^{41}K/^{39}K$ values of 10,610‰ and 3694‰, exceeding the highest value in the SN model. Therefore, although there might have been grains with ^{41}K excesses of a non-radiogenic origin and we might have overestimated their $^{41}Ca/^{40}Ca$ ratios, radiogenic ^{41}K is undoubtedly present in the grains. We inferred $^{41}Ca/^{40}Ca$ ratios by assuming that all ^{41}K excesses are due to the decay of ^{41}Ca.

For the Ti–Ca systematics, the situation is more complicated. There are grains with normal $^{42}Ca/^{40}Ca$ and $^{43}Ca/^{40}Ca$ ratios and excesses in ^{44}Ca outside of 2σ errors. They are grains KE3a-321, KE3a-322, KE3c-242, KE3d-1, KFA1e-562, KFA1i-201 and KFA1i-m141 (Table 4, the names are underlined in Figs. 12a and 12b, for KE3d-9, KFA1e-301, and KFA1e-743, which have $^{42,43}Ca$ excesses but is also underlined, see below and Section 3.13). In these cases, there is little doubt that the ^{44}Ca excesses can be attributed to ^{44}Ti decay. There is one case where the ^{44}Ca excess is so huge that the correction for non-radiogenic ^{44}Ca makes little difference: KFA1f-302 (Fig. 12b) shows the largest ^{44}Ca excess found in Murchison graphite grains, where the $^{44}Ca/^{40}Ca$ ratio is 138 times solar and the $^{43}Ca/^{40}Ca$ ratio is 3 times solar (but normal within 2σ errors).

Most of the grains measured for Ca isotopic ratios show ^{42}Ca and/or ^{43}Ca anomalies. When Ca isotopic abundances are modified by neutron capture, ^{44}Ca excesses are expected to be substantially smaller than ^{42}Ca and ^{43}Ca excesses. When the other Ca isotopic ratios of a grain are anomalous, we compared the pattern of the grain and predicted patterns of different zones in supernovae and estimated a radiogenic portion of ^{44}Ca. We will discuss the method in Section 3.13.

The sensitivity factor F between elements A and B is defined as $A/B = F \times A^+/B^+$. The sensitivity factors used to infer isotopic ratios for the extinct radionuclides are $F(Al^+/Mg^+) = 1.35$, $F(Ca^+/K^+) = 3$, and $F(Ti^+/Ca^+) = 3.0$ for IMS-3f analyses and 2.5 for NanoSIMS analyses.

3.9. $^{26}Al/^{27}Al$ ratios

Inferred $^{26}Al/^{27}Al$ ratios in graphite grains are shown in Fig. 9. Many KE3 grains show ratios up to ~0.1. The highest ratio (0.146 ± 0.008) is found in KE3a-152. All five Population III grains show high $^{26}Al/^{27}Al$ ratios, with the lowest ratio being $(2.24 \pm 0.15) \times 10^{-2}$. Many Population II grains also show high $^{26}Al/^{27}Al$ ratios although there are more grains with lower $^{26}Al/^{27}Al$ ratios than in Population III. There is no KE3 grain with $^{26}Al/^{27}Al$ ratio higher than 5×10^{-2} in Population I.

In KFA1, there are many Population II grains with high $^{26}Al/^{27}Al$ ratios, similar to KE3 grains. However, there are only few Population III grains with high $^{26}Al/^{27}Al$ ratios and that there are more Population I grains with high $^{26}Al/^{27}Al$ ratios in KFA1 than in KE3. Only a few KFB1 grains show resolvable ^{26}Al. The $^{26}Al/^{27}Al$ ratios of these grains range from $(4.3 \pm 1.1) \times 10^{-3}$ to $(8.6 \pm 1.8) \times 10^{-2}$. There was no KFC1 grain that contains detectable ^{26}Al.

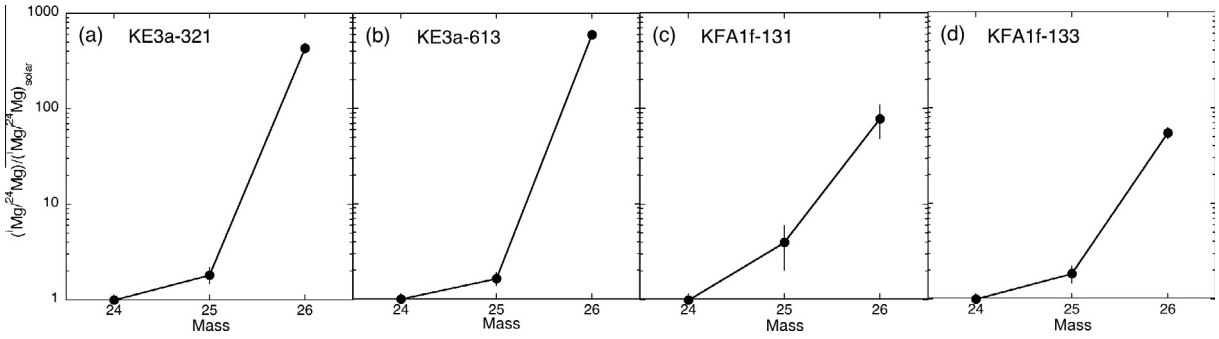

Fig. 8. $^{25}Mg/^{24}Mg$ and $^{26}Mg/^{24}Mg$ ratios of four grains, normalized to the solar ratios. The ^{26}Mg excesses are much larger than the ^{25}Mg excesses.

3.10. Silicon isotopic ratios

Fig. 10 shows the Si isotopic ratios of the grains. Grains with Si isotopic anomalies in at least one ratio outside of 2σ errors are shown as filled circles in the δ^{29}Si-C isotope plots on the right.

Both ^{28}Si excesses, and ^{29}Si and/or ^{30}Si excesses are observed in graphite grains, although the former are more common than the latter. The ^{29,30}Si excesses are most pronounced in Population II grains of KE3. The highest excess is observed in KE3d-9 ($\delta^{29}Si = 1272 \pm 75‰$, $\delta^{30}Si = 937 \pm 66‰$). This grain has an ^{18}O excess [$^{18}O/^{18}O = (8.77 \pm 0.15) \times 10^{-3}$], Ca and Ti isotopic anomalies (Fig. 12a and Fig. 14a), but close-to-normal $^{12}C/^{13}C$ (82.8 ± 0.3). We calculated the slope of the linear regression line for the 5 KE3 grains with ^{29,30}Si excesses (Fig. 10) and it is 1.39 ± 0.16, indicating that ^{29}Si is more enriched than ^{30}Si is in these grains. Interestingly, the slope is the same as that of the SiC mainstream grains, which formed in AGB stars. In KFA1, the largest ^{29,30}Si excesses (~500‰) are observed in a Population II grain (KFA1a1-471) and a Population III grain (KFA1e-463), the latter with its $^{12}C/^{13}C$ ratio (229 ± 2) lying close to the range of Population II. In the higher-density fractions KFB1 and KFC1, these excesses, albeit being smaller than in KE3 and KFA1, are also observed in Population II.

Silicon-28 excesses are observed in all the density fractions. They are observed in all Populations in KE3, while they are mainly observed in Population II in KFA1 and KFB1. Silicon-28 excesses are, along with ^{18}O excesses, evidence of a SN origin. The highest ^{28}Si excesses are seen in KE3. The lowest $^{29,30}Si/^{28}Si$ ratios are about half of the solar ratios, and are seen in KE3, KFA1, and KFB1 grains.

KFC1a-551 shows a very low $^{12}C/^{13}C$ ratio (8.46 ± 0.04), a high δ^{30}Si value ($761 \pm 72‰$) and a close-to-normal $^{29}Si/^{28}Si$ ratio. Its isotopic signature is indicative of a nova origin (Amari et al., 2001a), although Nittler and Hoppe (2005) proposed that such a signature can be also produced in supernovae.

3.11. $^{41}Ca/^{40}Ca$ ratios

KE3 and KFA1 were analyzed for the Ca–K systematics (Fig. 11). Seven KE3 grains and 9 KFA1 grains have ^{41}K excesses: $\delta^{41}K/^{39}K$ values range from $55 \pm 11‰$ to $10{,}610 \pm 326‰$ in the KE3 grains and from $44 \pm 11‰$ to $602 \pm 16‰$ in the KFA1 grains. The inferred $^{41}Ca/^{40}Ca$ ratios range from $(1.01 \pm 0.24) \times 10^{-3}$ (KFA1e-743) to $(2.52 \pm 0.01) \times 10^{-2}$ (KFA1i-741).

3.12. Calcium isotopic ratios

The Ca isotopic patterns of grains from KE3, KFA1, and KFC1 are shown in Figs. 12a–12c. We selected grains that show isotopic anomalies in at least one ratio outside of 2σ errors. Calcium-46 and ^{48}Ca were not analyzed because of their low abundances and interferences from ^{46}Ti and ^{48}Ti, respectively.

We classified the Ca isotopic patterns into four types. (1) Excesses in ^{42}Ca and ^{43}Ca are similar with much smaller ^{44}Ca excess as seen in KE3j-020 (Fig. 12a). The names of these grains are indicated with outlined letters in Figs. 12a–12c. (2) The largest excess is seen in ^{43}Ca, a smaller excess in ^{42}Ca, and even smaller excess in ^{44}Ca. This pattern is most widely seen in the graphite grains. In Fig. 12a, 6 grains, whose names are not outlined or underlined, show this pattern. (3) The pattern shows contributions from the decay of ^{44}Ti to ^{44}Ca. Four grains (KE3a-321, KE3a-322, KE3c-242 and KE3d-1) show ^{44}Ca excesses, while the other isotopic ratios are solar within 2σ errors. For these grains, we assumed that the ^{44}Ca excesses are due to the decay of ^{44}Ti ($T_{1/2} = 60$ a) as discussed in Section 3.8. The pattern of KE3d-9 can be classified as the second type except the high $^{44}Ca/^{40}Ca$ ratio. For this grain, we estimated the radiogenic portion of the ^{44}Ca as will be described in Section 3.13. (4) Either ^{42}Ca and/or ^{43}Ca are deficient. The names of grains of this type are shown in italics font (not in Fig. 12a).

In Fig. 12b, grains of the first type, having similar excesses in ^{42}Ca and ^{43}Ca, are KFA1e-301 and KFA1e-743. However, their $^{44}Ca/^{40}Ca$ ratios are higher than what is expected from stellar models. Therefore, we estimated the ^{44}Ca from the decay of ^{44}Ti as will be described in Section 3.13. (Their names are also underlined.) Grains of the second type, 7 grains whose names are not marked, are most abundant also in KFA1. The four grains (underlined in Fig. 12b) show ^{44}Ca excesses with close-to-solar $^{42}Ca/^{40}Ca$ and $^{43}Ca/^{40}Ca$ ratios, which belong to the third type, had their $^{44}Ti/^{48}Ti$ ratios calculated along with KFA1e-301 and KFA1e-743. Five grains are categorized

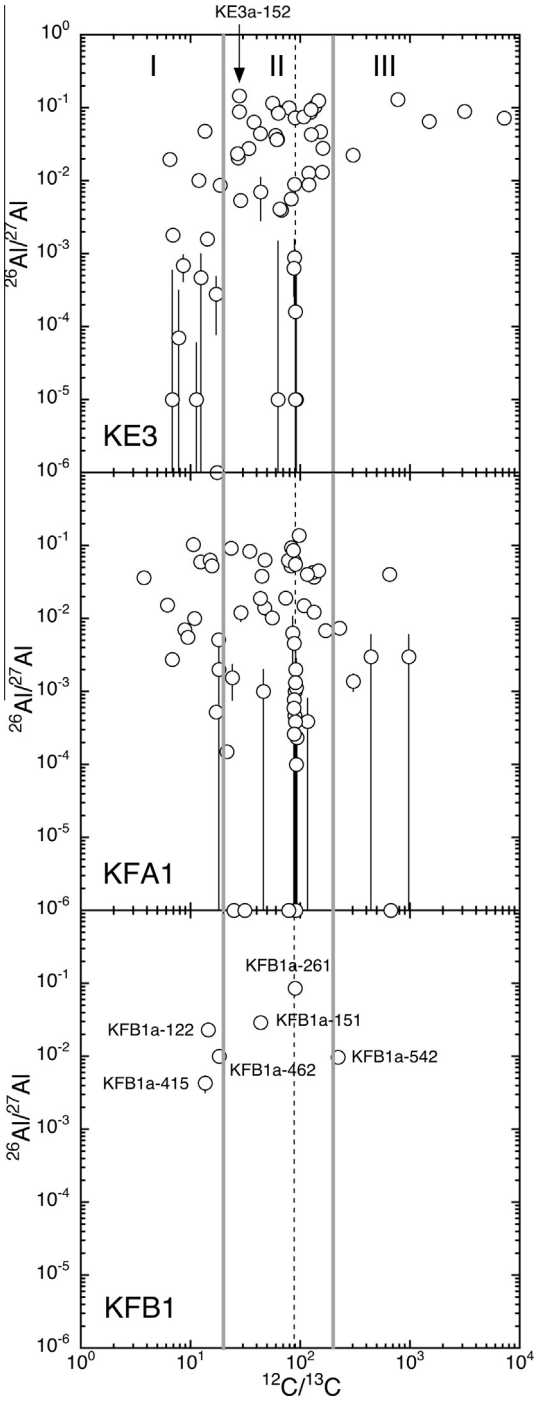

Fig. 9. ^{26}Al/^{27}Al ratios inferred from ^{26}Mg/^{24}Mg and Mg/Al ratios are plotted against ^{12}C/^{13}C ratios. KFC1 grains were not analyzed for Mg-Al. Part of the data have previously been published by Hoppe et al. (1995), Amari et al. (1993, 1996) and Travaglio et al. (1999).

into the fourth type. [The δ^{44}Ca/^{40}Ca value of KFA1i-741 is normal with 2σ errors (64 ± 32‰) and the ^{44}Ti/^{48}Ti ratio was not calculated.]

In Fig. 12c, KFC1a-357b and KFC1b2-2113 belong to the first type, with similar excesses in ^{42}Ca and ^{43}Ca, and KFC1b2-441 belongs to the second type. KFC1b2-231 and KFC1b2-521 have negative δ^{42}Ca/^{40}Ca and δ^{43}Ca/^{40}Ca values, respectively, making them members of the fourth type.

3.13. ^{44}Ti/^{48}Ti ratios

Inferred ^{44}Ti/^{48}Ti ratios of a few KE3 and KFA1 grains are shown in Fig. 13. If ^{44}Ca/^{40}Ca ratios are the only ratios that are higher than solar, we assumed that all ^{44}Ca excesses are due to the decay from ^{44}Ti. Such grains are KE3a-321, KE3a-322, KE3c-242, KE3d-1, KFA1e-562, KFA1i-201, KFA1i-m141 and KFA1f-302. If ^{42}Ca/^{40}Ca and ^{43}Ca/^{40}Ca ratios are higher than solar, we estimated the amount of ^{44}Ca from the decay from ^{44}Ti in the following way. If grains show the Ca isotopic pattern of the first type (Section 3.12), we compared the δ^{44}Ca/δ^{42}Ca ratios of the grains and that of the He/C zone (0.11) and took the excess in the δ^{44}Ca value (if it was anomalous outside of 2σ errors) as the portion of ^{44}Ca from ^{44}Ti decay. The ^{44}Ti/^{48}Ti ratios of KFA1e-301 and KFA1e-743 were inferred that way. If grains show the Ca isotopic pattern of the second type, we compared their δ^{44}Ca/δ^{42}Ca ratios and that of the O/C and O/N zones (0.40) and took the excess in the δ^{44}Ca value as the portion of ^{44}Ca from ^{44}Ti decay. Among the grains of the second type in KE3 and KFA1, KE3d-9 is the only grain that shows such an excess.

In KE3 and KFA1 together, 11 grains show evidence for initial ^{44}Ti, with inferred ^{44}Ti/^{48}Ti ratios between $(1.06 \pm 0.22) \times 10^{-3}$ (KE3a-321) and 0.41 ± 0.30 (KE3d-1).

3.14. Titanium isotopic ratios

Figs. 14a–14c show Ti isotopic patterns of the grains that show anomalies in at least one isotopic ratio outside of 2σ errors. Since ^{50}Ti$^+$ and ^{50}Cr$^+$ could not be separated (because a mass-resolution power of 40,000 would be needed), ^{50}Cr was estimated from ^{52}Cr, assuming the solar ^{50}Cr/^{52}Cr ratio. This was probably justified because $Na_2Cr_2O_7$ was used to destroy kerogen just before density separation to extract graphite grains, and the Cr must have been mostly from this chemical. Furthermore, the amount of indigenous Cr is probably much lower than that of Ti because Cr is more volatile than Ti and is not expected to condense into the grains. If the contribution of ^{50}Cr was overwhelming, which was the case especially for KFC1 grains, δ^{50}Ti/^{48}Ti values are not shown in the figures. Titanium-50 (+ ^{50}Cr) was not measured for grains on the KE3a mount.

Mount KFA1e was heavily contaminated and we had unusually high Ca counts. This affected the Ti isotopic analysis of the grains on this mount. Many grains showed negative Ti delta values because the ^{48}Ti$^+$ apparently had a significant contribution from ^{48}Ca$^+$. We corrected the contribution of ^{48}Ca$^+$ to the ^{48}Ti$^+$ counts when it was possible. Unfortunately, ^{40}Ca was not analyzed during the Ti analysis and we used ^{40}Ca$^+$/^{48}Ti$^+$ ratios measured during the K-Ca analysis. This means that grains that were not analyzed for K-Ca did not have their ^{40}Ca$^+$/^{48}Ti$^+$ ratios determined. We selected the Ti data for grains from the KFA1e mount

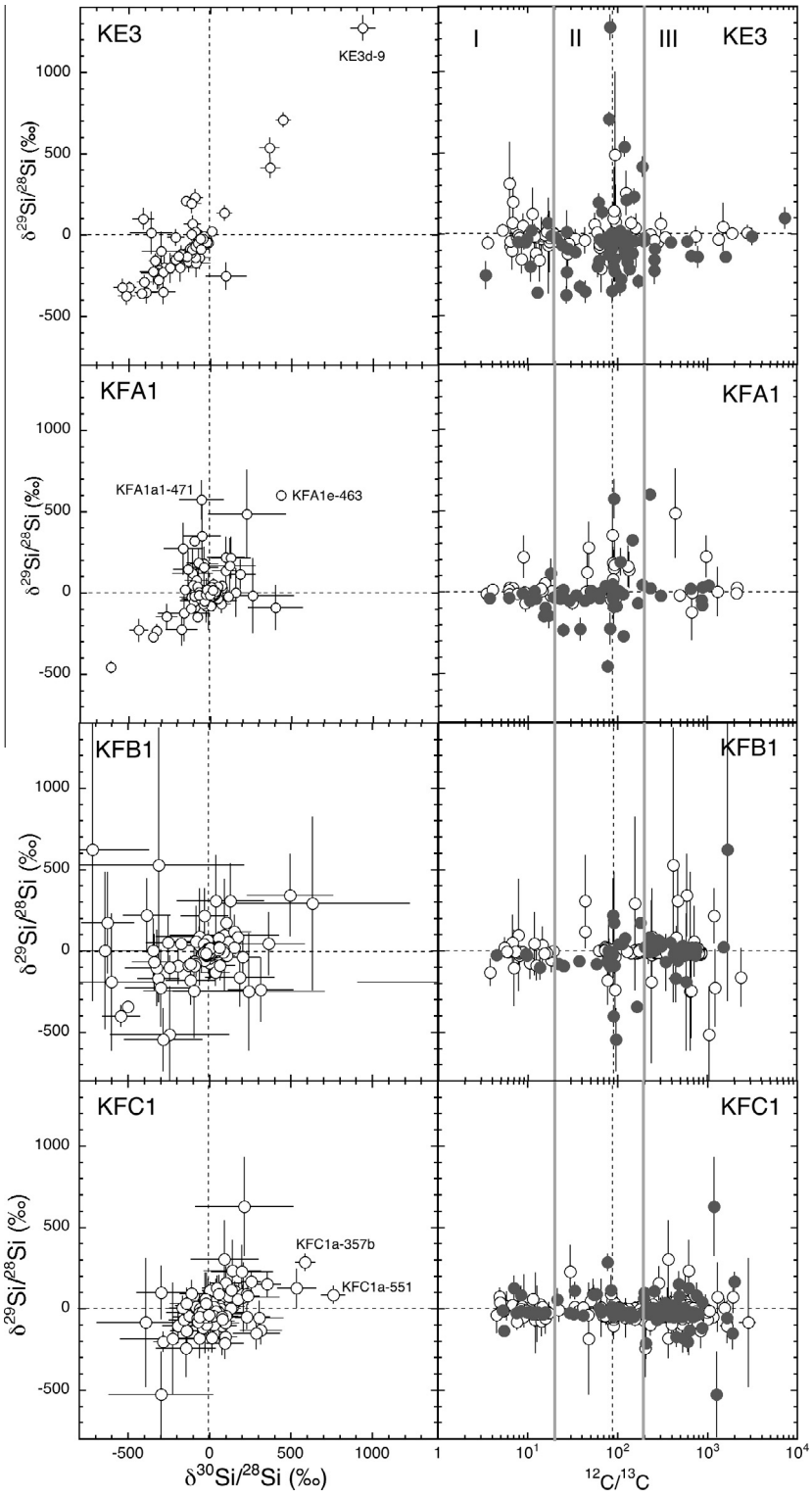

Fig. 10. Silicon isotopic ratios and $^{12}C/^{13}C$ ratios of Murchison graphite grains. In the $\delta^{29}Si/^{28}Si$–$^{12}C/^{13}C$ plots on the right, the open circles indicate grains with solar Si (within 2σ errors) and the dark solid circles indicate Si-anomalous grains. Part of the data have previously been published by Hoppe et al. (1995), Amari et al. (1995c), Travaglio et al. (1999), Croat et al. (2003) and Meier et al. (2012).

as follows. First, if $\delta^{49}Ti/^{48}Ti$ values are larger than 1000‰, we assumed that the Ca interference had little effect. KFA1e-413 and KFA1e-742 are examples. Both grains did not have their $^{40}Ca^+/^{48}Ti^+$ ratios determined. Second, we selected grains with $^{40}Ca^+/^{48}Ti^+$ ratios <100. Those of KFA1e-274b and KFA1e-731 are 29 and 16, respectively.

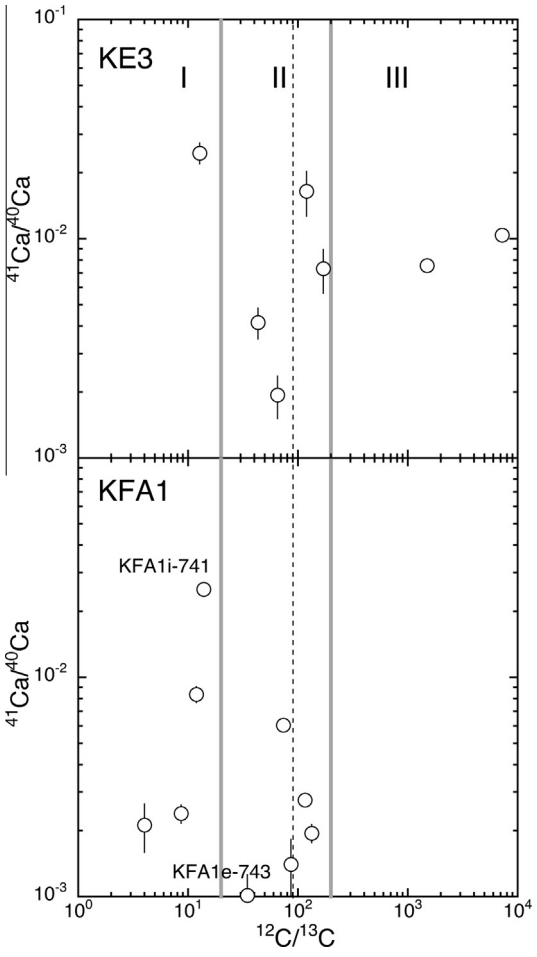

Fig. 11. $^{41}Ca/^{40}Ca$ ratios inferred from the $^{41}K/^{39}K$ and K/Ca ratios are plotted against $^{12}C/^{13}C$ ratios for KE3 and KFA1 grains. Part of the data have previously been published by Amari et al. (1996) and Travaglio et al. (1999).

We can identify several Ti isotopic patterns. (1) ^{49}Ti excesses are dominant compared with anomalies in other Ti isotopic ratios: ^{46}Ti excesses are small compared with the ^{49}Ti excesses. $^{47}Ti/^{48}Ti$ ratios are, in several cases, smaller than solar. In cases when $^{50}Ti/^{48}Ti$ ratios were obtained, ^{50}Ti excesses are smaller than ^{49}Ti excesses. Names of grains of this type are outlined in the Figs. 14a–14c. (2) ^{46}Ti and/or ^{47}Ti excesses are much more pronounced than in grains of the first type, thus the Ti isotopic patterns of grains of this type often show a V-shape. A few of the grains show ^{47}Ti excesses that are larger than ^{46}Ti excesses. The names of these grains are not marked. (3) Patterns that are not classified as either of the first or the second type. One or more Ti isotopic ratios are lower than solar. Grains of this type are labeled in italics.

The first type is dominant in KE3: 10 grains have the first type and 5 grains the second type. In KFA1, 5 grains have the first type, 9 grains the second type and 6 grains the third type. In KFC1, 5 grains each show the first type and the second type, while 2 grains have the third type. Titanium-47 excesses that are higher than ^{46}Ti excesses are observed in two grains, KE3d-9 and KFA1e-413, outside of 2σ errors.

We often observed that Ti counts changed significantly during the measurement in a few grains. Examples in Orgueil graphite are shown in Figs. 10–14 by Zinner and Jadhav (2013). The fluctuation was due to TiC subgrains in these graphite grains [see Fig. 1b by Nittler et al. (1996) and Fig. 2cd by Amari (2009)]. When the beam hit where TiC subgrains were populated inside a graphite grain, the ^{48}Ti count increased. Depending on ^{40}Ca and ^{48}Ti counts, the fluctuation of the ^{44}Ca count mimicked that of ^{48}Ti count (see Figs. 10–12 by Zinner and Jadhav 2013), indicating the most of the ^{44}Ca is due to the decay from ^{44}Ti.

4. DISCUSSION

4.1. Stellar evolution

Before we discuss the isotopic signatures of the graphite grains and their stellar sources, we will briefly summarize the evolution of stars, with emphasis of relevant aspects for the graphite grains. Detailed reviews of stellar evolution can be found elsewhere (e.g., Lattanzio and Boothroyd, 1997; Busso et al., 1999; Woosley et al., 2002; Herwig, 2005).

Stars spend most of their lives on the Main Sequence, burning H in the core. When H is exhausted in the core, stars ascend the Giant Branch and H burns in a shell surrounding the inert core. When the convective envelope penetrates deep into the region where partial H-burning has taken place (first dredge-up), the envelope composition changes. Helium-4 and the products in the CN cycle, primarily ^{14}N and ^{13}C, are mixed into the envelope and the $^{12}C/^{13}C$ ratio of the envelope is expected to be ~ 20. Next, ^{4}He violently ignites in the core (core He flash) and the stars quickly move to the Horizontal Branch while ^{4}He burns in the convective core and H burns in the H-shell. When central He is exhausted in the core, it becomes ^{12}C and ^{16}O-rich and the stars ascend the Asymptotic Giant Branch (AGB). For stars with $\geqslant 5\ M_{\odot}$, the second dredge-up takes place, where the inner edge of the convective envelope penetrates the H-shell, bringing the ashes of the complete H- burning into the envelope.

Stars with $<8\ M_{\odot}$ and $>8\ M_{\odot}$ follow different evolutionary paths. At this stage, $<8\ M_{\odot}$ stars consist of a CO core (product of He-burning), He-and H-burning shells, which burn alternately, and the convective envelope. The He-shell is thermally unstable and burns vigorously during thermal pulses. During a thermal pulse, due to a huge energy release in a short amount of time, the intershell region becomes convective and ^{12}C and *s*-process products are mixed in this region. Following the thermal pulse, the bottom of the convective envelope moves inward into the intershell region and brings nucleosynthetic products into the envelope (third dredge-up). With repeated thermal pulses, the envelope gradually becomes enriched in ^{12}C and *s*-process products. When the envelope becomes C-rich, the star becomes a carbon star and carbonaceous grains can form instead of oxides because in O-rich conditions, C is locked in CO molecules and is not available for the formation of carbonaceous grains. The number of thermal pulses depends on the mass and the metallicity of the star. Towards the end

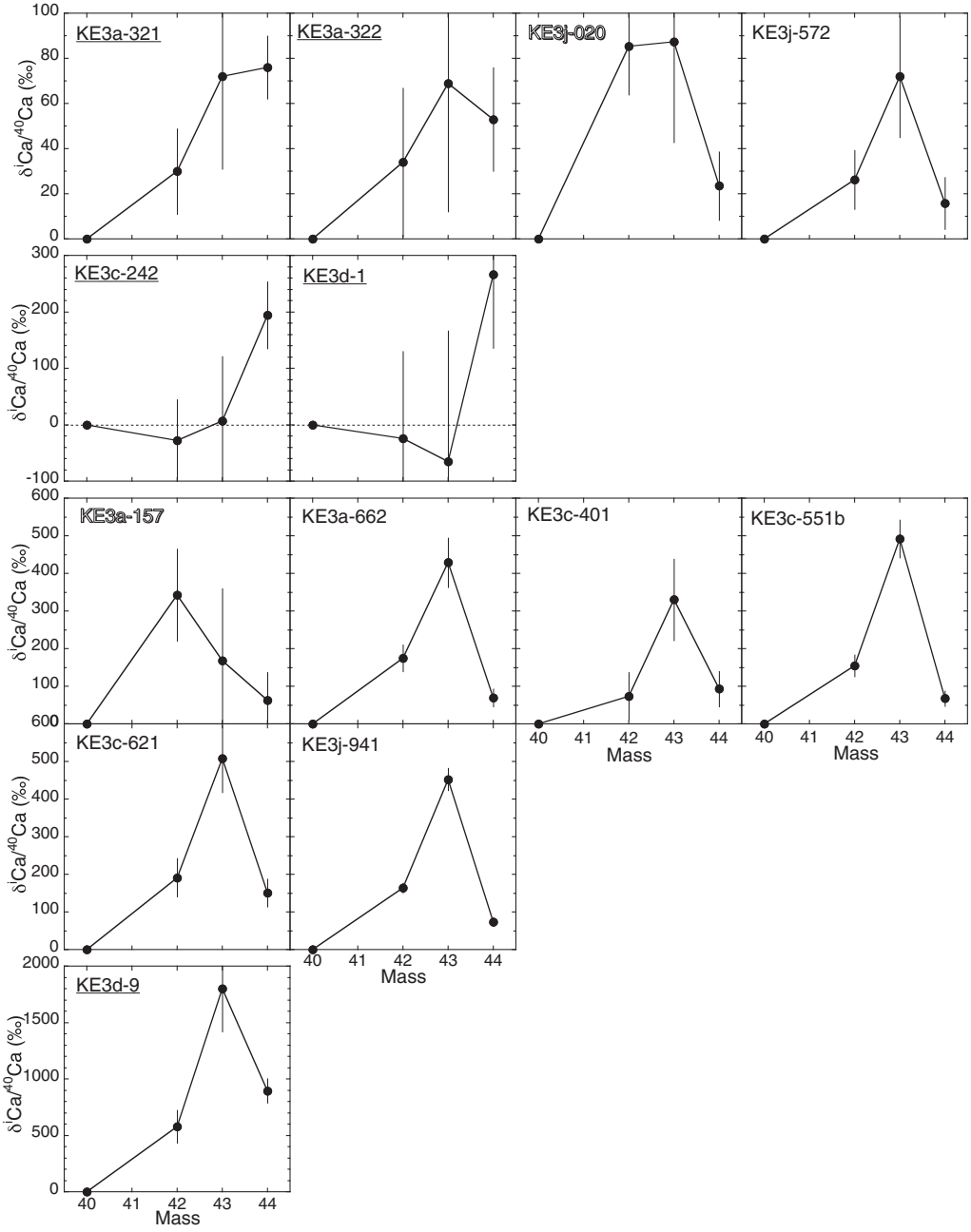

Fig. 12a. Calcium isotopic patterns, given as δ values normalized to ^{40}Ca, of graphite grains from KE3. The Ca isotopic patterns are classified into four types. For definition, see text. Part of the data have previously been published by Amari et al. (1996), Nittler et al. (1996) and Travaglio et al. (1999).

of the third dredge-up, mass loss rates increase to $\sim 10^{-5}$ $M_{\odot}$ a year and stars become proficient dust producers.

After stars undergo extensive mass loss during the superwind phase, they leave the AGB and move to the Planetary Nebula phase. It is estimated that 10–20% of all post-AGB stars experience a very late thermal pulse (VLTP) (Iben et al., 1983) that starts after H shell burning stops. The small remaining H-rich convective envelope transports protons into the hot intershell, burning H via $^{12}C(p,\gamma)^{13}N$. The amount of H in the envelope is quickly consumed and the convective H burning lasts about a month (Herwig et al., 1999). Sakurai's object (V4334 Sgr), an example of such stars, is a H-deficient, C-rich star enriched in the light *s*-process elements (Duerbeck and Benetti, 1996) and its $^{12}C/^{13}C$ ratio is quite low (4 ± 1, Pavlenko et al., 2004). This phase is estimated to last typically for 100–1000 years (Asplund et al., 1999) after which the stars return to the Planetary Nebula region in the Hertzsprung–Russell diagram and finally become white dwarfs.

Stars with mass $\geqslant 8$ $M_{\odot}$ become core-collapse supernovae and end their lives in an explosion. Supernovae are classified based on spectral features and light curves. Type II

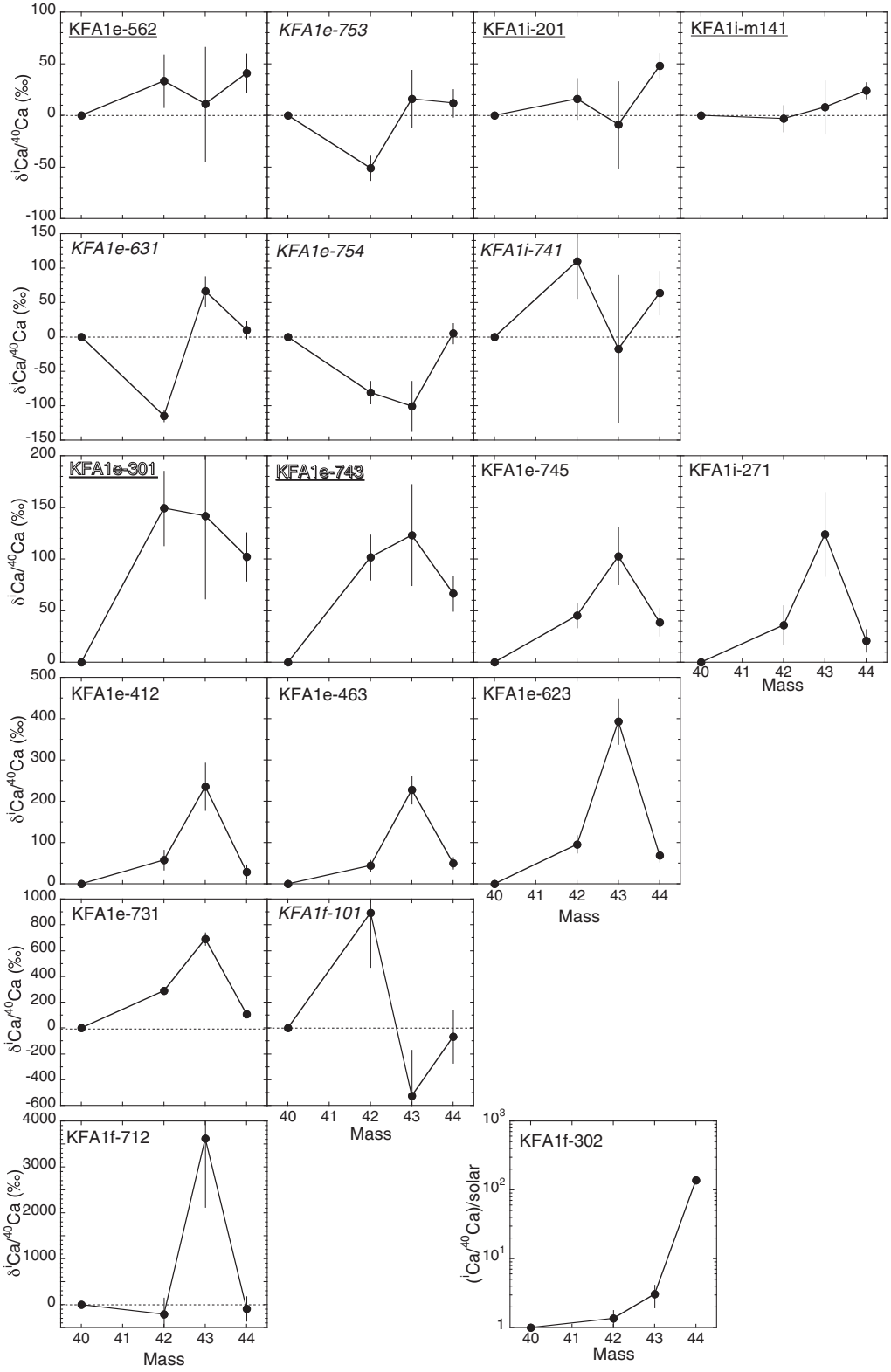

Fig. 12b. Calcium isotopic patterns, given as δ values normalized to ^{40}Ca, of graphite grains from KFA1. Part of the data have previously been published by Nittler et al. (1996).

supernovae show H features. Before explosion, they consist of different zones where different nuclear reactions had taken place. Meyer et al. (1995) named these zones according to the two most abundant elements. For example, the

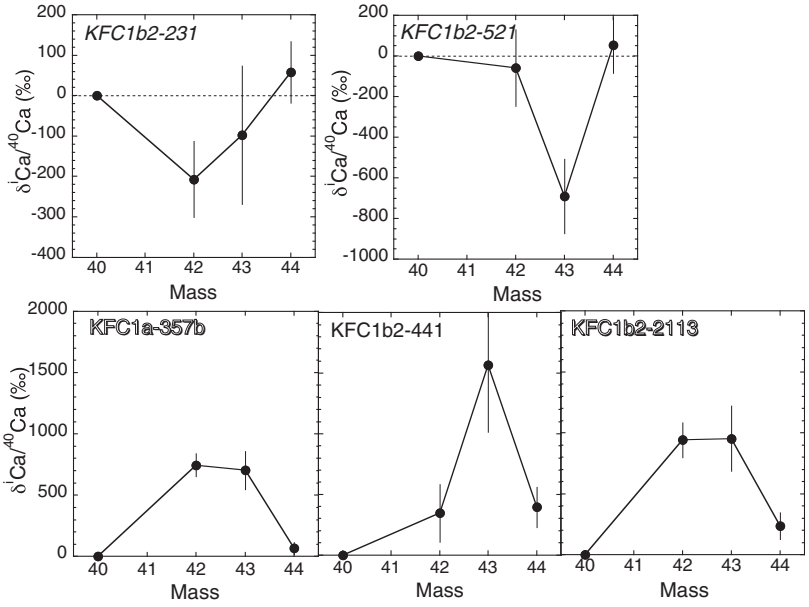

Fig. 12c. Calcium isotopic patterns, given as δ values normalized to ^{40}Ca, of graphite grains from KFC1.

zone where the CNO cycle has taken place is enriched in ^{14}N and is called the He/N zone. Beneath the zone is the He/C zone where partial He-burning occurs. Type I supernovae reveal no detectable H. Progenitors of both Type Ib and Ic supernovae are Wolf–Rayet stars. Type Ib supernovae lost the H-rich envelope, whereas Type Ic supernovae further lost most of the He/C zone before they explode.

For the discussion below, we will use the theoretical models by Rauscher et al. (2002) taken from the web (http://nucastro.org/nucleosynthesis/). We chose "Zonal Yields" among their data sets, where some of the radiogenic decays are included but the radiogenic isotopes of interest, such as ^{22}Na, ^{26}Al, ^{41}Ca and ^{44}Ti, are still alive. We will focus on the s15a28c case (Fig. 15) except as otherwise stated. It describes a 15 $M_\odot$ star with initial solar composition and an explosion energy of 1.2×10^{51} erg. The ratios in the SN model in the following sections are derived from this data set.

Pignatari et al. (2013a,b) presented models to focus on explosive burning at the bottom of the He/C zone. When the shock wave passes, the temperature of the He/C zone becomes $T > 3.5 \times 10^8$ K. At this temperature, the reaction rates of ^{16}O(α,γ)^{20}Ne, ^{20}Ne(α,γ)^{24}Mg and ^{24}Mg(α,γ)^{28}Si increase while that of ^{12}C(α,γ)^{16}O is less affected. Consequently, the bottom of the He/C zone becomes enriched in ^{12}C and ^{28}Si. One of the advantages of the models, from the perspective of reproducing the grain data, is that we do not have to invoke mixing of material at the outer He-rich zone and that of the inner Si-rich zone. However, we will not pursue the models to discuss the grain data because it will take more time to accommodate this feature into a whole network of model calculations.

4.2. KE3 and KFA1 grains: Grains from supernovae

KE3 and KFA1 grains show signatures of an origin in core-collapse supernovae as previously discussed for KE3 grains (Amari et al., 1995c, 1996; Travaglio et al., 1999; Croat et al., 2003; Stadermann et al., 2005). These grains show isotopic features of nucleosynthesis taking place in different SN zones. Oxygen-18 is produced via ^{14}N(α,γ)^{18}F($e^+\nu$)^{18}O in the He/C zone, and the ^{18}O/^{16}O ratio of this zone in a 15 $M_\odot$ star is predicted to be 1.68 (Rauscher et al., 2002). As shown in Table 7 and 70% of the KE3 grains and 42% of the KFA1 grains show ^{18}O excesses. Silicon-28 excesses, observed in many grains, reflect O-burning. ^{29,30}Si excesses are expected in the He/C zone and O-rich interior zones where neutron capture takes place. The high ^{26}Al/^{27}Al ratios of the grains, up to ~0.15, also reinforce their SN origin, because it reflects ^{25}Mg(p,γ)^{26}Al in the He/N zone where an ^{26}Al/^{27}Al ratio of 0.23 is predicted in the 15 $M_\odot$ model. The most definitive proof of their SN origin is the initial presence of ^{44}Ti because ^{44}Ti is only produced in the inner Si/S zone during explosive nucleosynthesis (Timmes et al., 1996; Travaglio et al., 1999). Therefore, the isotopic features of many KE3 and KFA1 grains, indicating contributions from different SN zones, can be qualitatively explained by a SN origin.

4.2.1. Mixing calculations to reproduce the graphite grain data

However, whether the isotopic signatures of KE3 grains as well as KFA1 grains can be quantitatively explained is another issue. Travaglio et al. (1999) carried out mixing calculations of different zones to quantitatively examine whether supernovae can account for the isotopic features of KE3 grains. They used the 15 $M_\odot$ model by Woosley and Weaver (1995), and mixed 7 different zones (excluding the H-rich envelope). Several constraints for the calculations included the C/O ratio of the mix (1, in a few cases, 3), the N amount from the He/N zone that should be mixed (1/20 of the N yield), and the ^{12}C/^{13}C ratios of the mix (5–10^4). They concluded that, if jets of material from the

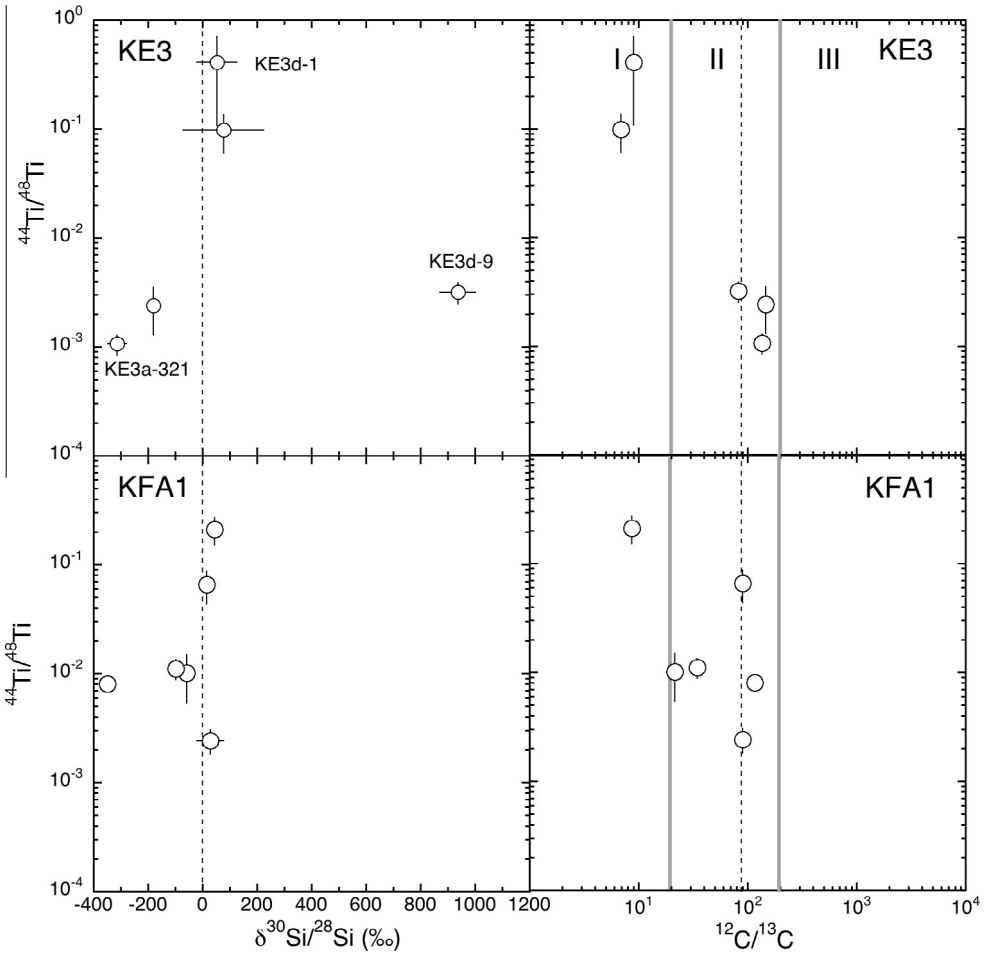

Fig. 13. $^{44}Ti/^{48}Ti$ ratios inferred from the $^{44}Ca/^{40}Ca$ and Ca/Ti ratios are plotted against $\delta^{30}Si/^{28}Si$ values and $^{12}C/^{13}C$ ratios. Eight out of 11 grains are Population II grains. Part of the data have previously been published by Nittler et al. (1996) and Travaglio et al. (1999).

Si-rich inner zone penetrate the intermediate O-rich zones and are mixed with the outer C-rich zone, the general features of the KE3 grains, namely $^{12}C/^{13}C$, $^{16}O/^{18}O$, $^{30}Si/^{28}Si$ and ^{44}Ti and ^{41}Ca can be reproduced.

Yoshida and Hashimoto (2004) adopted the 15 $M_\odot$ model by Nomoto and Hashimoto (1988). They considered two mixing cases involving the He/N, He/C and two additional zones (one case with the O/Ne and Si/S zones, the other with the Si/S and Ni zones), in an attempt to reproduce the isotopic features of 11 SiC X grains, as well as 3 KE3 and 1 KFA1 grains with evidence for initial ^{44}Ti, and could reproduce 3–4 isotopic ratios of 6 grains. Jadhav et al. (2013a) selected a few Orgueil graphite grains and mixed all zones of the 15 $M_\odot$ star model by Rauscher et al. (2002) to match as many isotopic ratios of these grains as possible.

We also performed mixing calculations of different zones. Mixing of SN ejecta and grain formation therein involve many complicated processes which we do not know in any detail. Furthermore, studies of SiC grains of a SN origin indicate that elemental fractionation takes place in SN ejecta. Marhas et al. (2008) reported that elemental fractionation between Si and Fe in the Si/S zone and fractionation between Ni and Fe in the He/C and He/N zones were required to explain their data on SiC X grains. Hoppe et al. (2012) also found that fractionation between Si and S was necessary to account for the S-isotopic compositions of SN SiC grains of type C. Therefore, we will not aim to explain all the isotopic ratios, but try to explain a few essential features of the SN graphite grains.

Supernova grains are abundant among KE3 and KFA1 grains (Table 7). Among the Populations, Population II contains most ^{18}O-rich grains in KE3, KFA1 and KFB1, showing that SN grains with $20 \leqslant {}^{12}C/^{13}C \leqslant 200$ are quite abundant throughout the whole density range except in KFC1, where there are hardly any ^{18}O-rich grains.

In the 15 $M_\odot$ SN model by Rauscher et al. (2002), the $^{12}C/^{13}C$ ratio of the He/C zone is predicted to be 2×10^5 and that of the He/N zone to be 4. Although a wide range of $^{12}C/^{13}C$ ratios, including ratios between 20 and 200, can be reproduced by mixing of these two zones with their extreme $^{12}C/^{13}C$ ratios, the presence of many SN grains in Population II indicates that the H-rich envelope with a $^{12}C/^{13}C$ ratio of 17 and/or material in the stellar wind with a $^{12}C/^{13}C$ ratio of 22, might also have contributed to the mix.

We performed mixing calculations of the He/C, He/N zones and the H-rich envelope in an attempt to reproduce

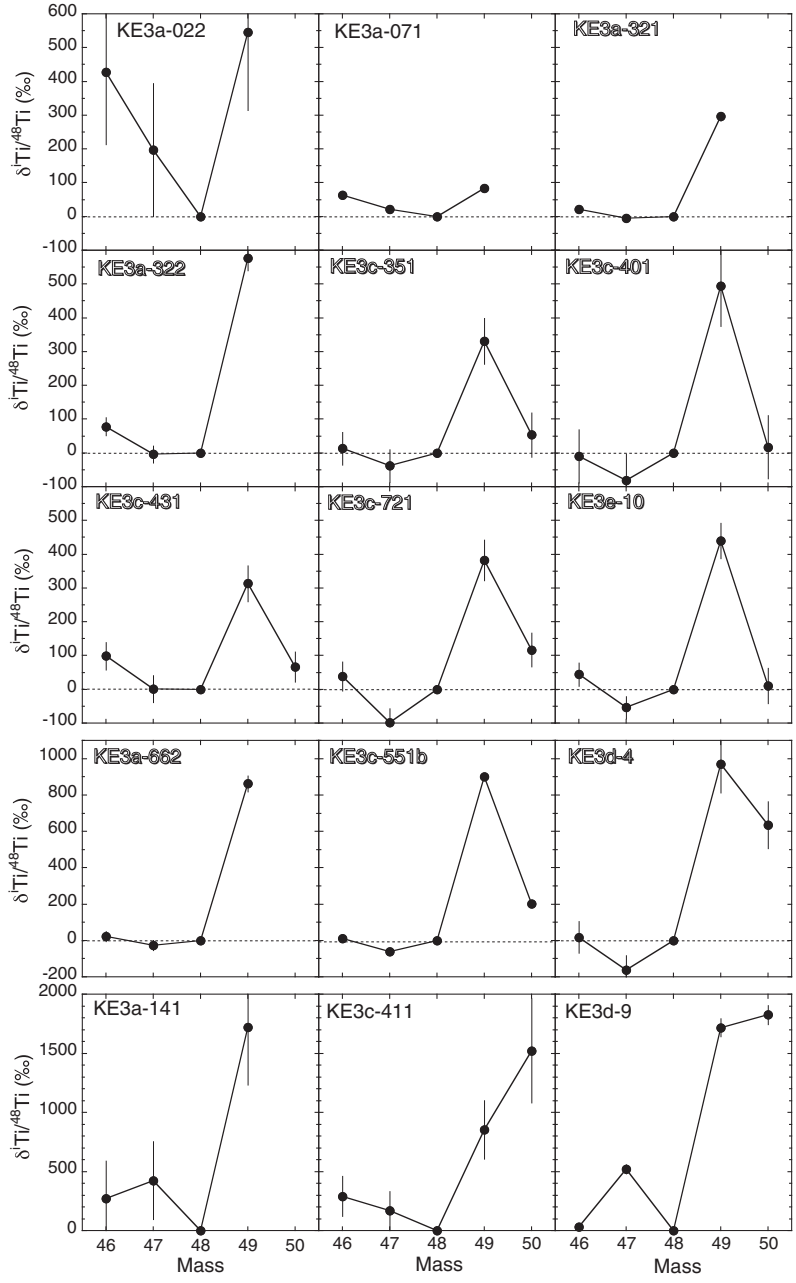

Fig. 14a. Titanium isotopic patterns, given as δ values normalized to ^{48}Ti, of graphite grains from KE3. In grains where ^{50}Ti is lacking in the plots, ^{50}Ti was not analyzed or it was overwhelmed by ^{50}Cr. The Ti isotopic patterns are classified into three types. For definition, see text. Part of the data have previously been published by Amari et al. (1995c, 1996), Nittler et al. (1996) and Travaglio et al. (1999).

the observed isotopic ratios. As mentioned earlier, we have evidence that elemental fractionation takes place in SN ejecta (Marhas et al., 2008; Hoppe et al., 2012), and that in many graphite grains Ti is carried by TiC subgrains (Bernatowicz et al., 1996; Nittler et al., 1996; Croat et al., 2003; Stadermann et al., 2005), which might have formed under conditions that were different from those under which the host graphite grains formed. Therefore, we focused on a few elements that might have been least affected by such fractionation. We chose C, O and Al for the mixing calculations. Carbon is the major element, thus it had to be present in the gas when the grains formed. The abundance of oxygen is critical for carbon grain formation. Under normal circumstances, C-rich conditions (C > O) are required for carbonaceous grain formation and we assumed that C-rich conditions are required for grain formation in SN environments. Since graphite grains of a likely SN origin have O isotopic anomalies, O must have been present in the ejecta where grains formed. Aluminum is refractory and is relatively abundant in graphite along with N (Hoppe et al., 1995) and a high ^{26}Al/^{27}Al ratio is a signature of the He/N zone.

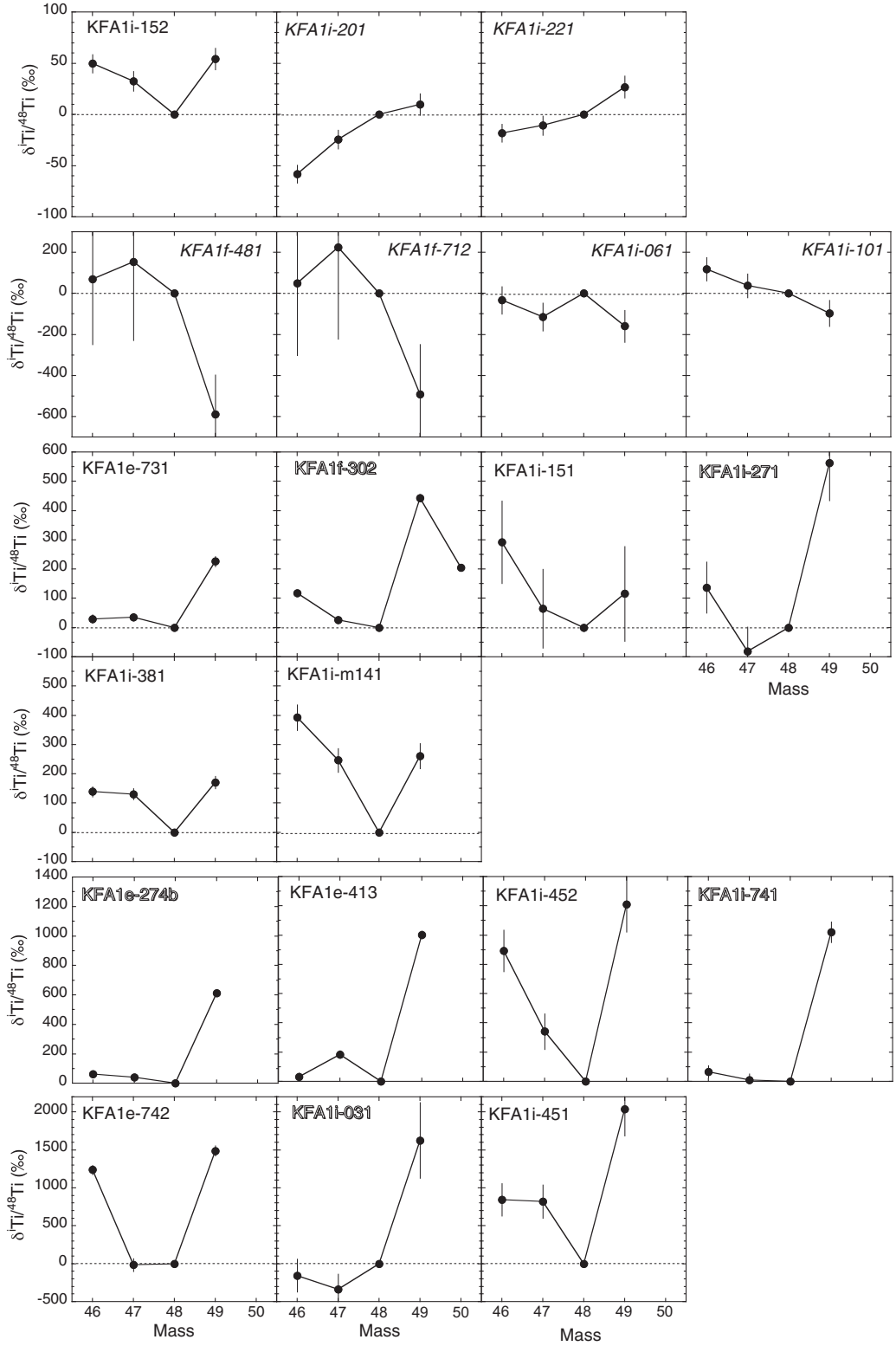

Fig. 14b. Titanium isotopic patterns, given as δ values normalized to ^{48}Ti, of graphite grains from KFA1. Part of the data have previously been published by Nittler et al. (1996).

We considered only the KE3 grains for comparison with mixing results (Fig. 16a). The reason is that one of the KFA1 mounts, the KFA1e mount, was heavily contaminated, most notably with a huge amount of isotopically normal Ca. Therefore, other isotopic ratios, including O and Al, might also have been compromised. Although there is a scatter in the KE3 grain data, we observe a trend (Fig. 16a): the ^{18}O/^{16}O ratios of the grains increase with

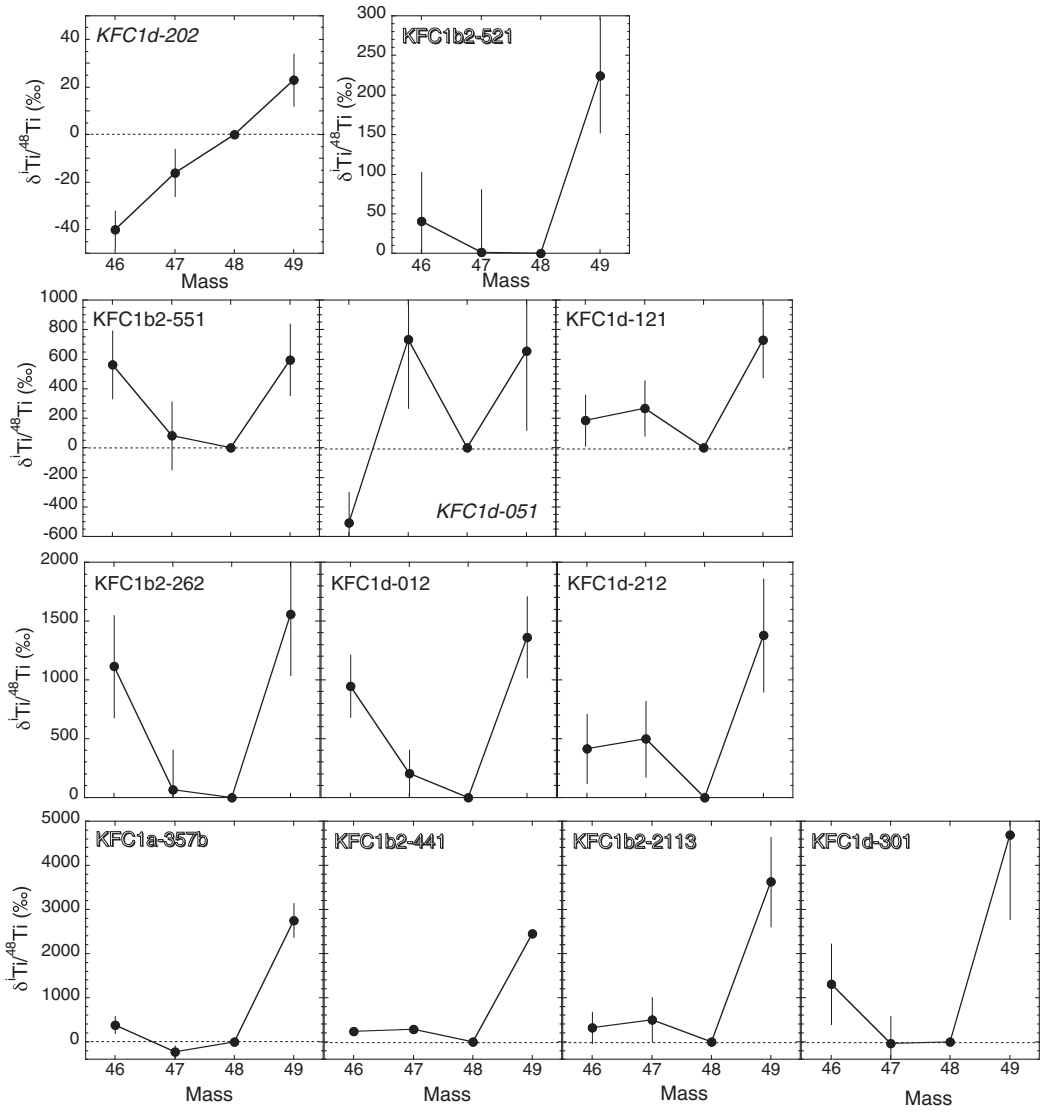

Fig. 14c. Titanium isotopic patterns, given as δ values normalized to ^{48}Ti, of graphite grains from KFC1.

population according to Population I < Population II < Population III. The Population III grains have high ^{18}O/^{16}O and ^{26}Al/^{27}Al ratios. The Population II grains have a range of ^{18}O/^{16}O ratios and ^{26}Al/^{27}Al ratios. The Population I grains show the lowest ^{18}O/^{16}O and ^{26}Al/^{27}Al ratios among the three Populations. A few Population I grains have solar ^{18}O/^{16}O ratios. We note that the fraction of ^{18}O-rich Population I grains is 37%. Since more than half of the grains may not be SN grains, grains with a solar ^{18}O/^{16}O ratio should not be considered for the mixing calculations.

To reproduce these trends, we mixed three zones [He/C, He/N and H-rich envelope, results are shown with solid symbols in Fig. 16b], as well as four zones (these three and O/C, shown with open symbols) of the 15 $M_{\odot}$ star model, assuming C > O. We mixed entire zones to calculate the composition of a zone. It is oversimplification because isotopic yields sometimes change rapidly in a zone (see ^{26}Al and ^{28}Si in the O/Ne zone in Fig. 15). However, if we had taken more restricted layers and mix them, we would have had infinite complexity. The symbols in Fig. 16b indicate different Populations for the mix based on the ^{12}C/^{13}C ratio. For example, circles indicate mixtures with ^{12}C/^{13}C ratios within the range defined for Population II. Diamonds and squares are for ^{12}C/^{13}C ratios within the ranges for Population I and III, respectively.

Along a given track, the mass fraction of the He/C zone, as well as that of the O/C zone for the four-zone mixing, is kept constant while the relative fractions of the other zones are changed. The tracks converge at the region of high ^{26}Al/^{27}Al and ^{18}O/^{16}O ratios. One may wonder why high ^{26}Al/^{27}Al, a signature of the He/N zone, and high ^{18}O/^{16}O, a signature of the He/C zone, appear together in the mix. It is because in a track, the relative proportions of the He/N zone and the H-rich envelope are changed. As the track moves toward the region of high ^{26}Al/^{27}Al and ^{18}O/^{16}O ratios, the proportion of the He/N zone in the mix increases. However, the ^{16}O yield in this zone is

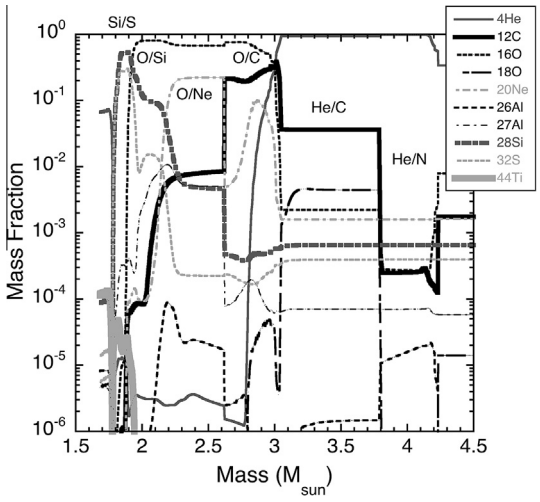

Fig. 15. Mass fractions of isotopes for a 15 $M_{\odot}$ SN model of solar composition by Rauscher et al. (2002). Plotted are the s15a28c case in Zonal Yields, abundances 25,000 seconds after the core bounce. The names of the zones, coined by Meyer et al. (1995), indicate the two most abundant elements.

the lowest among the 3 (or 4) zones of the mixing. Therefore, as the amount of the contribution of the He/N zone increases, the relative proportion of ^{16}O decreases, resulting in high $^{18}O/^{16}O$ ratios, a feature of the He/C zone.

The isotopic ratios of grains from Population III can be explained by the mixing. To achieve the high $^{12}C/^{13}C$ ratios observed in the Population III grains, a substantial amount of material from the He/C zone is required, which makes the mix C-rich. Therefore, it is possible to include material from the O-rich O/C zone with varying proportions and still keep the mix C-rich.

The Population II grains with high $^{18}O/^{16}O$ ratios can also be explained by the mixing. However, Population II grains with $^{18}O/^{16}O < 4 \times 10^{-2}$, which constitute a significant portion, cannot be reproduced by the mixing: since the ^{18}O content of the He/C zone is so high (4×10^{-3} in mass fraction. Fig. 15), a significant amount of ^{16}O is needed to lower the $^{18}O/^{16}O$ ratio, but this makes the mix O-rich. The situation is worst for the Population I grains. Only a small amount of material from the He/C zone can be in the mix to reproduce their low $^{12}C/^{13}C$ ratios, which means that the bulk of material in the mix is from the He/N zone with C/O = 0.97. However, even with a small amount of material from the He/C zone, the $^{18}O/^{16}O$ ratios of the mix are still $>10^{-2}$, and ^{16}O from other zones cannot lower the $^{18}O/^{16}O$ ratios if we keep C-rich conditions.

It has been proposed that carbonaceous grains can form in an O-rich SN environment (Clayton et al., 1999, 2001; Clayton, 2011): abundant and stable CO molecules are dissociated by energetic electrons produced by Compton scattering of gamma-rays from ^{56}Co ($T_{1/2} = 77$ d), making C available for graphite formation. However, it is not clear whether this scenario would work, even from the abundance of ^{56}Co alone. The ^{56}Co yield in the Ni zone ranges from 0.80 to 0.86 by mass fraction. In the Si/S zone, it changes from 0.88 down to 1.4×10^{-5}. It is even lower in the O/Si zone, falling from 1.0×10^{-5} to 4.6×10^{-8}. The ^{56}Co yields are even lower in the outer zones. Carbon, the major element of graphite, is abundant in the outer He-rich zones, where ^{56}Co is hardly present (the ^{56}Co yield in He/C: 3.4×10^{-8} to 8.9×10^{-14}). Even if extensive mixing between the innermost zone and the outer He-rich zones takes place, it is not clear whether or not a large amount of ^{56}Co can be mixed into the gas from which graphite forms. Furthermore, dust formation is usually detected a few hundred days after the explosion. In SN 1987A infrared (4–13 μm) continuum radiation was observed on day 350 and it was attributed to dust formation in the ejecta (Meikle et al., 1993). If we assume that grain formation started a few hundred days after the explosion, the ^{56}Co abundance in SN

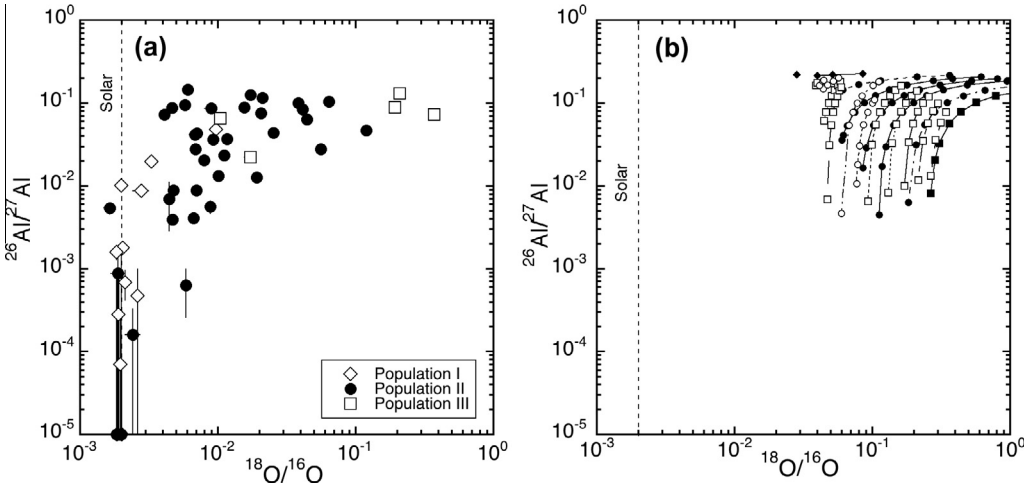

Fig. 16. $^{26}Al/^{27}Al$ and $^{18}O/^{16}O$ ratios in (a) KE3 grains and (b) mixtures of the He/C, He/N and the H envelope (solid symbols) and those with the O/C zone added (open symbols) from 15 $M_{\odot}$ SN model by Rauscher et al. (2002). For a given track, the contribution from the He/C zone (for the three-zone mixing) as well as the contribution from the O/C zone (for the four-zone mixing) are kept constant while the relative contributions from the other zones to the mixture vary. Diamonds, circles and squares indicate the ranges of $^{12}C/^{13}C$ ratios of Populations I, II and III, respectively, corresponding to the symbols in (a).

ejecta would be essentially close to zero. Therefore, it still remains to be seen whether carbonaceous grains form in an O-rich SN environment and in this study we assume that graphite forms in a C-rich environment.

4.2.2. Other isotopic signatures

As already mentioned, we have evidence of elemental fractionation in SN ejecta (Marhas et al., 2008; Hoppe et al., 2012). Therefore, for isotopic ratios of elements other than C, O and Al, we will discuss which zones contributed to grain formation but we will not attempt to quantitatively reproduce the isotopic ratios of the grains.

4.2.2.1. Magnesium. Magnesium-25 is depleted in the He/N zone ($\delta^{25}Mg/^{24}Mg = -917‰$) because it is destroyed via $^{25}Mg(p,\gamma)^{26}Al$, which yields a high $^{26}Al/^{27}Al$ ratio (0.23). The He/C zone still shows a ^{25}Mg deficit ($\delta^{25}Mg/^{24}Mg = -509‰$). In the O/C zone, it is produced via $^{22}Ne(\alpha,n)^{25}Mg$ but destroyed via $^{25}Mg(n,\gamma)^{26}Mg$. The net result is production of both isotopes ($\delta^{25}Mg/^{24}Mg = 21{,}500‰$, $\delta^{26}Mg/^{24}Mg = 19{,}900‰$). The ^{25}Mg yield significantly increases at the bottom of the He/C zone. Magnesium-25 excesses are observed mostly in Population II grains from KE3 (Fig. 7). In KFA1, ^{25}Mg excesses in Population I grains are higher than those in Population II grains. There is only one Population I grain each from KFB1 and KFC1 that shows an excess. We note that in KE3 and KFA1 all ^{25}Mg anomalies are excesses, not deficit, indicating a contribution from the bottom of the He/C zone and/or the O/C zone. It is puzzling that the Population I grains from KFA1 show the excesses. To keep low $^{12}C/^{13}C$ ratios, a significant amount of material from the He/N zone is required, where ^{25}Mg is depleted. This is yet another indication that elemental fractionation can take place in SN ejecta.

4.2.2.2. Silicon. Many KE3 grains and a few KFA1 grains show ^{28}Si excesses (Fig. 10). Hydrostatic and explosive O burning produce ^{28}Si, thus the Si in the Si/S zone is almost pure ^{28}Si ($\delta^{29}Si/^{28}Si = -985‰$, $\delta^{30}Si/^{28}Si = -998‰$). These grains must have had contributions from the Si/S zone. As discussed by Travaglio et al. (1999), an addition of a small amount of material from the inner Si-rich zones to material in the outer He-rich zones can explain the observed ^{28}Si excesses.

On the other hand, $^{29,30}Si$ excesses, due to neutron capture, are predicted for the He/C, O/C and O/Ne zones (^{30}Si excess only in the O/Si zone). The excesses are relatively small in the He/C zone ($\delta^{29}Si/^{28}Si = 244‰$, $\delta^{30}Si/^{28}Si = 244‰$), but those in the O/C ($\delta^{29}Si/^{28}Si = 5600‰$, $\delta^{30}Si/^{28}Si = 11{,}400‰$) and O/Ne ($\delta^{29}Si/^{28}Si = 4790‰$, $\delta^{30}Si/^{28}Si = 3550‰$) zones are much larger. The $\delta^{29}Si/\delta^{30}Si$ ratios in the He/C and O/Ne zones are 1 and 1.35, respectively, while the $\delta^{29}Si/\delta^{30}Si$ ratio in the O/C zone is only 0.49. All the $^{29,30}Si$-rich grains plot on a line through the origin whose slope (1.39) is close to the former values. The $\delta^{29}Si/\delta^{30}Si$ ratio of KE3d-9 is 1.36 ($\delta^{29}Si/^{28}Si = 1272 \pm 75‰$, $\delta^{30}Si/^{28}Si = 937 \pm 66‰$), almost a perfect match for Si from the O/Ne zone. Silicon-28 excesses are observed in KE3 grains from all three Populations, while $^{29,30}Si$ excesses are observed in Population II grains. Interestingly, SiC grains of type C (Hoppe et al., 2010), which most likely originated from core-collapse supernovae, show similar $^{29,30}Si$ excesses. Pignatari et al. (2013b) investigated SN models with different shock velocities and found that $^{29,30}Si$ excesses can be produced in the outer He/C zone when the shock velocities are less than a factor of four of the standard initial shock velocity (2×10^9 cm/s). With these models, there is no need to invoke a small addition of material from inner Si-rich zones or elemental fractionation in the ejecta.

4.2.2.3. Calcium. $^{41}Ca/^{40}Ca$ ratios of $1.15–2.17 \times 10^{-2}$ are predicted for the He/C, O/C and O/Ne zones, where neutron capture produces ^{41}Ca. These ratios are in line with the observed grain data where ratios range from 1.01×10^{-3} to 2.52×10^{-2} (Table 4b and Fig. 11). In the O/Si and Si/S zones, the ^{41}Ca yields are higher than in the outer zones, but the ^{40}Ca yields are also higher, lowering the $^{41}C/^{40}Ca$ ratios to 4.16×10^{-3} and 2.78×10^{-4} in the O/Si and Si/S zones, respectively.

In the 15 $M_\odot$ model, the Ca isotopic patterns predicted for various zones (Fig. 17a) can explain the observed Ca isotopic patterns (Figs. 12a and 12b). In the He/C zone, ^{42}Ca and ^{43}Ca show similar excesses along with a much smaller ^{44}Ca excess. This pattern is seen in the grains of the first type described in Section 3.12. In the O/C and O/Ne zones, ^{43}Ca has the highest enrichment, followed by ^{42}Ca and ^{44}Ca, a pattern defined as the second type. The ratios of the number of grains of the first type to that of the second type in KE3 and KFA1 are comparable (2/6 and 2/7, respectively). Since the grains of the second type are more abundant than those of the first type, contribution of Ca from the O-rich zone is widely seen in the KE3 and KFA1 grains.

4.2.2.4. Titanium. Titanium-44, definite proof of a SN origin of a few grains, is produced in the alpha-rich freezeout (Jordan et al., 2003, about alpha-rich freezeout) and its yield is sensitive to explosion mechanisms. Nagataki et al. (1997) performed explosive nucleosynthesis calculations of axisymmetrically deformed supernovae and found that $^{44}Ti/^{56}Ni$ ratios were enhanced by a stronger alpha-rich freezeout in the polar region. This can explain the high $^{44}Ti/^{56}Ni$ ratio in Cassiopeia A, which is known to have an asymmetric shape of the remnant (Nagataki et al., 1998). In the 15 $M_\odot$ star model by Rauscher et al. (2002), the $^{44}Ti/^{48}Ti$ ratio is 0.36 in the Ni zone, it decreases to 5.45×10^{-2} in the Si/S zone and it increases again to 1.76 in the 1.91–1.96 $M_\odot$ region due to the decrease of the ^{48}Ti yield, then it quickly goes down in the rest of the O/Si zone to 6.88×10^{-4}. These ratios in the ^{28}Si-rich zones are in line with the grain data (Fig. 13). However, only 5 out of 11 grains with ^{44}Ti are enriched in ^{28}Si. Five other grains have normal Si isotopic composition within their errors and KE3d-9 shows huge enrichments in $^{29,30}Si$. Titanium, in most cases, is carried by TiC subgrains. Since host graphite grains and TiC subgrains do not necessarily have to form from the same mixture, this lack of correlation between ^{44}Ti and ^{28}Si does not pose a puzzle. Croat et al. (2003) found significant variations in the V/Ti ratio among TiC

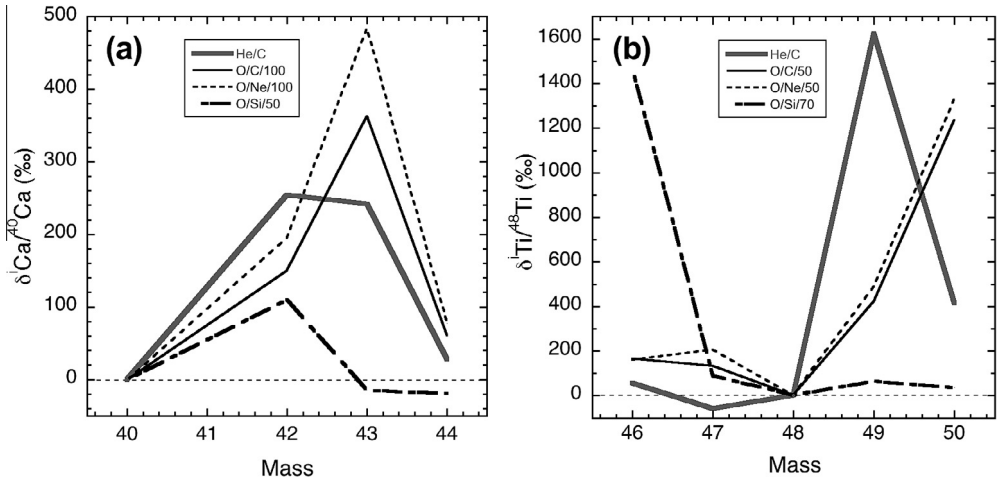

Fig. 17. Predicted isotopic patterns of (a) Ca and (b) Ti in different zones of a 15 $M_{\odot}$ star of solar composition (Rauscher et al. model s15a28c). The isotopic delta values of the zones are divided by the numbers after the zone names so that the patterns fit into the plot. The patterns in the O/C and O/Ne zones are similar for both Ca and Ti.

subgrains within the same graphite host and concluded that TiC subgrains had diverse histories. In addition, Si might be dominated by contamination. We note that 8 out of the 11 grains with ^{44}Ti are in Population II.

The Ti in the He/C zone is characterized by large excess in ^{49}Ti (2.6 times solar ^{49}Ti/^{48}Ti ratio), small excess in ^{46}Ti, a slight deficit in ^{47}Ti, and modest excess in ^{50}Ti (1.4 times solar ^{50}Ti/^{48}Ti ratio) (Fig. 17b). The O/C and O/Ne zones show similar Ti isotopic patterns: the largest excess is found in ^{50}Ti, followed by that in ^{49}Ti. The ^{46}Ti and ^{47}Ti excesses are smaller than ^{49}Ti excess, but they are much larger than those of Ti in the He/C zone.

There are similarities between the grain data and the predicted Ti patterns from the He/C, O/C (or O/Ne) zones (Figs. 14a and 14b). The grains classified into the first group have an isotopic pattern similar to that in the He/C zone. Fifteen (10 KE3 and 5 KFA1) grains fall into this group. (We note that these numbers have some uncertainties: not all grains have the ^{50}Ti/^{48}Ti ratios and a few grains have large errors. Even with these uncertainties, we could identify a trend in KE3 and KFA1.) The grains in the second group have Ti patterns similar to that in the O/C or O/Ne zone. Fourteen (5 KE3 and 9 KFA1) grains are in this group. Since the grains of the first group are more abundant in KE3 and those of the second group are more represented in KFA1, the KE3 grains received a substantial contribution of Ti from the He/C zone while the KFA1 grains received from the O/C and O/Ne zone.

A closer inspection reveals that it is not possible to reproduce all the observed patterns with the model if we mix entire zones. The ^{47}Ti excess that is larger than the ^{46}Ti excess is observed in the O/Ne zone (δ^{46}Ti/^{48}Ti = 7960‰, δ^{47}Ti/^{48}Ti = 10,300‰), but the pattern does not explain the ^{47}Ti excesses in KE3d-9 and KFA1e-413.

If we consider more restricted zones than the entire O/C and He/C zones, we may be able to better reproduce the grain data. Titanium isotopic yields significantly change at the bottom of the He/C zone and the outer part of the O/C zone in the model. The ^{46}Ti yield sharply decreases while the ^{47}Ti yield increases in the outer layers of the O/C zone, where He burning still take place and the He mass fraction rapidly decreases. Fig. 18 shows Ca and Ti isotopic patterns of a mix of the C-rich O/C zone and the bottom of the He/C zone with different proportions. The C-rich O/C zone (2.97–3.04 $M_{\odot}$), without contribution from the He/C zone, shows the largest Ca and Ti excesses. As the contribution from the He/C zone increases (2.97–3.11 $M_{\odot}$ and 2.97–3.49 $M_{\odot}$), the excesses decrease. The Ca isotopic patterns remain the same, showing the characteristic of the O/C zone, whereas the Ti isotopic patterns change. The ^{47}Ti excess that is larger than the ^{46}Ti excess, found in KE3d-9 and KFA1e-413, is observed in the C-rich O/C zone (δ^{46}Ti/^{48}Ti = 308‰, δ^{47}Ti/^{48}Ti = 2540‰). However, the δ^{49}Ti/δ^{47}Ti ratio (12.7, δ^{49}Ti/^{48}Ti = 32,200‰) is much higher than those of KE3d-9 and KFA1e-413 (3.3 and 5.4, respectively). KE3d-4 and KFA1f-302, classified as members of the first group, show much larger ^{50}Ti excesses than what is predicted in the He/C zone. The 2.97–3.49 $M_{\odot}$ case (Fig. 18b) has comparable ^{49}Ti and ^{50}Ti excesses (δ^{49}Ti/^{48}Ti = 3030‰, δ^{50}Ti/^{48}Ti = 2130‰). Thus, a small amount of material from the O/C zone can explain their patterns.

As shown above, the C-rich O/C zone and the bottom of the He/C zone may be able to explain a variety of the Ti isotopic patterns in the grains although it is still remains to been seen: the lack of ^{50}Ti/^{48}Ti ratios in a few grains makes it hard to fully evaluate and compare their Ti isotopic patterns with the models.

There are grains in KFA1 that show negative delta values (Fig. 14b). Except for five grains have huge uncertainties, KFA1i-201 has negative δ^{46}Ti and δ^{47}Ti values with small errors. This suggests that the grain contains a small amount of Ti originating from the Si/S and/or Ni zones (<1%) because these two zones are depleted in ^{46}Ti, except for the outer layers of the Si/S zone, which are extremely rich in ^{46}Ti, and ^{47}Ti.

We note that only a handful of grains (2 KE3 and 2 KFA1 grains) show the Ca pattern from the He/C zone

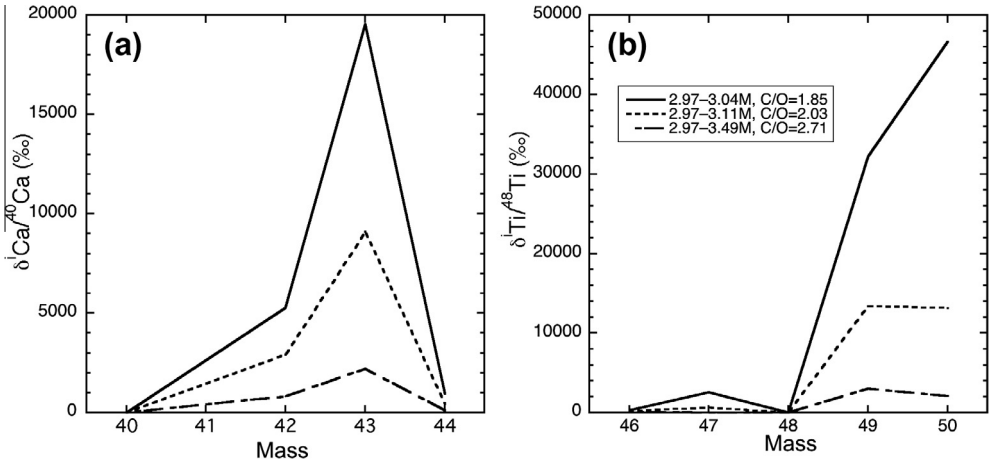

Fig. 18. Isotopic patterns of (a) Ca and (b) Ti of the C-rich O/C zone and the bottom of the He/C zone with various proportions. Mixed zones and the C/O ratios of the mixtures are shown in the legend in (b).

but a quite a few grains (10 KE3 and 5 KFA1 grains) with a Ti pattern from the He/C zone. As we have already seen for other elements, Ca and Ti did not always originate from the same zone. For example, KE3c-401 and KE3c-551b have Ca from the O/C zone and Ti from outer regions of the He/C zone. Calcium seems to be uniformly contained in the grains, while Ti, in most cases, is carried by TiC subgrains. Host graphite grains and the subgrains inside them might have different formation histories and the latter were incorporated into the former, demonstrating that mixing and grain formation in SN ejecta are complex.

In summary, the isotopic signatures of the KE3 and KFA1 grains can be qualitatively explained by SN model calculations, confirming that these grains formed in core-collapse supernovae. We took the 15 $M_{\odot}$ model (Rauscher et al., 2002) with which to compare the grain data. However, reproducing the isotopic ratios of these grains by uniformly mixing different layers of the 15 $M_{\odot}$ star does not work for many elements if material from different zones is mixed without elemental fractionation. Mixing more restricted layers may be able to better reproduce the isotopic ratios of the grains.

It should be noted that presolar oxides and silicates of SN origin have also been identified. Presolar oxides and silicates are classified into 4 groups according to their O isotopic compositions (Nittler et al., 1997). Grains of Groups 1, 2 and 3 formed in red giants or AGB stars. Group 4 grains, comprising 7.3% of presolar oxides and silicates (from the presolar grain database, Hynes and Gyngard, 2009), show higher-than-solar $^{18}O/^{16}O$ ratios and $^{17}O/^{16}O$ ratios that are moderately higher than solar or close-to-solar. These grains, although initially suggested to have formed in red giants and/or AGB stars with higher than solar metallicity (Nittler et al., 1997), most likely formed in core-collapse supernovae (Choi et al., 1998; Nittler et al., 2008) and received their ^{18}O from the He-C zone. Choi et al. (1998), Nittler et al. (2008) and Haenecour et al. (2013) performed SN mixing calculations in order to explain the O isotopic compositions of corundum, hibonite, spinel, and silica grains whose O isotopic ratios range up to 2.26 × solar for $^{17}O/^{16}O$ and 3.3 × solar for $^{18}O/^{16}O$. They could reproduce the grain's O isotopic compositions with varying mixtures from the O/C, He/C, He/N zones and the H-rich envelope. It is interesting that silicates and oxides, which condense in O-rich conditions (silicates also form in C-rich conditions although most of them form in O-rich conditions, for details, see Lodders and Fegley, 1997), show ^{18}O excesses, the same signature as that of SN graphite grains. Since except H and He, ^{16}O is the most abundant isotope in supernovae, one would expect that there are many more ^{16}O-rich SN oxides and silicates, but only two ^{16}O-rich SN oxide grains (e.g., Nittler et al., 1998; Gyngard et al., 2010a) have been found. Even if ^{16}O-rich oxides and silicates formed in the O-rich ejecta, most of them might have been destroyed by the reverse shock because they must have experienced a lot more gas-grain collision compared with grains formed in the outer zone. Another possibility is that because of high nucleation density, grains from ^{16}O-rich layers are extremely small and have either been destroyed or have not been detected. This may be the reason why most of the SN oxides and silicates in meteorites are ^{18}O-rich, which formed in the outer zones of supernovae.

4.3. KFB1 and KFC1 grains: Grains from AGB stars

Only a handful of grains in KFB1 and, to a lesser extent, KFC1, show SN signatures such as ^{18}O and ^{28}Si excesses and high $^{26}Al/^{27}Al$ ratios. Many grains in these fractions have isotopic properties different from those of KE3 and KFA1 grains.

4.3.1. $^{12}C/^{13}C$ ratios and s-process $^{86}Kr/^{82}Kr$ in KFB1 and KFC1

Amari et al. (1995b) pointed out that excesses in $^{29,30}Si$ in a few KFC1 grains indicate that they formed in low-mass low-metallicity AGB stars. Krypton isotopic ratios of KFC1 obtained from bulk noble gas analysis also indicate that KFC1 grains originated in low-metallicity AGB stars

($Z \leqslant 0.002$) (Amari et al., 1995a). Bernatowicz et al. (1996) and Croat et al. (2005) examined slices of 70-nm-thick KFC1 graphite slices by TEM and found that TiC subgrains inside the graphite grains are highly enriched in the *s*-process elements Zr, Mo, and Ru. Nicolussi et al. (1998) analyzed Mo and Zr isotopic ratios of 32 KFC1 grains with resonant ionization mass spectrometry and found *s*-process signatures in 8 grains, concluding that they formed in thermally-pulsing AGB stars. Meier et al. (2012) analyzed He and Ne in single KFC1 grains and found evidence that some of the grains originated from low-mass low-metallicity AGB stars. Heck et al. (2009a) analyzed He and Ne in 51 KFB1 grains that had been analyzed for their $^{12}C/^{13}C$ and $^{18}O/^{16}O$ ratios and concluded that grain KFB1g-34-4 formed in a low-mass AGB star with half-solar metallicity.

Here we examine the bulk Kr data of KFB1 and KFC1 (Amari et al., 1995a) and the C isotopic distribution of KFB1 and KFC1 grains, compare them with model calculations for the He-shell and the envelope of AGB stars with a range of masses (1.5, 2, 3 and 5 $M_\odot$) and metallicities ($Z = 3 \times 10^{-3}$, 6×10^{-3}, 1×10^{-2} and 2×10^{-2}), and discuss stellar sources of these grains. The models we are employed are briefly described by Bisterzo et al. (2010): the s-process nucleosynthesis is based on a post-process method based on full evolutionary models (Straniero et al., 2006). These models use the neutron capture cross sections published in 2009, which are complied in the KADoNiS Nuclear Database (http://www.kadonis.org/), and the revision of the solar abundance by Lodders et al. (2009).

KFB1 and KFC1 grains have similar C isotopic distributions, with two distinct peaks, one with $^{12}C/^{13}C$ ratios around 10, the other with ratios around 400–630 (500–630 for KFB1 and 400–500 for KFC1) (Fig. 4). In this section we will focus on the grains belonging to the second peak. The origin of grains with low $^{12}C/^{13}C$ ratios ($\leqslant$20) will be discussed in the next section.

Table 8 summarizes the results of the AGB model calculations. It lists the amount of ^{13}C-pocket, the total number of pulses, the range of $^{12}C/^{13}C$ ratios of the C-rich envelope, the C/O ratio after the last thermal pulse, and $^{86}Kr/^{82}Kr$ ratios in the He-shell after the last thermal pulse in stars with a range of mass and metallicity. The total number of thermal pulses increases with increasing stellar mass. In a star of given mass, the $^{12}C/^{13}C$ ratio in the envelope, when it becomes C-rich, increases with decreasing metallicity. This is because ^{13}C, a secondary isotope, is less abundant in lower metalliciy stars than in higher metallicity stars, while the amount of ^{12}C dredged up into the envelope does not change much with metallicity. We note that the 1.5 $M_\odot$ and 2 $M_\odot$ cases have similar $^{12}C/^{13}C$ ratios when the envelope becomes C-rich. The same can be said for the 3 $M_\odot$ and 5 $M_\odot$ cases. For a star of given mass, the C isotopic range from the time when the stars becomes C-rich to the time after the last thermal pulse increases with decreasing metallicity. For the 3 $M_\odot$ $Z = 3 \times 10^{-3}$ case, we list the results for different amounts of the ^{13}C pocket. Except for the $^{86}Kr/^{82}Kr$ ratios, which range from 4.5 to 6.1, the other parameters do not vary with the amounts of the ^{13}C pocket. The highest $^{12}C/^{13}C$ ratio of 2522 is found in the 3 $M_\odot$ $Z = 3 \times 10^{-3}$ case.

It is not likely that KFB1 and KFC1 grains of an AGB star origin originated from a single type of stars, with a specific mass and metallicity. It is more likely that stars with

Table 8
Values predicted for thermally pulsing AGB stars with various mass and metallicity.

				After the last thermal pulse		
				C-rich envelope		He-shell
Mass (M_{sun})	Metallicity (Z)	^{13}C-pocket	Total number of pulses	Range of $^{12}C/^{13}C$	C/O	$^{86}Kr/^{82}Kr$
1.5	*3 × 10⁻³*	*ST*	*20*	*67–761*	*12.50*	*6.320*
	6 × 10⁻³	ST	19	54–239	4.94	1.951
	1 × 10⁻²	ST	19	44–90	2.13	1.330
	2 × 10⁻²	ST	19	38–43	1.16	0.542
2	*3 × 10⁻³*	*ST*	*26*	*68–1305*	*18.95*	*8.675*
	6 × 10⁻³	ST	26	51–372	7.40	3.779
	1 × 10⁻²	ST	25	42–152	3.48	1.134
	2 × 10⁻²	ST	22	37–56	1.51	0.439
3	*3 × 10⁻³*	*ST*	*35*	*108–2521*	*16.72*	*5.101*
		ST/3	*35*	*108–2522*	*17.08*	*6.128*
		ST/2	*35*	*108–2522*	*16.99*	*5.913*
		ST/1.5	*35*	*108–2522*	*16.91*	*5.639*
		1.3 × ST	*35*	*108–2520*	*16.53*	*4.739*
		2 × ST	*35*	*108–2519*	*16.20*	*4.548*
	6 × 10⁻³	*ST*	*26*	*103–650*	*6.18*	*6.112*
	1 × 10⁻²	ST	25	93–349	3.82	2.038
	2 × 10⁻²	ST	25	84–141	1.80	0.988
5	3 × 10⁻³	ST	48	108–360	3.15	7.068
	6 × 10⁻³	ST	48	99–240	2.40	6.101
	1 × 10⁻²	ST	48	89–169	1.87	5.013
	2 × 10⁻²	ST	48	80–108	1.36	3.940

ST = the amount of ^{13}C and its profile in the ^{13}C pocket that best reproduce the solar-system *s*-process main component as the average of two AGB models of 1.5 and 3 $M_\odot$ with half-solar metallicity (Arlandini et al. 1999).

a range of mass and metallicity produced these grains. Since the peaks of the C isotopic distributions are around $^{12}C/^{13}C = 400–630$, stars that reach $^{12}C/^{13}C > 400$ are likely sources for these grains. The masses and metallicities of such stars are 1.5 $M_\odot$ $Z = 3 \times 10^{-3}$, 2 $M_\odot$ $Z = 3 \times 10^{-3}$, 3 $M_\odot$ $Z = 3 \times 10^{-3}$ and 3 $M_\odot$ $Z = 6 \times 10^{-3}$ (shown in italics in Table 8). They are low-mass (1–3 $M_\odot$) low-metallicity ($Z \leqslant 6 \times 10^{-3}$) stars. Particularly the 3 $M_\odot$ $Z = 3 \times 10^{-3}$ case can explain grains with high (>1000) $^{12}C/^{13}C$ ratios.

KFC1, despite having a C isotopic distribution similar to that of KFB1, shows a unique *s*-process Kr. Krypton-86 yields are a sensitive indicator of nucleosynthetic conditions. There is an *s*-process branching point at ^{85}Kr, which decays to ^{85}Rb with a half-life of 11 years. Therefore, $^{86}Kr/^{82}Kr$ ratios depend on neutron density. We will compare *s*-process Kr isotopic ratios derived from the grain data with *s*-process Kr isotopic ratios predicted for the He-shell, not the ratios predicted for the envelope as we did for the $^{12}C/^{13}C$ ratios. This is because Kr was analyzed in bulk (=aggregate) samples (Amari et al., 1995a), which were mixtures of presolar graphite and solar system grains (Table 5). The Kr of the samples was released from both types of grains thus did not represent envelope ratios of the stars from which the stellar grains formed. The method to derive *s*-process Kr from the graphite noble gas data has been described in detail by Amari et al. (1995a, 2006). The Kr data indicate that all the graphite fractions (KE1, KFA1, KFB1 and KFC1) contain *s*-process Kr (Kr-S). The lighter-density fractions, KE1, KFA1 and KFB1, contain Kr-S with a low $^{86}Kr/^{82}Kr$ ratio of $0.02 \sim 0.67$ (Kr-SL) [the ratio depends on the *s*-process $^{83}Kr/^{82}Kr$ ratio because the *s*-process $^{86}Kr/^{82}Kr$ ratios are determined from a $^{86}Kr/^{82}Kr$–$^{83}Kr/^{82}Kr$ plot, with a fixed *s*-process $^{83}Kr/^{82}Kr$ ratio at a certain nucleosynthetic condition. *s*-Process $^{83}Kr/^{82}Kr$ ratios vary with temperature, and this is the reason why the $^{86}Kr/^{82}Kr$ ratio of Kr-SL has a range (see Amari et al., 2006). In contrast, KFC1 contains Kr-S with a high $^{86}Kr/^{82}Kr$ ratio of 4.43 ± 0.46 (Kr-SH). [A close inspection shows that KE1 + KFA1 and KFB1 have a slightly different Kr-S, the data points of the latter plotting closer to solar Kr and plotting along a line with a shallower slope than those of the former in a $^{86}Kr/^{82}Kr$–$^{83}Kr/^{82}Kr$ plot. However, it is clearly seen that Kr-SH is largely absent from KFB1. For details, see Fig. 3 in Amari et al. (1995a).]

We compare the *s*-process $^{86}Kr/^{82}Kr$ ratio from KFC1 with the predicted ratios in the He-shell in AGB models of a range in mass and metallicity. The $^{86}Kr/^{82}Kr$ ratios in low-mass (1.5–3 $M_\odot$) stars with $Z \geqslant 1 \times 10^{-2}$ remain below 3, while those in low-metallicity stars ($Z \leqslant 6 \times 10^{-3}$) or higher-mass (5 $M_\odot$) stars reach 4 or above (Table 8). For the latter cases, the ratios for a series of thermal pulses after the envelope becomes C-rich are shown in Fig. 19.

As can be seen from the figure, only the $M = 3\ M_\odot$ $Z = 3 \times 10^{-3}$ case, the $M = 5\ M_\odot$ $Z = 1 \times 10^{-2}$ case, and the $M = 5\ M_\odot$ $Z = 2 \times 10^{-2}$ case (shown bold in Fig. 19) can account for Kr-SH (the $M = 3\ M_\odot$ $Z = 6 \times 10^{-3}$ case produces Kr-SH only for a few pulses). However, the two 5 $M_\odot$ cases cannot explain the whole C isotopic range of the second peak in the C isotope distribution in KFC1. The only case which satisfies both the C isotopic distribution and Kr-SH is the $M = 3\ M_\odot$ $Z = 3 \times 10^{-3}$ case and it is tempting to consider such stars as the stellar sources of the KFC1 grains.

However, we also have to take the KFB1 grains into account. These grains have a C isotopic distribution similar to that of the KFC1 grains (Fig. 4) but a completely different s-process Kr (Kr-SL). If the $M = 3\ M_\odot$ $Z = 3 \times 10^{-3}$ case produced Kr-SH found in KFC1, it is hard to explain why KFB1, which has a similar C isotopic distribution, lacks Kr-SH. Therefore, we have to conclude that stars with $M = 3\ M_\odot$ $Z = 3 \times 10^{-3}$ are not a source of the Kr-SH. It might be that graphite grains had already been carried away far from the star when a substantial amount of Kr was dredged-up into the envelope. A detailed inspection shows that there are more grains with $^{12}C/^{13}C$ ratios around ~100 in KFC1 than in KFB1 (Fig. 4). In the $M = 5\ M_\odot$ cases ($Z = 1 \times 10^{-2}$ and 2×10^{-2}), C isotopic ratios in the C-rich envelope are expected to range from 89 to 169 and from 80 to 108, respectively. Therefore, if these stars are sources of Kr-SH, the C and the Kr isotopic ratios of both KFC1 and KFB1 can be explained.

From the C isotopic ratios and the *s*-process Kr in KFC1 grains, we have identified AGB stars with somewhat different ranges of mass and metallicity as stellar sources of these KFC1 grains. The C isotopic ratios indicate that low-mass (1.5, 2 and 3 $M_\odot$) and low-metallicity [$Z = 3 \times 10^{-3}$ and $Z = 6 \times 10^{-3}$ (for 3 $M_\odot$ only)] stars are likely sources. From the Kr isotopic ratios, slightly higher mass stars with a range of metallicity (5 $M_\odot$ $Z = 1 \times 10^{-2}$, 5 $M_\odot$ $Z = 2 \times 10^{-2}$) are identified as the sources.

KE1, KFA1 and, to less extent, KFB1 contain Kr-SL. Kr-SL was first considered to have originated from high-metallicity AGB stars (Amari et al., 1995a). However, Amari et al. (2006) revisited the data and the theoretical models of supernovae and concluded that Kr-SL originated from either the O/C or the O/Ne zone in core-collapse supernovae. Since no Kr and Xe analysis on single graphite

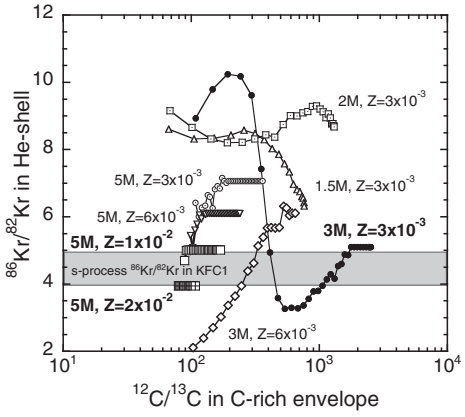

Fig. 19. Model $^{86}Kr/^{82}Kr$ ratios in the He-shell of AGB stars of different mass and metallicity, after the envelope became C-rich, are plotted against the $^{12}C/^{13}C$ ratios of the envelope as function of numbers of thermal pulses. The *s*-process $^{86}Kr/^{82}Kr$ ratio in KFC1 (Amari et al., 2006) is shown as the shadowed box. The data for *s*-process Kr are from Bisterzo et al. (2010). One 3 $M_\odot$ and two 5 $M_\odot$ cases, shown with bold font, can reproduce the *s*-process Kr in KFC1 (Kr-SH).

grains is performed, we do not know which grains contain the Kr. However, the distribution of the ^{18}O-rich grains gives us a hint. Population II from all three fractions contains ^{18}O-rich grains, but Population II in KFC1 does not. Therefore, grains containing Kr-SL may be in Population II.

To summarize the stellar sources of KFB1 grains, there are a few grains from core-collapse supernovae, mainly in Population II. KFB1 grains in the larger peak at higher ^{12}C/^{13}C ratios (Population III) likely formed in AGB stars with the same mass and metallicity as those identified from the C isotopic ratios of KFC1 grains: low-mass (1.5, 2 and 3 $M_\odot$) and low-metallicity [$Z = 3 \times 10^{-3}$ and $Z = 6 \times 10^{-3}$ (for 3 $M_\odot$ only)].

4.3.2. Oxygen isotopic ratios

As discussed in Section 4.2, ^{18}O excesses indicate a SN origin of the grains. Thirteen KFB1 grains have ^{18}O excesses up to $(1.53 \pm 0.04) \times 10^{-2}$ (KFB1f-632). Most of these grains that were analyzed for Si isotopic ratios show Si isotopic anomalies, which are consistent with a SN origin of these grains.

The O isotopic composition of the envelope after the first dredge-up in AGB stars depends on mass and metallicity of stars (Boothroyd and Sackmann, 1999). For stars with mass >1.5 $M_\odot$, ^{17}O is expected to be enriched and ^{18}O is slightly depleted. Many oxide and silicate grains in Group 1 (Nittler et al., 1997) reflect the envelope composition after the first dredge-up.

In thermally-pulsing AGB stars, ^{16}O is produced significantly only in the deeper radiative parts of the He shell (Herwig, 2005). The amount of ^{16}O in the intershell depends on overshooting. In low-mass and 5 $M_\odot$ stars, AGB nucleosynthesis hardly changes the O isotopic composition of the envelope. In low-metallicity stars, ^{16}O, a primary isotope, is more abundant relative to ^{17}O and ^{18}O, both being secondary isotopes. Therefore, the ^{17}O/^{16}O and ^{18}O/^{16}O ratios of the envelope depend on metallicity, but very little on mass. The ^{17}O/^{16}O and ^{18}O/^{16}O ratios in the envelope of low-mass (1.5, 2 and 3 $M_\odot$) and 5 $M_\odot$ stars are (2.21–2.91) $\times 10^{-4}$ and (0.90–1.15) $\times 10^{-3}$, (3.72–3.89) $\times 10^{-4}$ and (1.47–1.53) $\times 10^{-3}$, (4.82–4.93) $\times 10^{-4}$ and (1.91–1.95) $\times 10^{-3}$, and (6.46–6.58) $\times 10^{-4}$ and (2.56–2.60) $\times 10^{-3}$ for $Z = 3 \times 10^{-3}$, $Z = 6 \times 10^{-3}$, $Z = 1 \times 10^{-2}$, and $Z = 2 \times 10^{-2}$, respectively.

There are two KFB1 grains with ^{17}O excesses outside of 2σ errors but normal ^{18}O/^{16}O ratios and normal Si isotopic compositions (Table 4a). The ^{12}C/^{13}C ratios are 157 ± 6 and 333 ± 12 for KFB1f-171 and KFB1f-378, respectively. From their C, O and Si isotopic ratios, the parent stars of the two grains are likely to be 3 $M_\odot$ AGB stars with half to close-to-solar metallicity.

Fifteen grains show ^{17}O deficits, ranging from $(1.51 \pm 0.51) \times 10^{-4}$ to $(2.60 \pm 0.51) \times 10^{-4}$, with close-to-solar ^{18}O/^{16}O ratios with 2σ errors. One grain, KFB1f-763, shows also a ^{28}Si excess, indicating a SN origin. The ^{12}C/^{13}C ratios of the rest of the grains range from 83 to 1531, but most of them are between 400 and 600. Although their ^{18}O/^{16}O ratios are normal within 2σ errors, there is a hint of ^{18}O deficits. The O isotopic ratios, along with the ^{12}C/^{13}C ratios, of the grains are consistent that they originated from low-mass low-metallicity AGB stars.

Of them, three grains, KFB1f-024, KFB1f-202, and KFB1f-623 (^{12}C/^{13}C = 1531 ± 59, 758 ± 28, and 305 ± 11, respectively), show excesses in ^{29}Si and/or ^{30}Si. The Si in these grains is much more enriched in ^{30}Si than in ^{29}Si (Table 4a) and this signature is also consistent with an AGB star origin (Zinner et al., 2006).

We did not analyze ^{17}O in KFC1 grains. Of 120 grains analyzed for their ^{18}O/^{16}O ratios, only one grain, KFC1b-102 has an elevated ^{18}O/^{16}O ratio $(3.63 \pm 0.62) \times 10^{-3}$. It also shows a lower than solar ^{14}N/^{15}N ratio (93 ± 17), indicating a SN origin.

4.3.3. Al–Mg systematics and Si isotopic ratios

Six out of the 46 KFB1 grains analyzed for Al–Mg have resolvable ^{26}Mg excesses. The inferred ^{26}Al/^{27}Al ratios range from 4.3×10^{-3} to 8.6×10^{-2} (Fig. 9). The ^{26}Al/^{27}Al ratios alone can be explained by AGB stars (Fig. 20). However, after considering other isotopic signatures such as ^{12}C/^{13}C ratios, δ^{25}Mg/^{24}Mg values and Si isotopic ratios, we conclude that all 6 grains most likely originated in supernovae. (These grains were not analyzed for their O isotopic ratios.) Among the 6, three are Population I grains with ^{26}Al/^{27}Al ratios between 4.3×10^{-3} and 2.3×10^{-2}. In the AGB models, such ratios are predicted only when the ^{12}C/^{13}C ratio of the envelope becomes much higher than the ratios of these grains. In addition, KFB1a-122 (^{12}C/^{13}C = 14.5) has a ^{25}Mg excess (δ^{25}Mg/^{24}Mg = 670‰) and KFB1a-415 (^{12}C/^{13}C = 13.6) has a ^{28}Si excess (δ^{29}Si/^{28}Si = −103‰, δ^{29}Si/^{28}Si = −245‰), showing SN signatures. There are two Populations II grains and one Population III grain with ^{26}Al/^{27}Al ratios. KFB1a-151 has too low a ^{12}C/^{13}C ratio (43.5) to account for the high ^{26}Al/^{27}Al ratio (2.9×10^{-2}) to be from an AGB star. KFB1a-261 (^{26}Al/^{27}Al = 8.6×10^{-2}) has a large ^{28}Si excess (δ^{29}Si/^{28}Si = −402‰, δ^{29}Si/^{28}Si = −542‰), proof of a SN origin. KFB1a-542 has the highest ^{12}C/^{13}C ratio (221 ± 2) among the 6 grains, but still too low to explain the ^{26}Al/^{27}Al ratio (9.7×10^{-3}) with an AGB star origin (Fig. 20).

Fifty-nine KFC1 grains were analyzed for their Mg isotopic ratios and Al/Mg ratios, but none of them show a clear ^{26}Mg excess that can be attributed to the decay of ^{26}Al. This is puzzling because model calculations predict the ^{26}Al/^{27}Al ratios in the C-rich envelope in low-mass (1–3 $M_\odot$) low-metallicity ($Z = 3$ and 6×10^{-3}) AGB stars to range between 7.5×10^{-4} and 0.028 (Fig. 20). The Si isotopic ratios of KFC1 grains and those predicted for the C-rich envelope of low-mass low-metallicity stars are plotted in Fig. 21. Extremely high δ^{30}Si/^{28}Si values (>1000‰) are not observed in the grains, however, overall the Si isotopic range is produced with AGB stars models that can also reproduce the ^{12}C/^{13}C ratios of the KFC1 grains in the second peak in Fig. 4.

4.3.4. Calcium and Ti isotopic ratios of KFC1 grains

We compare the Ca and Ti isotopic patterns of the KFC1 grains (Figs. 12c and 14c) with those in the He-shell (Fig. 22) rather than those in the envelope of AGB stars. The reason is that there is a huge uncertainty on the

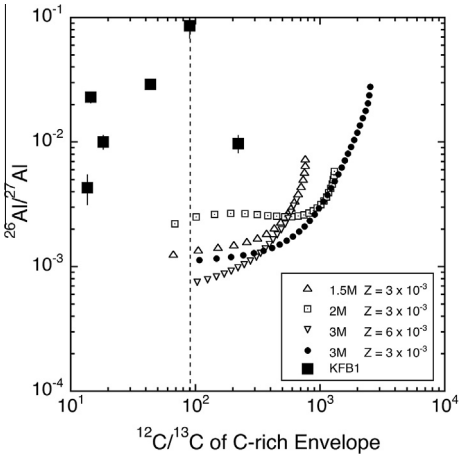

Fig. 20. $^{26}Al/^{27}Al$ and $^{12}C/^{13}C$ ratios of KFB1 grains (solid squares) are compared with those of the C-rich envelope as function of numbers of thermal pulses predicted for AGB stars of varying mass and metallicity. KFC1 grains do not have ^{26}Mg excesses from the decay of ^{26}Al.

original compositions of low-metallicity AGB stars. They are certainly not solar. In AGB models with lower-than-solar metallicities, the isotopic ratios of Ca and Ti were calculated by assuming that the abundances of all isotopes, except those of the alpha nuclei (^{40}Ca, ^{44}Ca, and ^{48}Ti), scale with the Fe abundance. The alpha nuclei, on the other hand, were assumed to be enhanced according to the enhancements observed in thin- and thick-disk stars, i.e. in stars close to the galactic plane and farther away from it (e.g., Zinner et al., 2007). However, the lower the metallicity, the more uncertainty is introduced in the isotopic ratios with this extrapolation method. In the models, a few isotopic ratios are expected to be lower than solar even after the last pulse, but this is not seen in many grains. Therefore, we compare the grain data with He-shell data in the following discussion.

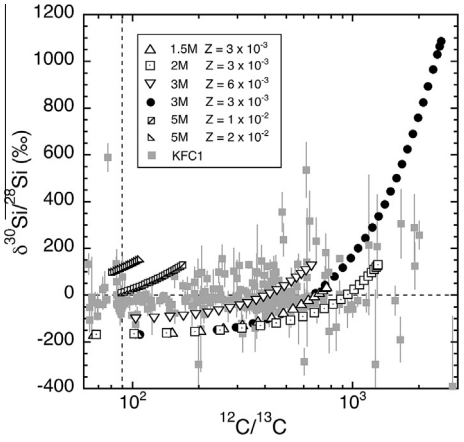

Fig. 21. $\delta^{30}Si/^{28}Si$ values and $^{12}C/^{13}C$ ratios of KFC1 grains (gray squares) are compared with those of the C-rich envelope as function of numbers of thermal pulses predicted for AGB stars of varying mass and metallicity. Low-metallicity stars can explain the overall trend.

Fig. 22 shows Ca and Ti isotopic patterns of the He-shell of the 3 $M_\odot$ AGB star model with $Z = 3 \times 10^{-3}$. ^{42}Ca and ^{43}Ca excesses are similar in the first few pulses, while ^{43}Ca excesses become larger than ^{42}Ca excesses in later pulses (Fig. 22a). The Ti isotopic patterns (Fig. 22b) have a V-shape with excesses in ^{46}Ti and ^{49}Ti when normalized to ^{48}Ti ($^{50}Ti/^{48}Ti$ ratios were not determined for the KFC1 grains due to high Cr/Ti ratios, therefore, the $^{50}Ti/^{48}Ti$ ratios of the models are not shown). The largest ^{49}Ti excess is found after the 8th pulse, during later pulses the $^{49}Ti/^{48}Ti$ ratio becomes ~15 times solar and remains around that ratio. The Ca and Ti patterns are similar to those predicted for the He/C, O/C and O/Ne zones in supernovae (Fig. 17). Therefore, we need to take isotopic signatures of other elements into account to investigate the origin of Ca and Ti isotopic anomalies.

KFC1b2-521 ($^{12}C/^{13}C = 2007$), KFC1a-357b (77.3), KFC1b2-441 (8.90) and KFC1b2-2113 (12.0) have both Ca and Ti isotopic anomalies (Figs. 12c and 14c). Both KFC1a-357b and KFC1b2-2113 show comparable ^{42}Ca and ^{43}Ca excesses (first group in Section 3.12), and KFC1b2-441 shows the highest excess in ^{43}Ca (second group). All grains show large ^{49}Ti excesses compared with $^{46,47}Ti$ excesses. The $^{12}C/^{13}C$ ratios of KFC1b2-441 and KFC1b2-2113 are too low to be accounted for by AGB stars, thus the grains most likely formed in supernovae. The Ca in KFC1b2-2113 has a signature of the He/C zone, while the Ca in KFC1b2-441 has a signature of O/C and O/Ne zones. The Ti in the two grains has a characteristic signature of the He/C zone.

The $^{12}C/^{13}C$ ratio of KFC1a-357b is higher than those of the two. Its $\delta^{29}Si/^{28}Si$ and $\delta^{30}Si/^{28}Si$ values are 285‰ and 582‰, respectively and the $\delta^{29}Si/\delta^{30}Si$ ratio is 0.49, which agrees with that in the O/C zone in the 15 $M_\odot$ star (0.49, $\delta^{29}Si/^{28}Si = 5600$‰, $\delta^{30}Si/^{28}Si = 11{,}400$‰). Thus, this grain also must have formed in a supernova. Its Ca and Ti isotopic patterns indicate the contribution from the He/C zone. The other two grains (KFC1b2-231 and KFC1b2-521, $^{12}C/^{13}C = 650$ and 2007, respectively) have negative $\delta^{42}Ca/^{40}Ca$ or $\delta^{43}Ca/^{40}Ca$ values. In AGB model calculations, if $\delta^{42}Ca$ and/or $\delta^{43}Ca$ values are negative in the envelope, $\delta^{44}Ca$ values are also expected to be negative because the initial composition was assumed to be enriched in ^{40}Ca relative to $^{42,43,44}Ca$ in low-metallicity stars. This is not the case in these grains. However, the errors are large and it is hard to discern the origin of these grains.

Five grains have Ti patterns of the first type (Fig. 14c and Section 3.14), 5 grains the pattern of the second type, and 2 grains the pattern of the third type. Among the 5 grains of the first type, 3 grains (KFC1a-357b, KFC1b2-441, KFC1b2-2113) have already been discussed and they are most likely SN grains. Of the 5 grains of the second type, two grains (KFC1d-121 and KFC1d-012) have slight ^{28}Si excesses and they can be interpreted to have originated either in supernovae or low-metallicity AGB stars. KFC1d-212 has $^{12}C/^{13}C$ ratio of 58.6 and $^{29,30}Si$ excesses ($\delta^{29}Si/^{28}Si = 88$‰, $\delta^{30}Si/^{28}Si = 229$‰). This relatively low $^{12}C/^{13}C$ ratio coupled with significant excesses in $^{29,30}Si$ indicate that this grain may be a SN grain. In contrast, KFC1d-301 has $^{12}C/^{13}C$ ratio of 437 ± 4 and ^{30}Si excess

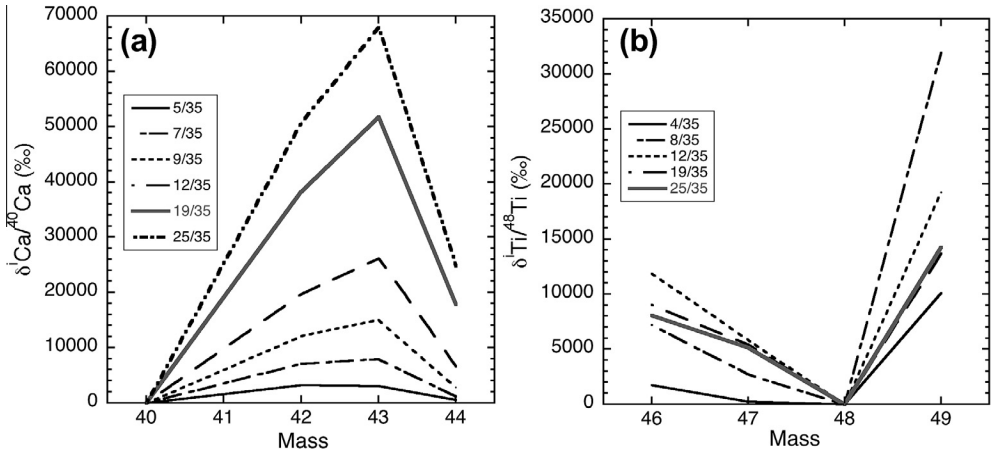

Fig. 22. Isotopic patterns of (a) Ca and (b) Ti predicted for the He-shell of a 3 $M_{\odot}$ AGB star with $Z = 3 \times 10^{-3}$. The patterns are plotted for different numbers of thermal pulses. The first numbers after the symbols in the legends indicate the pulse number. The total number of pulses is 35.

with normal $^{29}Si/^{28}Si$ ($\delta^{29}Si/^{28}Si = 3‰$, $\delta^{30}Si/^{28}Si = 66‰$) and it can be explained by an AGB star origin except that its ^{49}Ti excess is much higher than what is expected from its ^{30}Si excess.

4.4. Grains in Population I

Thirty-seven percent and 29% of the Population I grains in KE3 and KFA1, respectively, are ^{18}O-rich, thus, of a SN origin (Table 7). High $\delta^{25}Mg/^{24}Mg$ values of KFA1 grains (Fig. 7) also indicate a SN origin of these grains. There are only a few grains of a SN origin in Population I in the two higher-density fractions: six percent of KFB1 Population I grains are ^{18}O-rich and there are a few grains with ^{28}Si excesses or high $^{26}Al/^{27}Al$ ratios (up to 0.023), which are hard to explain other than by a SN origin. One KFC1 grain (KFC1a-042) shows a ^{25}Mg excess ($\delta^{25}Mg/^{24}Mg = 1387 \pm 522‰$), indicative of a SN origin. Population I contains SN graphite grains and the lower the density the higher their abundance.

KE3 and KFA1 have broad C isotopic distributions and they do not have distinct peaks in the Population I regions. This may be because grains from other stellar sources besides supernovae populate this region. In contrast, KFB1 and KFC1 have clear peaks with $^{12}C/^{13}C$ ratios around 10, which suggests a distinct origin of these grains. However, in these density fractions there are many grains that do not show isotopic anomalies except low $^{12}C/^{13}C$ ratios.

Amari et al. (2001c) have discussed origins of SiC grains of type A + B, defined as grains with $^{12}C/^{13}C$ ratios lower than 10, and proposed J stars and born-again AGB stars, such as Sakurai's object, as possible stellar sources of these grains. J stars are cool luminous carbon stars with low $^{12}C/^{13}C$ ratios (<10) and solar s-process abundances (Lambert et al., 1986; Ohnaka and Tsuji, 1999; Utsumi, 1985a, 1985b, 1988; Abia and Isern, 2000; Hedrosa et al., 2013). The fraction of J stars among cool carbon stars is estimated to be 5–15% (Lodders and Fegley, 1998). In spite of this significant fraction, the origin of J stars is not well understood. Their low $^{12}C/^{13}C$ ratios indicate that the CNO cycle was operating, but this would make the stars O-rich. If He-burning took place, the $^{12}C/^{13}C$ ratios would not remain low due to the triple alpha reaction. In addition, neutron capture by neutrons via $^{13}C(\alpha,n)^{16}O$ and $^{22}Ne(\alpha,n)^{25}Mg$ would have increased the abundances of *s*-process elements.

The other type of stars with low $^{12}C/^{13}C$ ratios is born-again AGB stars, which are undergoing a very late thermal pulse (VLTP) (Iben et al., 1983). Sakurai's object, a born-again AGB star, shows the low $^{12}C/^{13}C$ ratio (4 ± 1, Pavlenko et al., 2004). The presence of hot dust was evident from infra-red observations (Eyres et al., 1998; Kerber et al., 1999). It has been proposed that a small remaining H-rich envelope is convectively ingested into the He shell, resulting in an additional rapid H-driven nuclear burning (Hajduk et al., 2005). Herwig et al. (2011) performed detailed nucleosynthetic simulations of H-rich material being convectively mixed with the He-burning zone, with three-dimensional hydrodynamic He-shell flash convection models. Assuming a split of the convection zone into the original zone driven by He burning and a zone driven by ingested H burning, they could reproduce the abundances observed in Sakurai's object (Asplund et al., 1999), including the $^{12}C/^{13}C$ ratio, and overproduction of Rb, Sr, and Y by two orders of magnitude relative to the production of Ba and La.

J stars and born-again AGB stars are possible stellar sources of graphite grains with low $^{12}C/^{13}C$ ratios. First, these stars are carbon stars, thus graphite grains are expected to form. In addition, the carbon isotopic ratios of the grains agree with the stars' C isotopic ratios. Jadhav et al. (2013b) proposed that high-density Orgueil graphite grains with $^{12}C/^{13}C$ ratios < 20 and extreme Ca and Ti isotopic anomalies formed in born-again AGB stars. Using the post-AGB star models by Herwig et al. (2011), they could explain these grains' Ca and Ti isotopic anomalies. It remains to be seen whether this stellar object can also reproduce isotopic features of Murchison graphite grains with low $^{12}C/^{13}C$ ratios. The difference between the Murchison graphite and Orgueil graphite is that the former is devoid of extreme Ca and Ti isotopic anomalies that have been

seen in the Orgueil graphite: the highest $\delta^{43}Ca$ value found in the Murchison grains is 1569‰ (KFC1b2-441) and that in the Orgueil grains is 27,600‰ (OR1f2m-9), and the highest $\delta^{46}Ti$ value in the former is 319‰ (KFC1b2-2113) and that in the latter is 35,000‰ (OR1f2m-9).

4.5. Tentative identification of nova grains

Novae have traditionally been considered to be a source of Ne-E(L) (Clayton and Hoyle, 1976) because ONe novae produce a huge amount of ^{22}Na (e.g., José and Hernanz, 1998), which can explain ^{22}Ne enrichments. Graphite grain KFC1a-551 as well as a few SiC grains show the isotopic signature of ONe novae (Amari et al., 2001a; José et al., 2004): low $^{12}C/^{13}C$ ($4 \sim 9$) and $^{14}N/^{15}N$ ratios ($5 \sim 20$), high $^{26}Al/^{27}Al$ ratios (0.011), and ^{30}Si excesses (1.1∼2.1 times the solar $^{30}Si/^{28}Si$ ratio) with close-to-normal $^{29}Si/^{28}Si$ ratios. Although these isotopic signatures are consistent with those predicted in ONe novae, mixing calculations indicate that, to reproduce the grain data, more than 95% of the mix should have originated from material with a close-to-solar composition. Whether that kind of mixing takes place near nova ejecta is not clear. Nittler and Hoppe (2005) proposed that some of the grains that are classified as being of a nova origin might have formed in supernovae. Recent noble gas studies also suggest that supernovae are a main source of the ^{22}Na in the graphite grains (Amari, 2009; Heck et al., 2009a; Meier et al., 2012). Therefore, it remains to be seen whether novae are a stellar source of graphite grains. Even if it is so, novae are a minor stellar source of graphite grains found in meteorites.

There are also oxide grains of a tentative nova origin. Gyngard et al. (2010b, 2011) proposed that several oxide grains with $^{17}O/^{16}O$ ratios >0.004 (the predicted maximum ratio in low- and intermediate-mass AGB and RGB stars, Boothroyd and Sackmann, 1999) (Nguyen et al., 2010; Gyngard et al., 2010b, 2011; Nittler et al., 2010) had originated from novae. However, a significant amount of close-to-solar material has to be mixed into the ejecta in order to reproduce the O and Mg isotopic ratios of the grains, as in the case of SiC and graphite grains.

4.6. Abundances of grains from supernovae and AGB stars

We calculated abundances of grains from supernovae and AGB stars. Oxygen-18 rich grains are SN grains in all the density fractions. In KE3 and KFA1, along with the ^{18}O-rich grains, those with ^{26}Al (in most cases with $^{26}Al/^{27}Al > 1 \times 10^{-3}$), Si isotopic anomalies, and evidence of ^{44}Ti, are classified as SN grains.

For KFA1, SN signatures also include ^{25}Mg excesses. For KFB1, grains with ^{28}Si excesses (in all cases $^{30}Si/^{28}Si <$ solar) and/or with $^{26}Al/^{27}Al$ ratios ranging from $(4.3 \pm 1.1) \times 10^{-3}$ to $(8.6 \pm 1.8) \times 10^{-2}$, are classified as SN grains. In KFC1, there is one Population I grain with a ^{28}Si excess and one Population III grain with an ^{18}O excess. Also there are three grains (KFC1b2-441, KFC1b2-2113, KFC1a-357b) with Ca and Ti isotopic anomalies that can be attributed to supernovae, totaling 5 SN grains. For grains from AGB stars, we took grains with $^{12}C/^{13}C$ ratios $\geqslant 100$ in KFB1 and those with $^{12}C/^{13}C$ ratios $\geqslant 60$ in KFC1. It is because 5 $M_\odot$ stars with solar and half-solar metallicities are required to explain Kr-SH in KFC1.

Table 9 summarizes the abundances of grains from supernovae and AGB stars. KE3 is most abundant in SN grains followed by KFA1. This trend is already shown in Table 7, which gives the abundances of ^{18}O-rich grains. On the other hand, 76% and 80% of the grains in KFB1 and KFC1, respectively, are classified as having an AGB star origin. Because of the much higher KFC1 abundance, 77% of grains from AGB stars belong to KFC1.

The abundances of graphite grains from supernovae and AGB stars in the Murchison meteorite are 0.24 and 0.44 ppm, respectively. The biggest uncertainty of these numbers comes from the abundance of KE3 (Table 1), which was derived from the abundance of KE1 and comparison of the fractions of anomalous grains. Since the total abundance of presolar graphite grains in the Murchison meteorite is 0.88 ppm, grains from supernovae comprise 27% of the total graphite grains and those from AGB stars comprise 50%. We will compare these numbers with those for another presolar carbonaceous phase, SiC.

Size-separated SiC fractions have been extracted from the same fragments of the Murchison meteorite (Murchison K-series) and they are named KJA, KJB, KJC, KJD, KJE, KJF, KJG, KJH and KJI. The total abundance of SiC grains is 5.85 ppm (Amari et al., 1994). Since the graphite and the SiC fractions were extracted from the same Murchison fragments, we can compare the abundances of graphite and SiC of different stellar origins.

Silicon carbide grains are classified into several different populations based on their C, N and Si isotopic ratios

Table 9
Abundances of grains from supernovae and AGB stars.

Phase	Fraction	Fraction of SN grains	Abundance of SN grains (ppm)	Fraction of AGB grains	Abundance of AGB grains (ppm)
Graphite	KE3	0.761	0.167		
	KFA1	0.497	0.055		
	KFB1	0.072	0.009	0.76	0.10
	KFC1	0.009	0.004	0.80	0.34
	Total	0.27*	0.24	0.50*	0.44
SiC**	KJA–KJH	0.01 + 0.00077***	0.063	0.95	5.6

* 0.24 ppm/0.88 ppm (total of KE3–KFC1) and 0.44 ppm/0.88 ppm.
** The abundance of SiC grains in Murchison is 5.85 ppm (Amari et al., 1994).
*** The first number is for X grains and the second number for C grains.

(e.g., Hoppe and Ott, 1997). The major part (>93%) of SiC grains in meteorites are mainstream grains, having $^{12}C/^{13}C$ ratios between 10 and 100, higher $^{14}N/^{15}N$ ratios than that of air (272), and ^{29}Si and ^{30}Si excesses up to 20% relative to the solar ratios. Bulk isotopic analyses and single grain analyses of SiC grains indicate that they have formed in low-mass (1.5–3 $M_\odot$) AGB stars with close-to-solar metallicity (Lewis et al., 1990, 1994; Prombo et al., 1993; Hoppe et al., 1994; Savina et al., 2003; Podosek et al., 2004). Y grains are defined having $^{12}C/^{13}C$ ratios > 100, higher-than-terrestrial $^{14}N/^{15}N$ ratios, and ^{30}Si further enriched relative to the Si of mainstream grains (Amari et al., 2001b). Z grains show $^{12}C/^{13}C$ ratios similar to those of mainstream grains, but their $^{29}Si/^{28}Si$ ratios are lower than solar and they plot on the right side of the mainstream correlation line (Hoppe et al., 1997). Y and Z grains are considered to have formed also in AGB stars, but with around half-solar metallicity (Amari et al., 2001b) and one-third of solar metallicity (Hoppe et al., 1997). Y and Z grains together comprise a few percent of the total SiC grains. The abundances of Z grains increase with decreasing grain size (Zinner et al., 2007; Hoppe et al., 2010). Mainstream, Y and Z grains comprise ~95% of the SiC grains.

A + B grains, defined as having $^{12}C/^{13}C$ ratios lower than 10 with a range of $^{14}N/^{15}N$ ratios, comprise a few percent of SiC grains. Silicon carbide grains of type X, characterized by ^{15}N excesses, high $^{26}Al/^{27}Al$ ratios up to ~0.1, ^{28}Si excesses, and, in a few grains, evidence for the initial presence of ^{44}Ti, are believed to have formed in core-collapse supernovae. X grains comprise only 1% of the total SiC grains in meteorites (Amari et al., 1992; Hoppe et al., 2000). There are also grains of type C, characterized by excesses in ^{29}Si and ^{30}Si, and they are also considered to be of a SN origin (Hoppe et al., 2010; Croat et al., 2010; Pignatari et al., 2013b). However, their abundance is very low and strongly dependent on grain size: they are much more abundant in submicron grains and only one C grains are larger than 1 μm has been found (Amari et al., 1999). Among small SiC grains (KJA + KJB), 3 grains out of 2026 grains are C type grains (Hoppe et al., 2010). From the Presolar Grain Database (Hynes and Gyngard, 2009), we calculated the C grain abundance to be 0.077%, making the total abundance of SN grains 0.063 ppm. The ratio of SiC grains from supernovae and from AGB stars is ~0.011 (0.0108/0.95). Therefore, AGB stars are a dominant producer of SiC grains. This is markedly different from the situation of the graphite grains. For graphite grains, AGB stars are still a main producer, accounting for 50% of the graphite grains in the Murchison meteorite. However, supernovae are also a significant graphite dust source in that they produced 27% of these grains.

The abundance of SiC of an AGB star origin is much higher than that of graphite of an AGB star origin (5.6 ppm vs. 0.44 ppm, Table 9). When we compare abundances of SiC and graphite, we have to ask whether the numbers reflect the production abundances. The primary dust destruction processes are sputtering in gas-grain collisions and vaporization in grain–grain collisions in SN shock waves (Jones and Nuth, 2011), and interstellar residence times depend on the dust composition and structure (e.g., Jones et al., 1996): the interstellar residence time of hydrogenated amorphous carbon (~2×10^8 year) is estimated to be much shorter than that of graphite/amorphous carbon (~6×10^8 year, Jones et al., 1996). The residence times for SiC are expected to be longer than those of graphite because SiC grains are harder than graphite gains and are less susceptible to sputtering. (To date, interstellar residence times have been only determined for SiC grains (Gyngard et al., 2009; Heck et al., 2009b) and not for graphite grains.) If so, part of the higher SiC abundance is due to the higher survival rate of SiC than graphite. Alternatively, mainstream SiC grains formed in low-mass (1–3 $M_\odot$) AGB stars with close-to-solar metallicity, while high-density graphite grains formed in AGB stars with low-metallicity. Thus, the difference may also reflect an intrinsic difference of productions in different kinds of AGB stars.

The abundance of SN graphite in Murchison is 0.24 ppm, whereas that of SiC is 0.063 ppm (Table 9). For SN grains, dust destruction occurs in their birthplace because exploding supernovae are a hostile place. When the forward shock hits the H-rich envelope, material that was blown off from the star, or material in the interstellar medium (ISM), the reverse shock moves inward and when it reaches the ejecta, where gas and dust grains are mixed, grains will be decoupled from the ambient gas. Because grains are much heavier, they are not decelerated much and go through a hot (>10^6 K) gas that has been heated by both forward and reverse shocks. As the result, grains are sputtered, both kinetically and thermally. Bianchi and Schneider (2007) studied grain formation and survival in SN ejecta and concluded that 2–20% of the dust mass survives 4–8 × 10^4 years after the explosion. However, since they studied the grain destruction in the ejecta and did not include the destruction in the H-rich zone and the ISM, their estimate can be taken as upper limits. Nozawa et al. (2007) also investigated grain formation and destruction in SN ejecta, taking these additional destruction scenarios into account, and concluded that 0–80% of the dust survives. The survival rate of grains depends on grain type. We should probably define abundances after accounting for destruction as original abundances of SN grains. Considering the likelihood that SiC survives better than graphite in SN shock wave and the ISM, supernovae seem to be very proficient graphite producers.

5. SUMMARY

We studied presolar graphite grains from the density-separated Murchison fractions KE3 (1.65–1.72 g/cm^3), KFA1 (2.05–2.10 g/cm^3), KFB1 (2.10–2.15 g/cm^3) and KFC1 (2.15–2.20 g/cm^3) with SIMS. Isotopic features of graphite grains depend on density.

KE3 and KFA1 have broad distributions in the $^{12}C/^{13}C$ ratio, while KFB1 and KFC1 show two distinct peaks, one around 10 and the other around 400–630. We estimated abundances of presolar graphite grains and solar system grains in these fractions, assuming that the presolar graphite grains have smooth distributions in $^{12}C/^{13}C$. Only 52% of the

KFA1 grains are presolar, whereas 84–95% of the grains in the other fractions are presolar. Grains were classified according to their $^{12}C/^{13}C$ ratios: grains with $^{12}C/^{13}C < 20$ as Population I, those with $20 \leqslant {}^{12}C/^{13}C \leqslant 200$ as Population II and those with $^{12}C/^{13}C > 200$ as Population III.

Grains from supernovae are most abundant in KE3 and KFA1. We estimated that 76% and 50% of presolar grains in KE3 and KFA1, respectively, formed in core-collapse supernovae. Supernova grains are also present in the higher-density fractions. However, their abundances are much lower: 7.2% and 0.9% of the grains in KFB1 and KFC1, respectively. Characteristic isotopic features of these grains include ^{18}O excesses, ^{15}N excesses, high $^{26}Al/^{27}Al$ (up to ~0.1), Si isotopic anomalies (mainly ^{28}Si, but also ^{29}Si and/or ^{30}Si excesses), and the initial presence of ^{44}Ti.

Grains with ^{18}O excesses are most abundant in Population II. Since the two C-rich SN zones, the He/N and He/C zones, have extreme $^{12}C/^{13}C$ ratios (4 and 206,000, respectively), it is likely that other zones with $^{12}C/^{13}C$ ratios between these ratios might have contributed to the mix from which the graphite grains formed. The candidates are the H-rich envelope and possibly material blown off from the star as stellar wind before the explosion. To reproduce isotopic ratios of elements that would be least affected by elemental fractionation, we mixed three zones (the He/C, He/N and H-rich envelope) and four zones (these three and the O/C zone) to reproduce $^{12}C/^{13}C$, $^{18}O/^{16}O$ and $^{26}Al/^{27}Al$ ratios of the KE3 grains. The isotopic features of the Population III grains can be reproduced, however, those of Populations II and I are hard to be accounted for if C > O is required for graphite formation.

AGB model calculations can explain the peaks around 400–630 in the carbon isotopic distributions of KFB1 and KFC1 with low-mass (1.5, 2 and 3 $M_\odot$) low-metallicity ($Z = 3 \times 10^{-3}$ for 1.5, 2 and 3 $M_\odot$, $Z = 6 \times 10^{-3}$ for 3 $M_\odot$ only) stars. The C isotopic distribution and Kr-SH, the *s*-process Kr with $^{86}Kr/^{82}Kr$ of 4.43, in KFC1 are best explained with 5 $M_\odot$ stars of solar and/or half-solar metallicities. In KFB1 and KFC1, the fractions of grains from AGB stars are 76% and 80%, respectively. We did not find strong evidence that KE3 and KFA1 grains formed in AGB stars.

The abundance of presolar graphite in the Murchison meteorite was estimated to be 0.88 ppm. The abundances of the graphite grains from supernovae and AGB stars were calculated to be 0.24 ppm and 0.44 ppm, respectively. SiC fractions have been extracted from the same fragments of the Murchison meteorite. With an abundance of the total SiC grains of 5.85 ppm, the abundances of SiC grains from supernovae and AGB stars are 0.063 ppm and 5.6 ppm, respectively. In view of SiC being much harder than graphite and being likely to survive sputtering in the SN shock wave and the ISM, supernovae seem to be a proficient graphite producer. The abundance of graphite grains from AGB stars is much lower than that of SiC grains from AGB stars (0.44 ppm vs. 5.6 ppm). This difference may reflect the difference in their parent stars: graphite grains formed in low-metallicity stars, while SiC grains formed in close-to-solar metallicity stars.

ACKNOWLEDGEMENTS

We are grateful to Edward Anders and Roy S. Lewis at The University of Chicago for their roles in sample preparation of the Murchison K-series graphite and SiC grains. We thank Sara Russell and the anonymous reviewers for their constructive comments. This work was supported by a grant from McDonnell Center for the Space Sciences (S.A), as well as NASA grants NNX08AG56G (S.A), NNX10AI45G (S.A) and NNX11AH14G (S.A. and E.Z.).

APPENDIX A. SUPPLEMENTARY DATA

Supplementary data associated with this article can be found, in the online version, at http://dx.doi.org/10.1016/j.gca.2014.01.006.

REFERENCES

Abia C. and Isern J. (2000) The chemical composition of carbon stars II: The J-type stars. *Astrophys. J.* **536**, 438–449.

Amari S., Anders E., Virag A. and Zinner E. (1990) Interstellar graphite in meteorites. *Nature* **345**, 238–240.

Amari S., Hoppe P., Zinner E. and Lewis R. S. (1992) Interstellar SiC with unusual isotopic compositions: Grains from a supernova? *Astrophys. J.* **394**, L43–L46.

Amari S., Hoppe P., Zinner E. and Lewis R. S. (1993) The isotopic compositions and stellar sources of meteoritic graphite grains. *Nature* **365**, 806–809.

Amari S., Lewis R. S. and Anders E. (1994) Interstellar grains in meteorites: I. Isolation of SiC, graphite, and diamond; size distributions of SiC and graphite. *Geochim. Cosmochim. Acta* **58**, 459–470.

Amari S., Lewis R. S. and Anders E. (1995a) Interstellar grains in meteorites: III. Graphite and its noble gases. *Geochim. Cosmochim. Acta* **59**, 1411–1426.

Amari S., Zinner E. and Lewis R. S. (1995b) Interstellar graphite from the Murchison meteorite. In *Nuclei in the Cosmos III* (eds. M. Busso, R. Gallino and C. M. Raiteri). AIP, New York, pp. 581–584.

Amari S., Zinner E. and Lewis R. S. (1995c) Large ^{18}O excesses in circumstellar graphite grains from the Murchison meteorite: Indication of a massive star-origin. *Astrophys. J.* **447**, L147–L150.

Amari S., Zinner E. and Lewis R. S. (1996) ^{41}Ca in presolar graphite of supernova origin. *Astrophys. J.* **470**, L101–L104.

Amari S., Zinner E. and Lewis R. S. (1999) A singular presolar SiC grain with extreme ^{29}Si and ^{30}Si excesses. *Astrophys. J.* **517**, L59–L62.

Amari S., Gao X., Nittler L. R., Zinner E., José J., Hernanz M. and Lewis R. S. (2001a) Presolar grains from novae. *Astrophys. J.* **551**, 1065–1072.

Amari S., Nittler L. R., Zinner E., Gallino R., Lugaro M. and Lewis R. S. (2001b) Presolar SiC grains of type Y: Origin from low-metallicity asymptotic giant branch stars. *Astrophys. J.* **546**, 248–266.

Amari S., Nittler L. R., Zinner E., Lodders K. and Lewis R. S. (2001c) Presolar SiC grains of type A and B: Their isotopic compositions and stellar origins. *Astrophys. J.* **559**, 463–483.

Amari S., Gallino R., Limongi M. and Chieffi A. (2006) Presolar graphite from the Murchison meteorite: Imprint of nucleosynthesis and grain formation. In *Origin of Matter and Evolution of Galaxies: International Symposium on Origin of Matter and Evolution of Galaxies 2005: New Horizon of Nuclear Astrophys-*

ics and Cosmology (eds. S. Kubono, W. Aoki, T. Kajino, T. Motobayashi and K. Nomoto). AIP, New York, pp. 311–318.
Amari S. (2009) Sodium-22 from supernovae: A meteorite connection. *Astrophys. J.* **690**, 1424–1431.
Anders E. (1988) Circumstellar material in meteorites: Noble gases, carbon and nitrogen. In *Meteorites and the Early Solar System* (eds. J. F. Kerridge and M. S. Matthews). University of Arizona Press, Tucson, pp. 927–955.
Arlandini C., Käppeler F., Wisshak K., Gallino R., Lugaro M., Busso M. and Straniero O. (1999) Neutron capture in low-mass asymptotic giant branch stars: Cross sections and abundance signatures. *Astrophys. J.* **525**, 886–900.
Asplund M., Lambert D. L., Kipper T., Pollacco D. and Shetrone M. D. (1999) The rapid evolution of the born-again giant Sakurai's object. *Astron. Astrophys.* **343**, 507–518.
Bernatowicz T., Fraundorf G., Tang M., Anders E., Wopenka B., Zinner E. and Fraundorf P. (1987) Evidence for interstellar SiC in the Murray carbonaceous meteorite. *Nature* **330**, 728–730.
Bernatowicz T. J., Amari S., Zinner E. K. and Lewis R. S. (1991) Interstellar grains within interstellar grains. *Astrophys. J.* **373**, L73–L76.
Bernatowicz T. J., Amari S. and Lewis R. S. (1992) TEM studies of a circumstellar rock. *Lunar Planet. Sci.* **XXIII**, 91–92.
Bernatowicz T. J., Cowsik R., Gibbons P. C., Lodders K., Fegley, , B., Amari S. and Lewis R. S. (1996) Constraints on stellar grain formation from presolar graphite in the Murchison meteorite. *Astrophys. J.* **472**, 760–782.
Bernatowicz T. J. and Zinner E. (1997) Astrophysical implications of the laboratory study of presolar materials. In *AIP Conf. Proc. 402* (eds. T. Bernatowicz and E. Zinner). AIP, New York, p. 750.
Bianchi S. and Schneider R. (2007) Dust formation and survival in supernova ejecta. *Mon. Not. R. Astron. Soc.* **378**, 973–982.
Bisterzo S., Gallino R., Straniero O., Cristallo S. and Käppeler F. (2010) s-Process in low metallicity stars – I. Theoretical predictions. *Mon. Not. R. Astron. Soc.* **404**, 1529–1544.
Black D. C. and Pepin R. O. (1969) Trapped neon in meteorites. II. *Earth Planet. Sci. Lett.* **6**, 395–405.
Black D. C. (1972) On the origins of trapped helium, neon and argon isotopic variations in meteorites II. Carbonaceous meteorites. *Geochim. Cosmochim. Acta* **36**, 377–394.
Boothroyd A. I. and Sackmann I.-J. (1999) The CNO isotopes: deep circulation in red giants and first and second dredge-up. *Astrophys. J.* **510**, 232–250.
Busso M., Gallino R. and Wasserburg G. J. (1999) Nucleosynthesis in asymptotic giant branch stars: relevance for Galactic enrichment and solar system formation. *Ann. Rev. Astron. Astrophys.* **37**, 239–309.
Cameron A. G. W. (1962) The formation of the sun and planets. *Icarus* **1**, 13–69.
Choi B.-G., Huss G. R., Wasserburg G. J. and Gallino R. (1998) Presolar corundum and spinel in ordinary chondrites: Origins from AGB stars and a supernova. *Science* **282**, 1284–1289.
Choi B.-G., Wasserburg G. J. and Huss G. R. (1999) Circumstellar hibonite and corundum and nucleosynthesis in asymptotic giant branch stars. *Astrophys. J.* **522**, L133–L136.
Clayton D. D. (1968) *Principles of Stellar Evolution and Nucleosynthesis*. McGraw-Hill, New York.
Clayton D. D. (1975) Na-22, Ne-E, extinct radioactive anomalies and unsupported Ar-40. *Nature* **257**, 36–37.
Clayton D. D. and Hoyle F. (1976) Grains of anomalous isotopic composition from novae. *Astrophys. J.* **203**, 490–496.
Clayton D. D., Liu W. and Dalgarno A. (1999) Condensation of carbon in radioactive supernova gas. *Science* **283**, 1290–1292.
Clayton D. D., Deneault E. A.-N. and Meyer B. S. (2001) Condensation of carbon in radioactive supernova gas. *Astrophys. J.* **562**, 480–493.
Clayton D. D. and Nittler L. R. (2004) Astrophysics with presolar stardust. *Ann. Rev. Astron. Astrophys.* **42**, 39–78.
Clayton D. D. (2011) A new astronomy with radioactivity: Radiogenic carbon chemistry. *New Astron. Rev.* **55**, 155–165.
Croat T. K., Bernatowicz T., Amari S., Messenger S. and Stadermann F. J. (2003) Structural, chemical, and isotopic microanalytical investigations of graphite from supernovae. *Geochim. Cosmochim. Acta* **67**, 4705–4725.
Croat T. K., Stadermann F. J. and Bernatowicz T. J. (2005) Presolar graphite from AGB stars: Microstructure and s-process enrichment. *Astrophys. J.* **631**, 976–987.
Croat T. K., Stadermann F. and Bernatowicz T. (2008) Correlated isotopic and microstructural studies of turbostratic presolar graphites from the Murchison meteorite. *Meteorit. Planet. Sci.* **43**, 1497–1516.
Croat T. K., Stadermann F. J. and Bernatowicz T. J. (2010) Unusual ^{29,30}Si-rich SiCs of massive star origin found within graphites from the Murchison meteorite. *Astronom. J.* **139**, 2159–2169.
Croat T. K., Berg T., Bernatowicz T. J. and Jadhav M. (2013) Refractory metal nuggets within presolar graphite: First condensates from a circumstellar environment. *Meteorit. Planet. Sci.* **48**, 686–699.
Davis A. M. (2011) Stardust in meteorites. *Proc. Nat. Acad. Sci. USA* **29**, 19142–19146.
Duerbeck H. W. and Benetti S. (1996) Sakurai's object – A possible final helium flash in a planetary nebula nucleus. *Astrophys. J.* **468**, L111–L114.
Eyres S. P. S., Evans A., Geballe T. R., Salama A. and Smalley B. (1998) Infrared spectroscopy of Sakurai's object. *Mon. Not. R. Astron. Soc.* **298**, L37–L41.
Floss C., Stadermann F. J. and Bose M. (2008) Circumstellar Fe oxide from the Acfer 094 carbonaceous chondrite. *Astrophys. J.* **672**, 1266–1271.
Gallino R., Busso M., Picchio G. and Raiteri C. M. (1990) On the astrophysical interpretation of isotope anomalies in meteoritic SiC grains. *Nature* **348**, 298–302.
Gallino R., Raiteri C. M., Busso M. and Matteucci F. (1994) The puzzle of silicon, titanium and magnesium anomalies in meteoritic silicon carbide grains. *Astrophys. J.* **430**, 858–869.
Grady M. M. and Wright I. P. (2003) Elemental and isotopic abundances of carbon and nitrogen in meteorites. *Space Sci. Rev.* **106**, 231–248.
Gyngard F., Amari S., Zinner E. and Ott U. (2009) Interstellar exposure ages of large presolar SiC grains from the Murchison meteorite. *Astrophys. J.* **694**, 359–366.
Gyngard F., Zinner E., Nittler L. R., Morgand A., Stadermann F. J. and Hynes K. M. (2010a) Automated NanoSIMS measurements of spinel stardust from the Murray meteorite. *Astrophys. J.* **717**, 107–120.
Gyngard F., Nittler L. R., Zinner E. and Jose J. (2010b) Oxygen-rich stardust grains from novae. *Proc. of Science (NIC-XI)*, 141.
Gyngard F., Nittler L. R., Zinner E., Jose J. and Cristallo S. (2011) New reaction rates and implications for nova nucleosynthesis and presolar grains. *Lunar Planet Sci.* **XLII**. #2675 (abstr.).
Haenecour P., Zhao X., Floss C., Lin Y. and Zinner E. (2013) First laboratory observation of silica grains from core collapse supernovae. *Astrophys. J. Lett.* **768**, L17 (15pp).
Hajduk M., Zijlstra A. A., Herwig F., van Hoof P. A. M., Kerber F., Kimeswenger S., Pollacco D. L., Evans A., Lopéz J. A., Bryce M., Eyres S. P. S. and Matsuura M. (2005) The real-time stellar evolution of Sakurai's object. *Science* **308**, 231–233.
Heck P. R., Amari S., Hoppe P., Baur H., Lewis R. S. and Wieler R. (2009a) Ne isotopes in individual presolar graphite grains from the Murchison meteorite together with He, C, O, Mg–Al

isotopic analyses as tracers of their origins. *Astrophys. J.* **701**, 1415–1425.

Heck P. R., Gyngard F., Ott U., Meier M. M. M., Avila J. N., Amari S., Zinner E. K., Lewis R. S., Baur H. and Wieler R. (2009b) Interstellar residence times of presolar SiC dust grains from the Murchison carbonaceous meteorite. *Astrophys. J.* **698**, 1155–1164.

Hedrosa R. P., Abia C., Busso M., Cristallo S., Domínguez I., Palmerini S., Plez B. and Straniero O. (2013) Nitrogen isotopes in asymptotic giant branch carbon stars and presolar SiC grains: A challenge for stellar nucleosynthesis. *Astrophys. J. Lett.* **768**, L11 (15pp).

Herwig F., Blöcker T., Langer N. and Driebe T. (1999) On the formation of hydrogen-deficient post-AGB stars. *Astron. Astrophys.* **349**, L5–L8.

Herwig F. (2005) Evolution of asymptotic giant branch stars. *Ann. Rev. Astron. Astrophys.* **43**, 435–479.

Herwig F., Pignatari M., Woodward P. R., Porter D. H., Rockefeller G., Fryer C. L., Bennett M. and Hirschi R. (2011) Convective-relative proton-^{12}C combustion in Sakurai's object (V4334 Sagittarii) and implications for the evolution and yields from the first generation of stars. *Astrophys. J.* **727**, 89 (15pp).

Hoppe P., Amari S., Zinner E., Ireland T. and Lewis R. S. (1994) Carbon, nitrogen, magnesium, silicon and titanium isotopic compositions of single interstellar silicon carbide grains from the Murchison carbonaceous chondrite. *Astrophys. J.* **430**, 870–890.

Hoppe P., Amari S., Zinner E. and Lewis R. S. (1995) Isotopic compositions of C, N, O, Mg, and Si, trace element abundances, and morphologies of single circumstellar graphite grains in four density fractions from the Murchison meteorite. *Geochim. Cosmochim. Acta* **59**, 4029–4056.

Hoppe P., Annen P., Strebel R., Eberhardt P., Gallino R., Lugaro M., Amari S. and Lewis R. S. (1997) Meteoritic silicon carbide grains with unusual Si-isotopic compositions: Evidence for an origin in low-mass low-metallicity asymptotic giant branch stars. *Astrophys. J.* **487**, L101–L104.

Hoppe P. and Ott U. (1997) Mainstream silicon carbide grains from meteorites. In *Astrophysical Implications of the Laboratory Study of Presolar Materials* (eds. T. J. Bernatowicz and E. Zinner). AIP, New York, pp. 27–58.

Hoppe P., Strebel R., Eberhardt P., Amari S. and Lewis R. S. (2000) Isotopic properties of silicon carbide X grains from the Murchison meteorite in the size range 0.5–1.5μm. *Meteorit. Planet. Sci.* **35**, 1157–1176.

Hoppe P. and Zinner E. (2000) Presolar dust grains from meteorites and their stellar sources. *J. Geophys. Res.* **105**, 10371–10385.

Hoppe P., Leitner J., Groner E., Marhas K. K., Meyer B. S. and Amari S. (2010) NanoSIMS studies of small presolar SiC grains: New insights into supernova nucleosynthesis, chemistry, and dust formation. *Astrophys. J.* **719**, 1370–1384.

Hoppe P., Fujiya W. and Zinner E. (2012) Sulfur molecule chemistry in supernova ejecta recorded by silicon carbide stardust. *Astrophys. J. Lett.* **745**, L26–L30.

Huss G. R., Fahey A. J., Gallino R. and Wasserburg G. J. (1994) Oxygen isotopes in circumstellar Al_2O_3 grains from meteorites and stellar nucleosynthesis. *Astrophys. J.* **430**, L81–L84.

Hutcheon I. D., Huss G. R., Fahey A. J. and Wasserburg G. J. (1994) Extreme ^{26}Mg and ^{17}O enrichments in an Orgueil corundum: Identification of a presolar oxide grain. *Astrophys. J.* **425**, L97–L100.

Hynes K. M. and Gyngard F. (2009) The presolar grain database: http://presolar.wustl.edu/~pgd. *Lunar Planet. Sci.* **XL**. #1198 (abstr.).

Hynes K. M., Croat T. K., Amari S., Mertz A. F. and Bernatowicz T. J. (2010) Structual and isotopic microanalysis of presolar SiC from supernovae. *Meteorit. Planet. Sci.* **45**, 596–614.

Hynes K. M., Amari S., Bernatowicz T. J., Lebsack E., Gyngard F. and Nittler L. R. (2011) Combined TEM and NanoSIMS analysis of subgrains in a SiC AB grain. *Lunar Planet Sci.* **XLII**. #2332 (abstr.).

Iben, Jr., I., Kaler J. B., Truran J. W. and Renzini A. (1983) On the evolution of those nuclei of planetary nebulae that experience a final helium shell flash. *Astrophys. J.* **264**, 605–612.

Jadhav M., Amari S., Zinner E., Maruoka T., Marhas K. K. and Gallino R. (2013a) Multi-element isotopic analyses of presolar graphite grains from Orgueil. *Geochem. Cosmochim. Acta* **113**, 193–224.

Jadhav M., Pignatari M., Herwig F., Zinner E., Gallino R. and Huss G. R. (2013b) Relics of ancient post-AGB stars in a primitive meteorite. *Astrophys. J. Lett.* **777**, L27 (27pp).

Jones A. P., Tielens A. G. G. M. and Hollenbach D. J. (1996) Grain shattering in shocks: The interstellar grain size distribution. *Astrophys. J.* **469**, 740.

Jones A. P. and Nuth, III, J. A. (2011) Dust destruction in the ISM: a re-evaluation of dust lifetimes. *Astron. Astrophys.* **530**, A44 (12pp).

Jordan G. C., Gupta S. S. and Meyer B. S. (2003) Nucelar reactions important in α-rich freeze-outs. *Phys. Rev. C* **68**, id. 065801.

José J. and Hernanz M. (1998) Nucleosynthesis in classical novae: CO versus ONe white dwarfs. *Astrophys. J.* **494**, 680–690.

José J., Hernanz M., Amari S., Lodders K. and Zinner E. (2004) The imprint of nova nucleosynthesis in presolar grains. *Astrophys. J.* **612**, 414–428.

Jungck M. H. A. (1982) *Pure ^{22}Ne in the Meteorite Orgueil*. E. Reinhardt, München.

Kerber F., Blommaert J. A. D. L., Groenewegen M. A. T., Kimeswenger S., Käufl H. U. and Asplund M. (1999) ISO observations of dust formation in Sakurai's object. *Astron. Astrophys.* **350**, L27–L30.

Lambert D. L., Gustafsson B., Eriksson K. and Hinkle K. H. (1986) The chemical composition of carbon stars. I. Carbon, nitrogen, and oxygen in 30 cool carbon stars in the galactic disk. *Astrophys. J. Suppl.* **62**, 373–425.

Lattanzio J. C. and Boothroyd A. I. (1997) Nucleosynthesis of elements in low to intermediate mass stars through the AGB phase. In *Astrophysical Implications of the Laboratory Study of Presolar Materials* (eds. T. J. Bernatowicz and E. Zinner). AIP, New York, pp. 85–114.

Lewis R. S., Srinivasan B. and Anders E. (1975) Host phase of a strange xenon component in Allende. *Science* **190**, 1251–1262.

Lewis R. S., Tang M., Wacker J. F., Anders E. and Steel E. (1987) Interstellar diamonds in meteorites. *Nature* **326**, 160–162.

Lewis R. S., Amari S. and Anders E. (1990) Meteoritic silicon carbide: Pristine material from carbon stars. *Nature* **348**, 293–298.

Lewis R. S., Amari S. and Anders E. (1994) Interstellar grains in meteorites: II. SiC and its noble gases. *Geochim. Cosmochim. Acta* **58**, 471–494.

Lodders K. and Fegley, Jr., B. (1997) Condensation chemistry of carbon stars. In *Astrophysical Implications of the Laboratory Study of Presolar Materials* (eds. T. J. Bernatowicz and E. Zinner). AIP, New York, pp. 391–423.

Lodders K. and Fegley, Jr., B. (1998) Presolar silicon carbide grains and their parent stars. *Meteorit. Planet. Sci.* **33**, 871–880.

Lodders K. and Amari S. (2005) Presolar grains from meteorites: Remnants from the early times of the solar system. *Chem. Erde* **65**, 93–166.

Lodders K., Palme H. and Gail H.-P. (2009) Abundances of the elements in the solar system. In *Landolt-Börnstein, New Series,*

Vol. VI Astronomy and Astrophysics Numerical Data and Functional Relationship in Science and Technology 4B: Solar System (ed. J. E. Trümper). Springer-Verlag, Berlin, pp. 560–630.

Marhas K. K., Amari S., Gyngard F., Zinner E. and Gallino R. (2008) Iron and nickel isotopic ratios in presolar SiC grains. *Astrophys. J.* **689**, 622–645.

Meier M. M. M., Heck P. R., Amari S., Baur H. and Wieler R. (2012) Graphite grains in supernova ejecta – Insights from a noble gas study of 91 individual KFC1 presolar graphite grains from the Murchison meteorite. *Geochem. Cosmochim. Acta* **76**, 147–160.

Meikle W. P. S., Spyromilio J., Allen D. A., Varani G.-F. and Cumming R. J. (1993) Spectroscopy of supernova 1987A at 1–4 μm – II. Days 377 to 1114. *Mon. Not. R. Astron. Soc.* **261**, 535–572.

Messenger S., Keller L. P., Stadermann F. J., Walker R. M. and Zinner E. (2003) Samples of stars beyond the solar system: Silicate grains in interplanetary dust. *Science* **300**, 105–108.

Meyer B. S., Weaver T. A. and Woosley S. E. (1995) Isotope source table for a 25 Mö supernova. *Meteoritics* **30**, 325–334.

Mostefaoui S. and Hoppe P. (2004) Discovery of abundant in situ silicate and spinel grains from red giant stars in a primitive meteorite. *Astrophys. J.* **613**, L149–L152.

Nagashima K., Krot A. N. and Yurimoto H. (2004) Stardust silicates from primitive meteorites. *Nature* **428**, 921–924.

Nagataki S., Hashimoto M., Sato K. and Yamada S. (1997) Explosive nucleosynthesis in asymmetrically deformed type II supernovae. *Astrophys. J.* **486**, 1026–1035.

Nagataki S., Hashimoto M., Sato K., Yamada S. and Mochizuki Y. S. (1998) The high ratio of 44Ti/56Ni in Cassiopeia A and the axisymmetric collapse-driven supernova explosion. *Astrophys. J.* **492**, L45–L48.

Nguyen A. N. and Zinner E. (2004) Discovery of ancient silicate stardust in a meteorite. *Science* **303**, 1496–1499.

Nguyen A. N., Messenger S., Ito M. and Rahman Z. (2010) Mg isotopic measurement of FIB-isolated presolar silicate grains. *Lunar Planet. Sci.* **41**. #2413 (abstr.).

Nicolussi G. K., Pellin M. J., Lewis R. S., Davis A. M., Clayton R. N. and Amari S. (1998) Zirconium and molybdenum in individual circumstellar graphite grains: New isotopic data on the nucleosynthesis of heavy elements. *Astrophys. J.* **504**, 492–499.

Nittler L. R., Alexander C. M. O'D., Gao X., Walker R. M. and Zinner E. K. (1994) Interstellar oxide grains from the Tieschitz ordinary chondrite. *Nature* **370**, 443–446.

Nittler L. R., Hoppe P., Alexander C. M. O'D., Amari S., Eberhardt P., Gao X., Lewis R. S., Strebel R., Walker R. M. and Zinner E. (1995) Silicon nitride from supernovae. *Astrophys. J.* **453**, L25–L28.

Nittler L. R., Amari S., Zinner E., Woosley S. E. and Lewis R. S. (1996) Extinct ^{44}Ti in presolar graphite and SiC: Proof of a supernova origin. *Astrophys. J.* **462**, L31–L34.

Nittler L. R., Alexander C. M. O'D., Gao X., Walker R. M. and Zinner E. (1997) Stellar sapphires: The properties and origins of presolar Al_2O_3 in meteorites. *Astrophys. J.* **483**, 475–495.

Nittler L. R., Alexander C. M. O'D., Wang J. and Gao X. (1998) Meteoritic oxide grain from supernova found. *Nature* **393**, 222.

Nittler L. R. and Hoppe P. (2005) Are presolar silicon carbide grains from novae actually from supernovae? *Astrophys. J.* **631**, L89–L92.

Nittler L. R., Alexander C. M. O'D., Gallino R., Hoppe P., Nguyen A. N., Stadermann F. J. and Zinner E. K. (2008) Aluminum-, calcium- and titanium-rich oxide stardust in ordinary chondrite meteorites. *Astrophys. J.* **682**, 1450–1478.

Nittler L. R., Gyngard F. and Zinner E. (2010) Extreme O isotopic anomalies in presolar oxides from the Murray CM2 chondrite. *Meteorit. Planet. Sci.* **45**, A153.

Nomoto K. and Hashimoto M. (1988) Presupernova evolution of massive stars. *Phys. Rep.* **163**, 13–36.

Nozawa T., Kozasa T., Habe A., Dwek E., Umeda H., Tominaga N., Maeda K. and Nomoto K. (2007) Evolution of dust in primordial supernova remnants: Can dust grains formed in the ejecta surive and be injected into the early interstellar medium? *Astrophys. J.* **666**, 955–966.

Ohnaka K. and Tsuji T. (1999) Quantitative analysis of carbon isotopic ratios in carbon stars. III. 26 J-type carbon stars including 5 silicate carbon stars. *Astron. Astrophys.* **345**, 233–243.

Pavlenko Y. V., Geballe T. R., Evans A., Smalley B., Eyres S. P. S., Tyne V. H. and Yakovina L. A. (2004) CO bands in V4334 Sgr (Sakurai's Object): The ^{12}C/^{13}C ratio. *Astron. Astrophys.* **417**, L39–L43.

Pignatari M., Wiescher M., Timmes F. X., de Boer R. J., Thielemann F.-K., Fryer C., Heger A., Herwig F. and Hirschi R. (2013a) Production of carbon-rich presolar grains from massive stars. *Astrophys. J. Lett.* **767**, L22 (26pp).

Pignatari M., Zinner E., Bertolli M. G., Trappitsch R., Hoppe P., Rauscher T., Fryer C., Herwig F., Hirschi R., Timmes F. X. and Thielemann F.-K. (2013b) Silicon carbide grains of type C provide evidence for the production of the unstable isotope ^{32}Si in supernovae. *Astrophys. J. Lett.* **771**, L7 (5pp).

Podosek F. A. (1978) Isotopic structures in solar system materials. *Ann. Rev. Astron. Astrophys.* **16**, 293–334.

Podosek F. A., Prombo C. A., Amari S. and Lewis R. S. (2004) s-Process Sr isotopic compositions in presolar SiC from the Murchsion meteorite. *Astrophys. J.* **605**, 960–965.

Prombo C. A., Podosek F. A., Amari S. and Lewis R. S. (1993) s-Process Ba isotopic compositions in presolar SiC from the Murchison meteorite. *Astrophys. J.* **410**, 393–399.

Rauscher T., Heger A., Hoffman R. D. and Woosley S. E. (2002) Nucleosynthesis in massive stars with improved nuclear and stellar physics. *Astrophys. J.* **576**, 323–348.

Rugel G., Faestermann T., Knie K., Korschinek G., Poutivtsev M., Schumann D., Kivel N., Günther-Leopold I., Weinreich R. and Wohlmuther M. (2009) New measurement of the ^{60}Fe half-life. *Phys. Res. Lett.* **103**, 072502-072501–072502-072504.

Savina M. R., Davis A. M., Tripa C. E., Pellin M. J., Clayton R. N., Lewis R. S., Amari S., Gallino R. and Lugaro M. (2003) Barium isotopes in individual presolar silicon carbide grains from the Murchison meteorite. *Geochim. Cosmochim. Acta* **67**, 3201–3214.

Srinivasan B. and Anders E. (1978) Noble gases in the Murchison meteorite: Possible relics of *s*-process nucleosynthesis. *Science* **201**, 51–56.

Stadermann F. J., Croat T. K., Bernatowicz T. J., Amari S., Messenger S., Walker R. M. and Zinner E. (2005) Supernova graphite in the NanoSIMS: Carbon, oxygen and titanium isotopic compositions of a spherule and its TiC sub-components. *Geochim. Cosmochim. Acta* **69**, 177–188.

Straniero O., Gallino R. and Cristallo S. (2006) S process in low-mass asymptotic giant branch stars. *Nucl. Phys. A* **777**, 311–339.

Tang M. and Anders E. (1988) Isotopic anomalies of Ne, Xe, and C in meteorites. II. Interstellar diamond and SiC: Carriers of exotic noble gases. *Geochim. Cosmochim. Acta* **52**, 1235–1244.

Timmes F. X., Woosley S. E., Hartmann D. H. and Hoffman R. D. (1996) The production of ^{44}Ti and ^{60}Co in supernovae. *Astrophys. J.* **464**, 332–341.

Travaglio C., Gallino R., Amari S., Zinner E., Woosley S. and Lewis R. S. (1999) Low-density graphite grains and mixing in type II supernovae. *Astrophys. J.* **510**, 325–354.

Utsumi K. (1985a) Abundance analyses of thirty cool carbon stars. *Proc. Jpn. Acad.* **61B**, 193–196.

Utsumi K. (1985b) Abundance analysis of cool carbon stars. In *Cool stars with excesses of heavy elements* (eds. M. Jaschek and P. C. Keenan). Reidel Publishing Co., Dortrecht, pp. 243–247.

Utsumi K. (1988) Abundances in J-type carbon stars. In *Atmospheric Diagnostics of Stellar Evolution. Chemical Peculiarity, Mass Loss, and Explosion* (ed. K. Nomoto). Springer-Verlag, Berlin, New York, pp. 44–45.

Woosley S. E. and Weaver T. A. (1995) The evolution and explosion of massive stars, II. Explosive hydrodynamics and nucleosynthesis. *Astrophys. J. Suppl.* **101**, 181–235.

Woosley S. E., Heger A. and Weaver T. A. (2002) The evolution and explosion of massive stars. *Rev. Mod. Phys.* **74**, 1015–1071.

Wopenka B., Xu Y. C., Zinner E. and Amari S. (2013) Murchison presolar carbon grains of different density fractions: A Raman spectroscopic perspective. *Geochem. Cosmochim. Acta* **106**, 463–489.

Yoshida T. and Hashimoto M. (2004) Numerical analyses of isotopic ratios of presolar grains from supernovae. *Astrophys. J.* **606**, 592–604.

Zinner E., Tang M. and Anders E. (1989) Interstellar SiC in the Murchison and Murray meteorites: Isotopic composition of Ne, Xe, Si, C, and N. *Geochim. Cosmochim. Acta* **53**, 3273–3290.

Zinner E. (2004) Presolar grains. In *Meteorites, Planets, and Comets* (ed. A. M. Davis), *Vol. 1. Treatise on Geochemistry* (eds. H. D. Holland and K. K. Turekian). Elsevier-Pergamon, Oxford, pp. 17–39.

Zinner E., Nittler L. R., Gallino R., Karakas A. I., Lugaro M., Straniero O. and Lattanzio J. C. (2006) Silicon and carbon isotopic ratios in AGB stars: SiC grain data, models, and the Galactic evolution of the Si isotopes. *Astrophys. J.* **650**, 350–373.

Zinner E., Amari S., Guinness R., Jennings C., Mertz A. F., Nguyen A. N., Gallino R., Hoppe P., Lugaro M., Nittler L. R. and Lewis R. S. (2007) NanoSIMS isotopic analysis of small presolar grains: Search for Si_3N_4 grains from AGB stars, and Al and Ti isotopic compositions of rare presolar SiC grains. *Geochim. Cosmochim. Acta* **71**, 4786–4813.

Zinner E. (2013) Laboratory analysis of stardust. *Anal. Chem.* **85**, 1264–1270.

Zinner E. and Jadhav M. (2013) Isochrons in presolar graphite grains from Orgueil. *Astrophys. J.* **768**, 100 (19pp).

Associate editor: Sara S. Russell